



SAPIENZA
UNIVERSITÀ DI ROMA

FACOLTÀ DI INGEGNERIA DELL'INFORMAZIONE
INFORMATICA E STATISTICA

Corso di Laurea in Ingegneria Elettronica

Tesi di Laurea Magistrale

**Study of longitudinal multibunch
instabilities for LHC-type beams at the CERN
Proton Synchrotron**

Candidate
Letizia Ventura

Thesis Advisor
Prof. Luigi Palumbo

Thesis Co-Advisor
Prof. Mauro Migliorati

CERN Supervisor
Dott. Simone Silvano Gilardoni



A nonna Attilia

Contents

Acronyms Table	ix
Introduction	1
1 Basic concepts of Beam Dynamics	4
1.1 Guiding particles in an accelerator	4
1.2 Transverse beam dynamics	5
1.3 Equation of motion and betatron oscillations	7
1.4 Longitudinal beam dynamics	12
1.5 RF cavities	12
1.6 Bunch, Buckets and Phase Stability	13
1.7 Collective effects and Beam Instabilities	17
2 The CERN Proton Synchrotron	20
2.1 Beams in the CERN PS	22
2.2 The PS as LHC Injector	24
2.3 Alternative schemes for 25/50 ns beam production	25
2.4 The LHC Injectors Upgrade project	26
2.4.1 Main principles of the upgrade	27
3 Wakefield and Longitudinal Beam Instabilities	28
3.1 Basic mechanism driving an instability	28
3.2 Wakefield and potentials	29
3.3 Coupling Impedance	30
3.4 Longitudinal wake field of a resonant mode	32
3.5 Coupling impedances of a resonant mode	34
3.6 Instabilities in circular accelerators	34
3.7 Longitudinal coupled-bunch instabilities:qualitative analysis	35
3.8 Basic principle of Longitudinal Multi-bunch Instabilities	37
4 Simulation Code and Benchmarking	41
4.1 Longitudinal Coupled Bunch simulation Code (LCBC)	41
4.2 Benchmarks	43
4.3 Review of Feedback System Theory	46
4.3.1 Frequency domain FB: the PS choice	47
4.4 Overview of the feedback system in the LCBC code	48
4.4.1 Application of the feedback system to damp an unstable mode	49

5	Coupled bunch studies for the CERN Proton Synchrotron	52
5.1	External Excitation	52
5.2	10 MHz RF cavity system	55
5.3	Simulations at 3.3 MHz for $h = 7$	58
5.4	Simulations at 10 MHz for $h = 21$	61
5.5	Suppression of one mode at 10 MHz for $h = 21$	64
6	Preliminary results	69
6.1	40 and 80 MHz cavities	69
6.2	Finemet© cavity	71
7	Conclusion	75
	Acknowledgments	77
	Bibliography	79

List of Figures

1.1	Path of integration used to compute the quadrupole gradient as a function of the current	6
1.2	Schematic drawing of a symmetric FODO-cell [12]	7
1.3	Coordinate system	8
1.4	Schematic view of a dipole magnet, showing the path of integration to compute the field in the gap [13]	8
1.5	Cross-section of a quadrupole magnet [13]	9
1.6	Transverse oscillations inside a synchrotron of circumference s_c . . .	10
1.7	The parameters of a phase-space ellipse containing an emittance at a point in the lattice between quadrupoles. Points on the ellipse represent different turns of the particle	11
1.8	Energy variation of two circulating particles passing by the RF cavity [20].	14
1.9	Relative motion of A and B in the longitudinal phase space [20] . . .	15
1.10	Motion of particle inside and outside the bucket limit [20]	16
1.11	a) beam interacts with itself, b) beam interacts with localized electron cloud, c) beam interacts with machine	17
1.12	Cylindrical cross section of a beam	18
1.13	Proton beam moving in a beam pipe	19
2.1	Proton Synchrotron complex layout	21
2.2	Open and closed single block of the main magnet units	22
2.3	Example of magnetic field cycle for the ToF beam [34]	23
2.4	Example of magnetic field cycle for the nominal LHC 25 ns beam [34]	23
2.5	Production of the LHC 25 ns beam in the PS with the double batch injection on the 1.2 s long flat bottom plateau. The blue curve is the magnetic field as a function of time, the red is the beam intensity in number of protons and as a function of the harmonic number changed by the successive RF gymnastics.	25
2.6	RF gymnastic for the production of the BCMS scheme at intermediate energy. The batch compression is followed by a bunch merging and a triple splitting [27]	26
2.7	Longitudinal stability limits according to observations from 2009 to 2011 [37]	27
3.1	Image or wall current induced by a circulating bunch	29

3.2	The real part of a longitudinal coupling impedance for an RF cavity with adjacent beam pipes [6]	31
3.3	Parallel RLC circuit	32
3.4	RF cavity and the equivalent RLC parallel circuit model driven by a current generator	33
3.5	Real and imaginary parts of impedance Z of a resonator	34
3.6	Charged particle passing into a cavity	35
3.7	Motion of the four bunches in the longitudinal phase plane	36
3.8	Voltages induced by each of four bunches in a cavity tuned at the revolution frequency. Bunches do not perform synchrotron oscillations in this case	36
3.9	Voltages induced by two out of four bunches performing coupled synchrotron oscillations with a bunch-to-bunch phase shift of $\pi/2$	37
4.1	Flow chart of the code developed for $DA\Phi NE$ with the previous FB system in time domain [9]	42
4.2	Real part of the shunt impedance with indication of the lines of stable and unstable modes	44
4.3	Growth rate mode $\mu = 19$ in function of the number of turns in the machine	45
4.4	Fit	45
4.5	Diagram of a feedback system	47
4.6	Longitudinal position (on the right) and amplitude (on the left) of one bunch with FB off and with excitation	50
4.7	Longitudinal position (on the right) and amplitude (on the left) of one bunch with FB on and without excitation of an HOM	51
4.8	Longitudinal position (on the right) and amplitude (on the left) of one bunch with FB on and the mode excited	51
5.1	Synchrotron frequency sidebands of the f_{rev} harmonics [55]	53
5.2	Synchrotron frequency sidebands for LHC-type beams	53
5.3	Example mode spectrum of 21 bunches in $h = 21$, excited at the upper SB of $19f_0$	54
5.4	Example mode spectrum of 18 bunches in $h = 21$, excited at the upper SB of $19f_0$ [53]	55
5.5	On of the CERN PS 10 MHz cavity	56
5.6	Simplified model of the 10 MHz RF system, including ferrite loaded cavities and power amplifier with a tuned grid resonator and the fast feedback around the amplifier [47]	57
5.7	Real part of the total impedance of the 10 MHz cavities [47]	58
5.8	Real part of the total impedance of the 10 MHz cavities and best fit obtained and used in simulations for $h = 7$	59
5.9	Mode pattern for $h = 7$ using 7 bunches	59
5.10	Open and closed loop transfer function of one of the cavities at 3.3 MHz (right) and 10 MHz (left)	61
5.11	Closed loop transfer function at 3.3 Mhz (shifted) and at 10 MHz	61
5.12	Machine model impedance at 3.3 and 10 MHz	62

5.13	Real part of the total impedance of the 10 MHz cavities and best fit obtained and used in simulations for $h = 21$	63
5.14	LHC50ns: Development of the CB mode spectrum during acceleration for $h = 21$ with 21 bunches[54]	63
5.15	LHC50ns: CB mode spectrum during acceleration for $h = 21$ with 18 bunches[54]	64
5.16	Simulation of the LHC50ns CB mode spectrum during acceleration for $h = 21$ with 18 bunches	65
5.17	Simulation of the LHC50ns CB mode spectrum during acceleration for $h = 21$ with 21 bunches	65
5.18	Mode amplitude of all oscillation modes excited, the blu line is referred to $\mu = 2$	66
5.19	Mode amplitude of oscillation mode $\mu = 2$, the green line is referred to the mode and the red one is the fit	67
5.20	Exponential fit on the oscillation mode $\mu = 2$ when the FB is switched on	67
5.21	Mode pattern of all the oscillation modes once that the FB and the HOMs are on. The blu line is referred to the dumped mode $\mu = 2$	68
6.1	Mode amplitude of 10 and 40 MHz cavities (up) and 10 and 80 MHz cavities (down)	69
6.2	Mode amplitude of all cavities	70
6.3	One cell CST model of the Finemet cavity [58]	71
6.4	Longitudinal impedance of the one cell Finemet cavity [58]	71
6.5	Fit of the impedance of Finemet© cavity and study of the excited modes. The real part of impedance is expressed in Ω	72
6.6	Mode amplitude of Finemet cavity	73
6.7	Mode amplitude of Finemet© cavity and 10 MHz cavity	74

List of Tables

I	General parameters of the CERN Proton Synchrotron	21
II	Beam parameters of the LHC 25ns, TOF and AD beams	24
III	Parameters of the LHC beams produced in the PS at extraction . . .	24
IV	Robinson Instability	40
V	Parameters used for benchmark simulations of the LCBC code.	44
VI	Theoretical and simulated rise time of instability for mode $\mu = 19$ in harmonic number 21 with 21 bunches	46
VII	Parameters used to benchmark the FB system in the code (for beam parameters see table V)	49
VIII	Parameters used for benchmark simulations of the LCBC code.	55
IX	CB growth rates from eigenvalues system	58
X	Parameters resulting from the fit on the real part of the 10 MHz system impedance indicating the HOMs used in simulations to excite the coherent oscillation modes for $h = 7$	60
XI	Parameters used for simulations for $h = 7$	60
XII	Comparison between CB growth rates for $h = 7$ and for 7 bunches as simulations by LCBC code and values from the theoretical eigenvalues system.	60
XIII	Parameters resulting from the fit on the real part of the 10 MHz system impedance indicating the HOMs used in simulations to excite the coherent oscillation modes for $h = 21$	62
XIV	Input parameters for LHC50ns beams during acceleration	62
XV	Characteristic parameters of 40 and 80 MHz cavities	70

Acronyms Table

AD	Antiproton Decelerator
BCMS	Buch Compression Merging and Splitting
CBI	Coupled Bunch Instabilities
CERN	European Organization for Nuclear Research
CNGS	CERN neutrinos to Gran Sasso
DAΦNE	Double Annular Factory for Nice Experiments
FB	Feedback
HL-LHC	High Luminosity LHC
HOM	Higher Order Modes
INFN	Istituto Nazionale di Fisica Nucleare
L	Luminosity
LCBC	Longitudinal Coupled Bunch Simulation Code
LEIR	Low Energy Ion Ring
LHC	Large Hadron Collider
LINAC	Linear Accelerator
LIU	LHC Injector Upgrade
LNF	Laboratory Nazionali of Frascati
LS1	Long Shutdown 1
MU	Magnets Unit
nTOF	neutron Time-Of-Flight facility
OPERA	Oscillation Project with Emulsion-Racking Apparatus
PS	Proton Synchrotron
PSB	Proton Synchrotron Booster
Q	Quality Factor
RF	Radio Frequency
SBs	Sidebands
SPS	Super Proton Synchrotron
TE	Transverse electric
TEM	Transverse Electromagnetic
TM	Transverse Magnetic

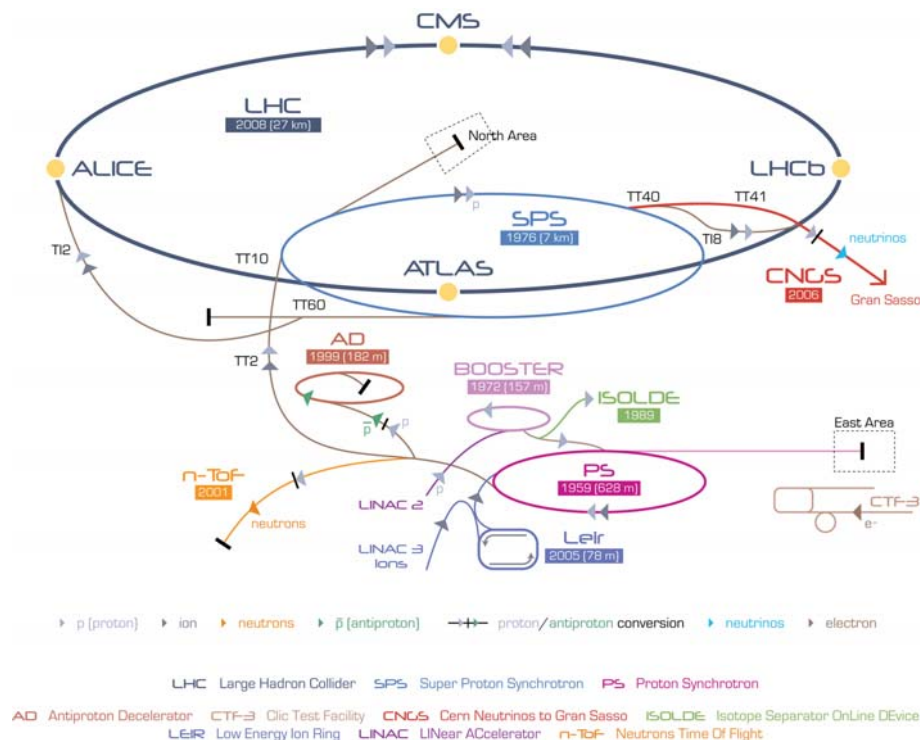
Abstract

This Master thesis work has been carried out at CERN in the framework of the LHC (Large Hadron Collider) Injector upgrade program (LIU). Longitudinal coupled-bunch (CB) oscillations are an important limitation for the high-brightness beam accelerated in the CERN Proton Synchrotron. Up to present intensities they are suppressed by a dedicated feedback system limited to the first two dominant oscillation modes. In view of the proposed installation of a new wide-band FB system in the framework of the LIU program, measurements have been performed on the old system with the aim of dimensioning the new one. A new simulation program, called LCBC (Longitudinal Coupled Bunch Simulation), has been used to study the behaviour of the CB FB. By means of this code I have started an extensive simulation campaign to benchmark the code with the theory of coupled bunch and to confirm that the 10 MHz cavity system is the main cause of the coupled bunch instabilities in the CERN PS.

Introduction

The LHC [1] it's the world's largest and most powerful particle accelerator. It mainly consists of a 27-kilometres ring of superconducting magnets with a number of accelerating structures to boost the energy of the particles along the way.

In the accelerator two beams of particles travel close to the speed of light with very high energies before colliding. The beams travel in opposite directions in separate beam pipes – two tubes kept at ultrahigh vacuum and are guided around the accelerator ring by a strong magnetic field, achieved using superconducting electromagnets. These are built from coils of special electric cables that operate in a superconducting state, efficiently conducting electricity without resistance. This requires chilling the magnets to about $1.9^{\circ}K$, a temperature colder than outer space. For this reason, much of the accelerator is connected to a distribution system of liquid helium, which cools the magnets.



CERN accelerator complex

The path of a proton accelerated through the accelerator complex at CERN is as follows: hydrogen atoms are stored in form of a gas and then protons are obtained by stripping orbiting electrons from them. Protons are injected into the PS Booster (PSB) [2] at an energy of 50 MeV from the Linac2 [3]. The Booster accelerates them to 1.4 GeV; the beam is fed to the Proton Synchrotron (PS) [4] where it is accelerated to 25 GeV. Protons are then sent to the Super Proton Synchrotron (SPS) [5] where they are accelerated to 450 GeV. They are finally transferred to the LHC .

At CERN high energies are achieved by accelerating particles in circular machine, so called synchrotrons. Modern synchrotrons require very high quality particle beams with high intensity, low transverse emittances, and low energy spread to achieve high brightness. This requirement of a high quality particle beam presents a number of challenges, including stabilizing beam orbits, and suppression of beam instabilities. The beam intensity is limited by single-particle effects as well as collective effects. Single-particle effects are mostly determined by the guiding magnetic elements of the accelerator, which are the most fundamental and important devices in the design of a circular accelerator. Collective effects are caused by the interactions between charged particles and their surroundings. They become more significant, and therefore more disrupting, at a high beam intensity. Space charge effect are caused by Coulomb interaction within a beam of many charged particles. This effect is important at low energy, especially in a low energy proton accelerator. However, it is negligible for ultra-relativistic particle beams in storage rings. In these storage rings, the electromagnetic field produced by the interaction between protons and their surroundings, such as vacuum chamber, the so-called wakefield, is the main source of beam instabilities. Wakefield effects can lead to longitudinal and transverse instabilities (coherent effects), which limit the ultimate achievable beam current because typically produces beam losses. Among these instabilities, the coupled bunch instabilities (CBIs) are very important in accelerators operated with multiple bunches at a high beam current. The wake effect can be minimized using various techniques and methods, such as increasing Landau damping (increase frequency spread of the beam), minimizing vacuum chamber transition and resistance, using single-mode RF cavities, and using active feedback systems. Among these measures, for an existing accelerator, one effective method to combat beam instabilities is the use of active feedback systems. The feedback system is a universal solution to beam instabilities regardless of the sources of wakefields [6].

The work of this thesis is dedicated to the study of longitudinal coupled bunch instabilities in the CERN PS. In view of the installation of a new feedback system to control longitudinal multi-bunch instabilities, within the framework of the LHC Injectors Upgrade project (LIU) [7], measurements have been performed with the existing damping system with the aim of dimensioning the new one. The goal is to compare measurement results and simulations, carried out with the Longitudinal Coupled Bunch simulation Code (LCBC) developed in ref.[8].

This code has been used to investigate the effect of a bunch-by-bunch feedback system for the longitudinal coupled bunch instabilities in DAΦNE [9]. The code tracks the longitudinal dipole motion of all the bunches and it includes the effects of

the HOMs, the synchrotron radiation and the fast RF feedback. A frequency domain longitudinal feedback, instead of the bunch-by-bunch one has been implemented in LCBC according with the PS future installation. While tracking the bunches, the code carries out a mode analysis to obtain amplitude, frequency and phase of the modes into which the phase oscillation of all the bunches can be decomposed. For each selected mode to be damped, the code applies a kick proportional to the FB gain and mode amplitude with a proper phase.

Simulations have been performed in different configurations by using an impedance model for the 10 MHz RF system, which is supposed to be the most probable impedance source of the coupled bunch instability in the PS. It appears that a good agreement between simulations and measurements can be obtained with and without the feedback system.

Chapter 1

Basic concepts of Beam Dynamics

The development of the first particle accelerators in the 1920s led to revolutionary possibilities for the understanding of the constitution of matter. At today's high energy frontier, physicists benefit from the Large Hadron Collider (LHC) at CERN with a design beam energy of 7 TeV, an increase of energy of six orders of magnitude compared to the first machines. The following introduction to accelerator physics is based on [10],[11],[1], where more detailed explanations can be found.

1.1 Guiding particles in an accelerator

Particle accelerators are machine that accelerate charged particles to high energies by applying electromagnetic fields. The processes of acceleration and guiding are exclusively based on the Lorentz force:

$$\vec{F} = q (\vec{E} + \vec{v} \times \vec{B}) \quad (1.1)$$

This is the non-relativistic formula where \vec{F} is the force excited by an electric field and a magnetic one on a particle of charge q and velocity v .

Particle energy increase is the main goal of an accelerator. The accelerator provides kinetic energy to charged particles, hence increasing their momentum. In order to do so, it is necessary to have an electric field along the direction of the initial momentum:

$$\frac{dp}{dt} = eE \quad (1.2)$$

Bending is generated by a magnetic field perpendicular to the plane of the particle trajectory. Focusing is a second way of using a magnetic field, in which the bending effect is used to bring the particles trajectory closer to the axis.

As we eyelight, at CERN high level of energies are achieved using synchrotron machines. A synchrotron is a circular accelerator where the nominal particle trajectory is kept at a constant physical radius by means of a magnetic field variation, as well as RF variation, to follow the energy increase.

1.2 Transverse beam dynamics

In any kind of accelerator there is exactly one curve - the design orbit- on which ideally all particles should move. If this design orbit is curved, which may be required for many reasons, bending forces are needed. In reality most particles of the beam will deviate slightly from the design orbit. In order to keep this deviations small, on the whole way, focusing forces are required. In order to obtain that, Lorentz force is applied as a:

- Bending Force (using dipoles) to guide particles along an ideal path, the 'design orbit', on which, ideally, all particles should move;
- Focusing Force (using quadrupoles) to confine the particles in the vicinity of the ideal path.

Bending and focusing magnets are interspace in the ring in a pattern called the lattice.

A dipole magnet is an electromagnet used in particle accelerators to create a homogeneous magnetic field over some distance. Particle motion in that field will be circular in a plane perpendicular to the field and collinear to the direction of particle motion and free in the direction orthogonal to it. Thus, a particle injected into a dipole magnet will travel on a circular or helical trajectory. A quadrupole is a magnetic element generating a force that focuses the particle in the vicinity of the ideal path as will be explained in section 1.3.

The new accelerators and storage ring are equipped with a "separated-function" magnets: dipoles for deflection and quadrupole for focusing.

The basis for a concept called 'Lattice design' was laid out in 1952 when Courant, Livingston, and Snyder developed the theory of strong focusing accelerators (or alternating-gradient machines) [12]. Lattice design is the design and optimization of the principal elements — the lattice cells — of a (circular) accelerator, and it includes the dedicated variation of lattice elements (for example, position and strength of the magnets in the machine) to get well-defined and predictable parameters of the stored particle beam.

Neglecting the electric field and considering a constant transverse magnetic field we divide by the velocity and get a relation between the magnetic field and the momentum p of the particle from which we obtain the expression of beam rigidity:

$$B * \rho = p/e \tag{1.3}$$

p is the momentum vector and connects the magnetic dipole field needed for a circular orbit of radius ρ to the particles momentum and charge. (Note that here we often refer to protons or electrons and the charge is just the elementary charge e). As general rule:

$$\frac{1}{\rho} \simeq 0.3 \frac{B [T]}{p [GeV/c]} \quad (1.4)$$

which defines the bending strenght of the dipole. With an ideal circular orbit, for each segment of the path ds we get the relation :

$$\alpha_c = \frac{ds}{\rho} \rightarrow \int B ds = 2\pi * \frac{p}{q} \quad (1.5)$$

α is called momentum compaction. As in any circular accelerator the angle swept in one turn for the design particle is 2π . Eq. (1.5) tells us that the integral of all bending magnets in the ring has to be 2π times the momentum of the beam once every quantities is expressed in the right unit. If the path lenght inside the dipole magnet does not differ much from the lenght of the magnet itself, the integral of eq. (1.5) can be approximated by $\int B dl$, where dl refers to the magnet lenght. For lattice designer, the integrated B field along the particles design orbit, is the most important parameter, as it is the value that enters eq. (1.5) and defines the field strenght and how many of these magnets are needed for a full circle. In general for a high-energy storage ring or synchrotron, a large number of bending magnets with very high magnetic field are needed to determine the design orbit.

If we look at fig. 1.1 we define:

$$nI = \oint H \cdot ds = \int_0^R H(r) ds + \int_1^2 H_E ds + \int_2^0 H ds \quad (1.6)$$

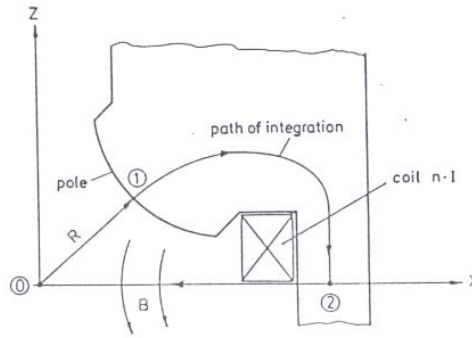


Figure 1.1. Path of integration used to compute the quadrupole gradient as a function of the current

On the first path $H(r) = gr/\mu_0$. The second integral is very small for $\mu_r \gg 1$. The third integral vanishes identically since $H \perp ds$. So we get in good approximation:

$$nI = \frac{1}{\mu_0} \int_0^R gr dr \quad (1.7)$$

In analogy with the bending strenght (eq. (1.4)) of a dipole magnet, it is convenient to relate the field gradient of the quadrupole magnet to its optical effect:

$$g = \frac{2\mu_0 n I}{R^2} \quad (1.8)$$

The field gradient is normalised to the momentum of the particles, thus defining the quadrupole strenght:

$$k = \frac{eg}{p} k [m^2] \simeq 0.3 \frac{g [T/m]}{p [GeV/c]} \quad (1.9)$$

A magnet structure consisting of focusing and defocusing quadrupole lenses in alternating order with basically nothing in between, is called a FODO lattice, and the elementary cell a FODO cell [12]. ‘Basically nothing’ in that context means any element with negligible effect on the focusing properties, as, for example, drift spaces, RF-structures or, under certain circumstances, even bending magnets. A FODO cell is shown in fig. 1.2

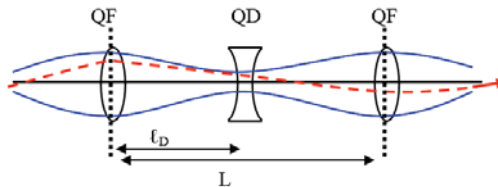


Figure 1.2. Schematic drawing of a symmetric FODO-cell [12]

In linear beam-optics the transfer matrix of a number of optical elements is given by the product of the matrices of the single elements.

1.3 Equation of motion and betatron oscillations

At any instant, particles may be displaced horizontally by x and vertically by z from the ideal position and may also have divergence angles horizontally and vertically with respect to the central orbit :

$$x' = \frac{dx}{ds} \quad (1.10)$$

$$z' = \frac{dz}{ds} \quad (1.11)$$

The coordinate system is shown in fig. 1.3.

In eq. (1.10) and eq. (1.11) the variation of x' and y' are due to the angular kick:

$$\Delta x' = xkl \quad (1.12)$$

and

$$\Delta y' = -ykl \quad (1.13)$$

These kicks depend on the current particle position (x, y) , the normalized quadrupole gradient k and the magnet length l .

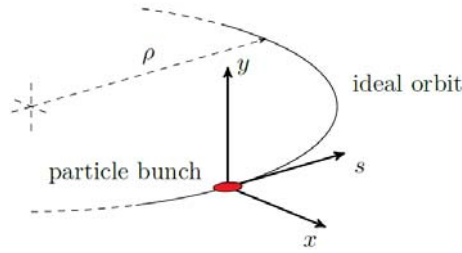


Figure 1.3. Coordinate system

According to eq. (1.12) and eq. (1.13), it is impossible to apply focusing forces in both transverse planes at the same time. A focusing quadrupole is therefore defined to have a focusing effect in the horizontal and a defocusing effect in the vertical plane. Rotating such an element by 90° about its longitudinal axis, or inverting its excitation currents, leads to a defocusing quadrupole, which is vertically focusing (see fig. 1.4 and fig. 1.5).

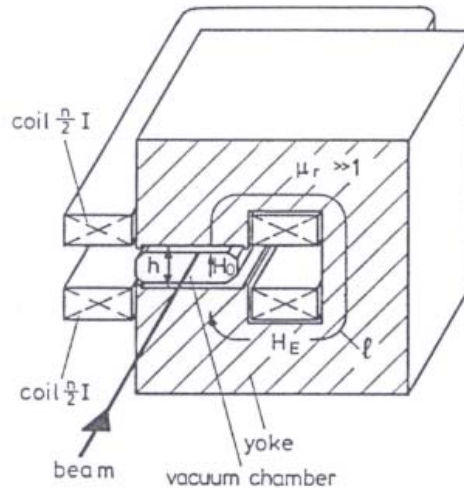


Figure 1.4. Schematic view of a dipole magnet, showing the path of integration to compute the field in the gap [13]

The resulting distribution of focusing forces around a machine can be described by the equation for the horizontal motion, that can be written as:

$$x'' + K(s)x = \frac{1}{\rho} \cdot \frac{\Delta p}{p_0} \quad (1.14)$$

where:

$$K(s) = -k(s) + \frac{1}{\rho^2(s)} \quad (1.15)$$

We can introduce the dispersion function $D(s)$ as the dispersion created by the momentum dependency of the bending radius in dipole magnets and appears

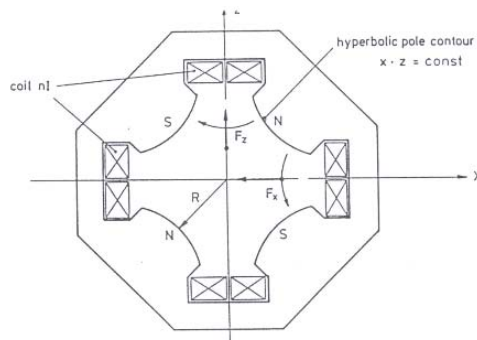


Figure 1.5. Cross-section of a quadrupole magnet [13]

therefore only in the plane of bending (generally the horizontal plane) and it is defined as the ratio between the inhomogeneous solution of eq. (4.14) and the momentum deviation of the particle $\frac{\Delta p}{p_0}$.

$$D(s) = \frac{x}{\Delta p/p_0} \quad (1.16)$$

$D(s)$ is the dispersion trajectory.

We assume that the circular accelerator has a median plane, taken to be the horizontal plane $z=0$, and that the magnetic guide and focusing fields are perpendicular to this plane. We assume even that there is a closed curve in this plane, called equilibrium orbit, on which a particle with reference momentum p_0 can move for an arbitrary number of revolutions. The differential equation for $x(s)$ and $z(s)$ in linear approximation can be written as [14]:

$$x'' - \left(k - \frac{1}{\rho^2}\right)x = \frac{1}{p} \frac{\Delta p}{p_0} z'' + kz = 0 \quad (1.17)$$

(s) and $\rho(s)$ are periodic functions of s because the orbit is a closed curve. In the following we consider only particles of momentum $p = p_0$ and $\Delta p = 0$. Moreover from now on we will write the equation of motion like:

$$x'' + Kx = 0 \quad (1.18)$$

with $K = 1/\rho^2 - k$ in the horizontal plane and $K = k$ in the vertical one. Eq. (1.18) is called the Hill's equation and it is reminiscent of simple harmonic motion but has a restoring force which varies around the accelerator. The general solution of Hill's equation is a pseudo-harmonic oscillation, with varying amplitude and frequency, called betatron oscillations:

$$x(s) = \sqrt{\varepsilon} \sqrt{\beta(s)} \cdot \cos(\Psi(s) + \Phi) \quad (1.19)$$

ε, Φ are integration constants determined by initial conditions and $\beta(s)$ is a periodic function given by focusing properties of the lattice (quadrupoles). Inserting the solution $x(s)$ into the equation of motion we obtain:

$$\Psi(s) = \int_0^s \frac{d\tilde{s}}{\beta(\tilde{s})} \quad (1.20)$$

which is the phase advanced of oscillation between point 0 and s in the lattice.

Another important parameter in accelerator physics is the number of transverse oscillations a particle carries out each turn. This value is obviously closely correlated to the phase advance per turn and defined as the betatron tune:

$$Q = \frac{1}{2\pi} \oint \frac{ds}{\beta(s)} \quad (1.21)$$

For two different values of Q the resulting oscillations are shown in fig. 1.6.

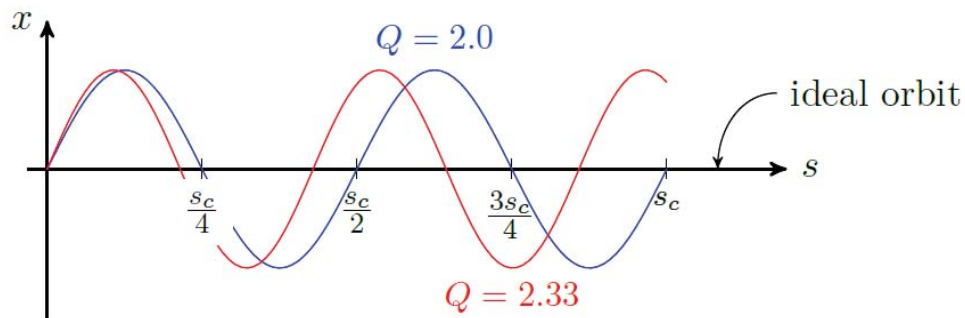


Figure 1.6. Transverse oscillations inside a synchrotron of circumference s_c

Normally accelerators are operated so that Q (Q_x, Q_y) are far from certain values called resonances, mainly due to magnetic errors. If Q is an integer the solution of the equation of motion is periodic and so any imperfection in the magnetic field act as a perturbation which are synchronous with the oscillation frequency. This will excite resonances causing an increasing amplitude and instable motion. One has to avoid to have:

$$kQ_x + lQ_y = m \quad (1.22)$$

where k, l, m are integers. This equation describes a set of lines in the $Q_x - Q_y$ plane which should be avoided. Tunes are normally chosen far from the lowest order resonances. This position in the plane is called working point.

In the eq. (1.19), the constant ε can be expressed through $x(s)$ and its derivative:

$$x' = \frac{\beta'}{2} \sqrt{\frac{\varepsilon}{\beta}} \cos(\phi) - \sqrt{\varepsilon \beta} \phi' \sin(\phi) \quad (1.23)$$

We obtain [14]:

$$\varepsilon = \gamma(s)x^2(s) + 2\alpha(s)x(s)x'(s) + \beta(s)x'^2(s) \quad (1.24)$$

which is called Courant-Snyder invariant [15]. α, β, γ are the Twiss parameters and offer a complete and compact description of the beam dynamics [16] and they are defined as:

$$\alpha(s) = -\frac{\beta'(s)}{2} \quad (1.25)$$

$$\gamma(s) = \frac{1 + \alpha^2(s)}{\beta(s)} \quad (1.26)$$

Both equations eq. (1.19) and eq. (1.23) lead to a parametric representation of an ellipse in the transverse phase space (x, x') , as the phase advance $\phi(s)$ goes from 0 to 2π . While a particle moves around an accelerator in real space it follows an ellipse in the phase space.

In fig. 1.7 we can see how the various features of the ellipse are related to the Twiss Parameters [17].

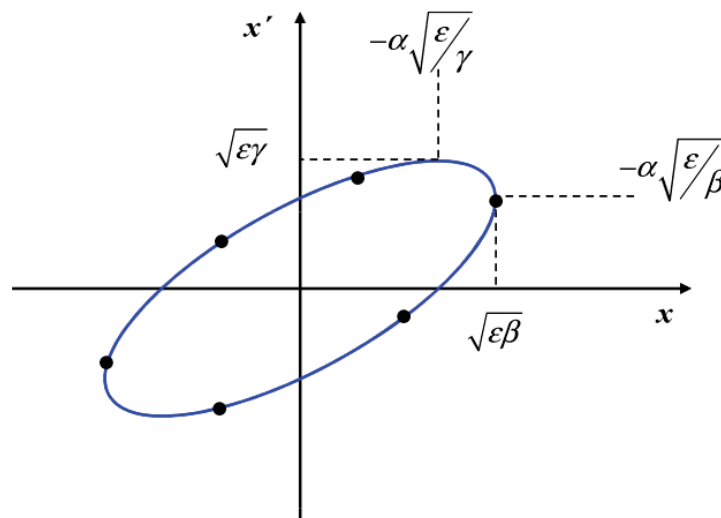


Figure 1.7. The parameters of a phase-space ellipse containing an emittance at a point in the lattice between quadrupoles. Points on the ellipse represent different turns of the particle

The orientation and the shape of the ellipse is determined by the lattice, i.e. the arrangement of magnets within an accelerator, and varies depending on the longitudinal position. The ellipse is furthermore characterized by its area $\pi\epsilon$, which, according to Liouville's theorem [18], is a constant of motion as long as only conservative forces are present and the energy of the particle remain constant. The term ϵ is referred to as emittance with $mm \cdot mrad$ being its unit. Neglecting higher order magnetic fields and other coupling mechanisms, the horizontal, vertical and longitudinal phase space can be treated independently and, therefore, one can define an emittance in each plane.

When the particles are accelerated, the emittance decreases inversely proportional to the momentum. This can be understood intuitively from the observation that only the longitudinal component of the momentum vector is increased in the accelerating cavities whereas the transverse components remain invariant, so that the beam divergence shrinks. This phenomenon is often called adiabatic damping which is

somewhat misleading since no dissipative effect is involved. The energy dependence of the emittance can be derived in a rigorous way within the Hamiltonian formalism. The key point is that the canonically conjugate momenta of the position variables x and z are not the slopes but rather the transverse momenta. The phase-space trajectory in the plane, corresponding to the emittance ellipse, is of course also an ellipse since $\varepsilon_N = (\frac{p_0}{m_0c})\varepsilon$. The area is $\pi\varepsilon_n \cdot (m_0c)$. Here we have defined the normalized emittance by

$$\varepsilon_N = \left(\frac{p_0}{m_0c}\right)\varepsilon \quad (1.27)$$

1.4 Longitudinal beam dynamics

From the expression of the Lorentz force (eq. (1.1)), now we take into consideration the term of electric field:

$$\vec{F} = q(\vec{E} + \vec{v} \times \vec{B}) \rightarrow \vec{F} = \frac{d\vec{p}}{dt} = e\vec{E} \quad (1.28)$$

The bending radius ρ should remain constant in a synchrotron as acceleration proceeds. To achieve this, particle momentum must be incremented on each turn by a precise voltage:

$$V = V_0 \sin\Phi_s \quad (1.29)$$

The amplitude V_0 is pre-programmed and controlled by automatic voltage control while the synchronous phase Φ_s is controlled by another system which compare the phase of the RF voltage with the passage of the bunch.

1.5 RF cavities

In order to accelerate the beam particles we need a longitudinal electric field. Magnetic field cause deflection to the particle trajectory but they do not change the particle momentum. So we must generate a longitudinal voltage, which is applied across isolated gap in the vacuum chamber. We need an oscillating voltage so that the particles see an accelerating voltage in the gap and the voltage than cancel out as the particle goes around the rest of the machine. To do this we use RF cavities.

A radio frequency (RF) cavity is a special type of resonator, consisting of a closed metal structure that confines electromagnetic fields. The structure is either hollow or filled with dielectric material. This cavity acts similarly to a resonant circuit with extremely low loss at its frequency of operation. In addition to their use in electrical networks, RF cavities can manipulate charged particles passing through them by application of acceleration voltage and are thus used in particle accelerators.

Most resonant cavities are made from closed or short-circuited sections of waveguide or high-permittivity dielectric material. Electric and magnetic energy is stored in the cavity and the only losses are due to finite conductivity of cavity walls and

dielectric losses of material filling the cavity. Every cavity has numerous resonant frequencies that correspond to electromagnetic field modes satisfying necessary boundary conditions on the walls of the cavity. Because of these boundary conditions that must be satisfied at resonance (tangential electric fields must be zero at cavity walls), it follows that cavity length must be an integer multiple of half-wavelength at resonance. Hence, a resonant cavity can be thought of as a waveguide equivalent of short circuited half-wavelength transmission line resonator.

The electromagnetic fields in the cavity are excited via external coupling. An external power source is usually coupled to the cavity by a small aperture, a small wire probe or a loop. Considering RF acceleration, it is obvious that when particles get high velocities the drift spaces get longer and one loses on the efficiency. The solution consists of using a higher operating frequency. The power lost by radiation, due to circulating currents on the electrodes, is proportional to the RF frequency. The solution consists of enclosing the system in a cavity which resonant frequency matches the RF generator frequency. Each such cavity can be independently powered from the RF generator. The electromagnetic power is now constrained in the resonant volume.

With the alternating electric field the cavity becomes a resonating structure and resonates at a specific design frequency and any noise or other frequency will not resonate in the cavity. The beam sees only the desired frequency.

RF cavities can be used to:

- accelerate;
- RF deflection and RF gymnastic.

Usually in a pillbox [19], TM (transverse magnetic) mode are the ones used for acceleration but one can even accelerate using TE (transverse electric) modes that have less magnetic field on the inner surface of the cavity. In this case one need to bend the electric field onto the axis. TE and TM mode cavity are ideal for frequencies in the several 100 MHz range. For lower frequencies the cavity dimension becomes too large. One can use TEM cavities where the f_{RF} isn't related to the transverse dimension of the cavity but to its length.

One example are the synchrotron cavities where part of the volume can be filled with a dielectric or magnetic material in order to shorten the cavity at the expenses of higher losses. By filling it with ferrites, one can change the frequency by changing the permeability of the ferrite with external fields. Of course lossy materials reduce the Q and make it possible to rapidly change the frequency.

1.6 Bunch, Buckets and Phase Stability

We always must make sure that a particle in an accelerator sees an accelerating voltage at the gap, so the RF frequency f_{RF} must always be an integer multiple (h) of the revolution frequency f_{rev} .

$$f_{RF} = hf_{rev} \quad (1.30)$$

where h is known as the harmonic number.

A synchronous particle will circulate forever on the design orbit, and it is synchronous with f_{RF} . All the other protons in the accelerator will oscillate in energy and in s around the synchronous particles under the influence of the RF system. This means that instead of being spread uniformly around the circumference of the accelerator the particles get "clumped" around the synchronous particle in a bunch.

For small energy deviations the particles follow a circular path and for larger energy deviations these circles get flattered into an ellipse.

To qualitatively explain the oscillations the particles perform in energy and time, we consider two particles: particle A, which is synchronous with the RF voltage and a second one, particle B, whose momentum is slightly higher than A's. In Fig. 1.8, particle A always passes through the cavity when there is no RF voltage (neither accelerating nor decelerating), assuming to neglect the radiation damping effect. Particle B, instead, arrives at the same time as A but with a higher energy, therefore on the second turn it arrives later than A and sees a decelerating RF voltage, which reduces its energy to exactly that of A. On the third turn it still arrives later than A as it has exactly the same energy/frequency, B is decelerated still more and now has a lower energy than A. On the fourth turn B now arrives at the same time as A, as its energy is lower and its revolution frequency is higher, so B sees no acceleration or deceleration and is still at a lower energy than A. On the fifth turn B now arrives before A and sees an accelerating voltage, which means it now has the same energy and revolution frequency as A again. In the sixth turn B still arrives before A and is accelerated again. Now B has a higher energy and a lower revolution frequency than A. At the last turn B arrives at the same time as A but with a higher energy. This is just the situation that we had at the beginning. These oscillations are called synchrotron oscillations. Fig. 1.9 shows the motion of the two particles in the longitudinal phase space. Stable phase space region is called a bucket while the boundary is the separatrix (see fig. 1.10) which separates stable and unstable oscillations. If a particle is injected at a point outside the separatrix it is lost. Bunches of particles occupy buckets; but not all buckets need be occupied. Batches (or bunch trains) are groupings of bunches formed in specific patterns, often from upstream accelerators.

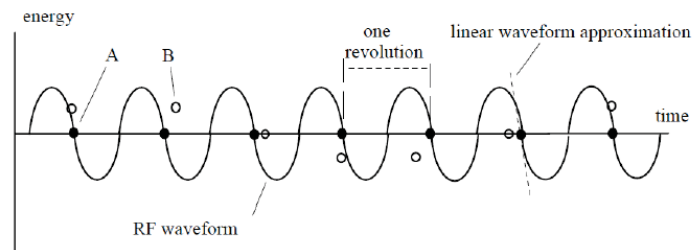


Figure 1.8. Energy variation of two circulating particles passing by the RF cavity [20].

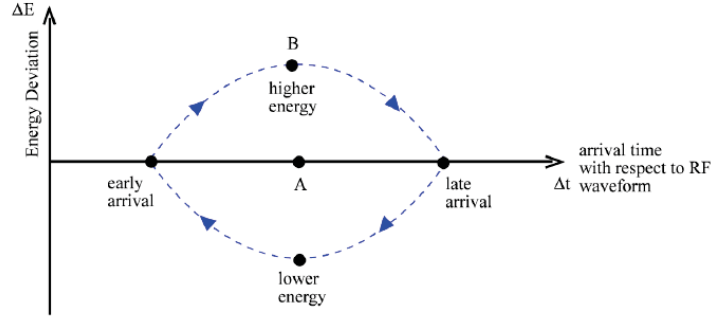


Figure 1.9. Relative motion of A and B in the longitudinal phase space [20]

The RF cavities are normally kept active also after the nominal energy is reached in order to provide a focussing in energy, since an ensemble of particles always has a momentum spread. Particles with an energy smaller than the nominal one ($p < p_0$) are accelerated by the cavities, while particles with a higher energy ($p > p_0$) are decelerated. Moreover, a circulating particle loses energy continuously through synchrotron radiation when it bends. The RF cavities serve then to replenish this energy loss on every turn which is negligible for protons at low energy. The RF system uses with good approximation a sinusoidal voltage $V(t) = V \sin(\varphi(t))$ and, for a particle with charge q , the energy gained at each passage across the cavity to compensate the energy loss turn by turn is:

$$\Delta E = qV \sin(\varphi(t)) \quad (1.31)$$

with V maximum amplitude of the RF accelerating potential and $\varphi(t)$ relative phase between the particle and the RF phase as function of time. The momentum offset is related to the energy deviation by:

$$\delta = \frac{\Delta p}{p} = \frac{1}{\beta^2} \frac{\Delta E}{E} \quad (1.32)$$

where $\beta = v/c$ is the relativistic beta. Similarly, the length of the orbit followed by the particle will also be modified according to:

$$\frac{\Delta L}{L} = \alpha_c \delta \quad (1.33)$$

where α_c is the momentum compaction factor, which is a fixed property of the lattice depending only on the bending radius of the particle orbit and the dispersion. It represents the difference in path length travelled by a particle at a given relative momentum deviation within one revolution of the reference particle. The phase focusing principle determines the longitudinal stability of the bunch by:

$$\frac{\Delta T}{T} = \left(\alpha_c - \frac{1}{\gamma^2}\right) \delta \quad (1.34)$$

with T revolution period of the proton in the ring and $E = mc^2$ is the relativistic gamma. According to the value of $\left(\alpha_c - \frac{1}{\gamma^2}\right)$, $\frac{\Delta T}{T}$ can be either positive and negative,

depending on the particle energy. The energy at which it changes sign is the transition energy:

$$\gamma_{tr} = \sqrt{\frac{1}{\alpha_c}} \quad (1.35)$$

The synchronous RF phase at which the synchronous particles passes the RF cavities on every turn, must be chosen depending on the particle relativistic γ , being below or above the transition. Two different regimes can, hence, be identified: $\gamma < \gamma_{tr}$ and $\gamma > \gamma_{tr}$.

In case $\gamma < \gamma_{tr}$, $0 < \varphi_s < \frac{\pi}{2}$ ensures the bunch stability, that corresponds to the particle which is on the positive slope of Eq. (1.31). More energetic protons will reach the RF earlier than the reference particle, they will lose energy and in the next turn they will get closer to the synchronous proton when they will pass by the cavities again. Less energetic particles, instead, will arrive late in the RF, receiving a larger kick by the system that allows them to approach the reference proton in the following turn. Similarly, above transition $\gamma > \gamma_{tr}$ a particle with a higher energy has a longer revolution time and arrives later, meaning that the decelerating voltage should be later in time. Hence, the stable motion occurs on the negative slope of Eq. (1.31), or for $\frac{\pi}{2} < \varphi_s < \pi$. Particles with small longitudinal amplitude, which occurs as long as they are close to the center of the bucket and not at the edges, even if the motion is still stable, perform synchrotron oscillations around the nominal particle (see Fig. 1.10).

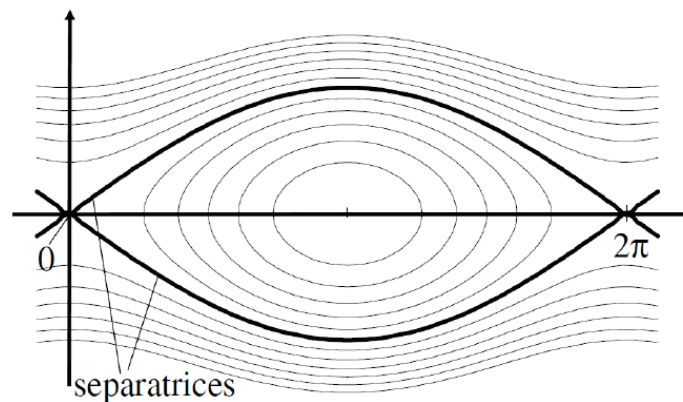


Figure 1.10. Motion of particle inside and outside the bucket limit [20]

Particle trajectories in phase space can be distinguished in two different types: closed orbits inside the RF-bucket in which particles perform stable motion and unstable motion outside for those particles having an energy large enough to go beyond the bucket limit. The specific trajectories in phase space which separate the stable region from the region where the motion is unstable leading the particle away from the synchronous phase and from the ideal momentum are called separatrices. If a proton injected in a storage ring has an energy corresponding to a point outside the separatrix, it will perform unbounded motion. The energy deviation that matches the separatrix determines the energy aperture of the ring. Now we take a particle

starting outside of the energy aperture, considering also the radiation damping effect (that means the particle is losing energy through emission of synchrotron radiation): its motion starts outside the stable region and it will stay outside forever. Moreover, the energy loss moves the particle further away from the nominal energy and, then, from the synchronous particle. When the accumulated energy deviation is large enough, the particle could hit the aperture of the machine and be lost.

In eq. (4.14), there was a term that in first approximation we didn't consider; now let's see what happens for particles with $\Delta p \neq 0$. These particles are focused differently in the quadrupoles and this lead to a shift of the Q value:

$$\Delta Q = -\frac{1}{4\pi} \oint \beta(s) K(s) ds \frac{\Delta p}{p_0} = \xi \frac{\Delta p}{p_0} \quad (1.36)$$

$$\xi = -\frac{1}{4\pi} \oint \beta(s) K(s) ds \quad (1.37)$$

ξ is called chromaticity of the machine. For a linear magnet lattice it is always negative. The main contribution to the chromaticity comes from quadrupoles which are strongly excited and where the β function is large. In big accelerators the chromaticity arising from the linear lattice is a large quantity, Then, the "tune" spread due to finite momentum band becomes so large that some part of the beam unavoidably hits dangerous resonance lines. For this reason, and in order to avoid the so-called "head-tail" instability [21], one has to compensate the chromaticity. This can be achieved with sextupoles [22]. The sextupoles magnets have to be placed at locations where the closed dispersion orbit $D(s)$ is nonzero.

1.7 Collective effects and Beam Instabilities

In order to control a beam of particle we apply external fields that focus the beam trasversely and accelerate it and focus it longitudinally. In addition to this externally applied fields, a particle within the beam feels a field due to the charge and the current of all the other particle of the beam. By collective effects we mean all those modifications to the beam behaviour which are due to this beam-induced force. In a very general sense, we can break collective effects down into three catagories: Beam-self, beam-beam, and beam-environment, as we can see in fig. 1.11

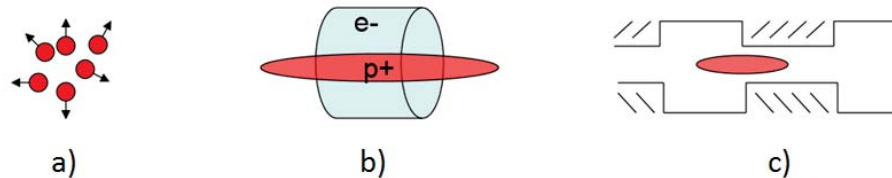


Figure 1.11. a) beam interacts with itself, b) beam interacts with localized electron cloud, c) beam interacts with machine

In picture a) we can see the case in which the beam interacts with itself: this is the case of space charge [23] and beam-beam effects [24]; in picture b) the beam interacts with localized electron cloud (e-p instability) and in picture c) it interacts with the machine, for example the vacuum chamber, in this case we will have so called impedances-related instabilities (as described in chapter 3). Collective effects and instabilities caused by collective effects is an entire topic of its own. Here we only briefly review some of the more common effects as an example.

Space charge is the simplest and most fundamental of collective effects whose impact generally is proportional to the beam intensity. The charge and current of the beam create self-fields and image fields which alter its dynamic behaviour and influence the single particle motion as well as coherent oscillations of the beam as a whole. If we consider a beam of cylindrical cross section as the one in fig. 1.12, a proton located at (r, Φ) experiences only the electrostatic fields from its neighbours:

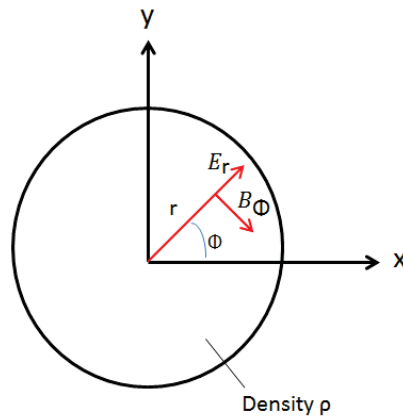


Figure 1.12. Cylindrical cross section of a beam

$$E_r = \frac{\rho}{2\epsilon_0} r \quad (1.38)$$

where ρ is the radius of the accelerator and ϵ_0 is the electric permeability. Due to symmetry, the electric field has just a radial component while the magnetic field lines are just circles around the cylinder:

$$B_\Phi = \frac{\rho}{2\epsilon_0} \frac{v}{c^2} r \quad (1.39)$$

We can define the defocusing term acting all around the circumference:

$$k = -\frac{rN}{\beta^2 \gamma^3 RS} \quad (1.40)$$

where N is the number of circulating protons, R is the radius of the machine and S is the beam cross-section, γ is the charge density [Cb/m^3] and $v = \beta c$ the velocity. The direct space charge leads to defocusing in either planes, and therefore one would expect that particles in a high-intensity beam will experience a lowering

of their betatron tunes Q by ΔQ . If we consider an unbunched beam, circular cross section everywhere in the accelerator and constant charge density, the Hill's equation $x'' + k(s)x = 0$ to a synchrotron lattice will yield to an unperturbed horizontal Q_{x0} while the expression $x'' + x(\frac{1}{\rho^2(s)} - k(s))x = 0$ introduces a space-charge defocusing ΔQ_x . In general we have for the direct space-charge tune shift:

$$\Delta Q_{x,y} = -\frac{r_0 N}{2\pi E_{x,y} \beta^2 \gamma^3} \quad (1.41)$$

where $E_{x,y}$ is the transverse emittance in either plane containing all of the particles, β is a periodic function given by focusing properties of the lattice and γ is the relativistic one.

An “electron-Proton” instability can be generated when the proton beam interacts with ambient electrons in the vacuum chamber (fig. 1.13).

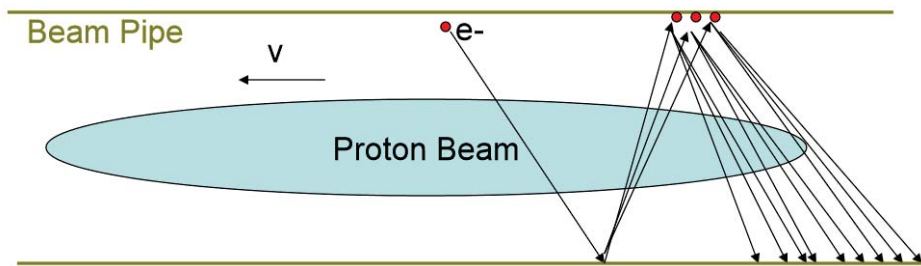


Figure 1.13. Proton beam moving in a beam pipe

Consider that an electron enters in the pipe and it is accelerated through beam potential, it strikes the wall on the opposite side and ejects more electrons. These electrons are accelerated through the beam and strike the opposite side wall, ejecting more electrons. If electrons live until the beam returns on the next pass, the “electron cloud” grows until it causes an instability in the proton beam.

Then we have the impedances-related instabilities. Since particles travel in the accelerator environment, with beam pipes and magnets, etc, they induce fields in the accelerator structures. These fields can act back on a trailing particle. Wakefields are generated in a smooth pipe of constant radius if it has finite resistance: the resistive wall impedance. Wakefields are also generated in a conducting pipe near the intersection of a geometry change. This kind of instability will be treated in detail in chapter 3 since is the main object of this thesis work.

Chapter 2

The CERN Proton Synchrotron

The Proton Synchrotron (PS) is a key component in CERN's accelerator complex, where it usually accelerates either protons delivered by the PS Booster or heavy ions from the Low Energy Ion Ring (LEIR [25]). In the course of its history it has juggled many different kinds of particles, feeding them directly to experiments or to more powerful accelerators and the first strong focusing synchrotron to be put in operation.

The PS first accelerated protons on 24 November 1959, becoming for a brief period the world's highest energy particle accelerator. It was initially CERN's flagship accelerator, but when the laboratory built new accelerators in the 1970s, the PS's principal role became to supply particles to the new machines. Over the years, it has undergone many modifications and the intensity of its proton beam has increased a thousandfold.

With a circumference of 628 metres, the PS has 277 conventional (room-temperature) electromagnets, including 100 dipoles to bend the beams round the ring. The accelerator operates at energy up to 25 GeV. In addition to protons, it has accelerated alpha particles (helium nuclei), oxygen and sulphur nuclei, electrons, positrons and antiprotons [26].

Today the PS complex (fig. 2.1) can accelerate all stable and electrically charged particles (electrons, protons), their antiparticles (antiprotons), and different kind of heavy ions (oxygen, lead). Proton beams from the PS complex are also used for physics experiments (ISOLDE, East Hall) or for the production of antiprotons (Antiproton Decelerator). The final design of the CERN PS was adopted in 1954; the first beam accelerated up to 24 GeV happened in 1959 [28]. At that time, the linear accelerator LINAC1 was the injector of PS with 50 MeV proton beams until the LINAC2 and the PSBooster took over in 1978. Today the PS accelerator complex is composed by the LINAC2 and LINAC3, PSBooster, LEIR (Low Energy Ions Ring), the Antiproton Decelerator (AD) and the PS.

The PS main magnet system consists of a ring-shaped structure 200 m in diameter [29]. This structure comprises 100 combined-function magnet units (MU) each composed of a focusing (F) half-unit and a defocusing (D) half-unit. A reference unit (MU 101) is located outside the tunnel in a dedicated air-conditioned room.

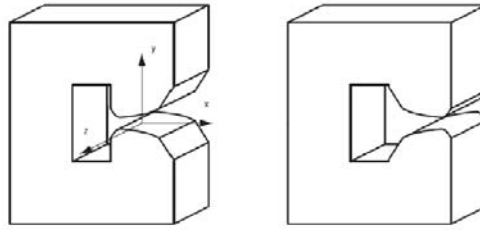


Figure 2.2. Open and closed single block of the main magnet units

2.1 Beams in the CERN PS

A typical magnetic cycle duration of the PS is a multiple of 1.2 s, defined as a basic period. During this time, the beam is injected, accelerated, extracted and the time left is dedicated to the magnetic field decreasing. Since the end of the 90's, the injection kinetic energy of the PS is 1.4 GeV for the proton beams. Fig. 2.3 shows a typical cycle where the protons are kept at constant magnetic field at least 30 ms on a flat bottom plateau in such a way the beam reaches an equilibrium state before acceleration in the transverse and longitudinal planes, in case of injection errors. Indeed the beam can experiment a trajectory transient if injected at the wrong position in the phase space (x, x') and (y, y') , resulting in transverse emittance blow up. The beam is then accelerated with a magnetic field rate dB/dt of 21 Gauss/ms or a momentum rate of 46 GeV/c/s. Finally the beam is extracted toward the SPS or a PS experiment. In fig. 2.3 the extraction momentum is 20 GeV/c and the beam is sent to a neutron production target (nTOF).

The Proton Synchrotron is used to accelerate different types of particle over its more than 50 years of operation: proton, electron/positrons, ions, antiprotons and even deuterons and α^- in the 80's. Currently only protons and ions are used in operation for the LHC and other experiments such as:

- nToF (Neutron Time of Flight) is a PS dedicated experiment [30];
- AD is a ring decelerating antiprotons which are produced by 26 GeV/c protons hitting a target [31] ;
- the experiments in the East Area of the PS such as an irradiation zone;
- beams are provided to the SPS for fixed target experiments, like CNGS in the past which aimed to produce neutrinos observed in the OPERA detector in Italy [32].

Table II shows the beam parameters for the nominal LHC beam. The next paragraph will focus on the PS as LHC injector and how the LHC beams are produced [33].

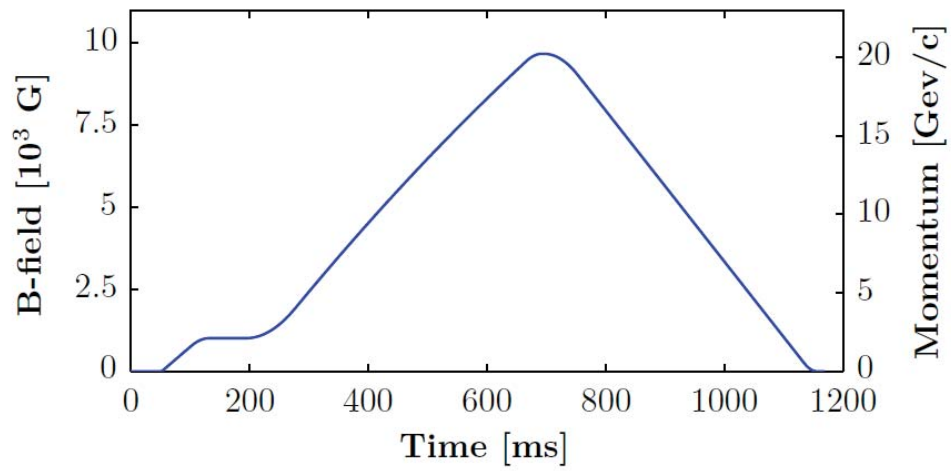


Figure 2.3. Example of magnetic field cycle for the ToF beam [34]

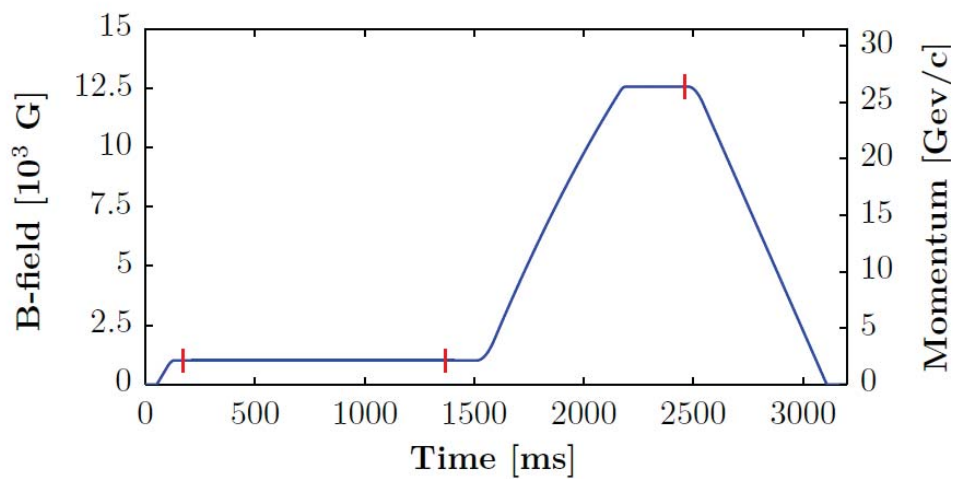


Figure 2.4. Example of magnetic field cycle for the nominal LHC 25 ns beam [34]

Table II. Beam parameters of the LHC 25ns, TOF and AD beams

Beam	TOF	AD	LHC 25ns
Total Intensity [10^{10}] p	850	1600	940
Bunches	1	4	12 to 72
Transverse emittance ($\varepsilon_{x,y}^*(1\sigma)$)	12.5-10.4	11.5-6.4	3 \ 3
Longitudinal emittance ($\varepsilon_l(2\sigma)$)	2.3	1.8	0.35 (4σ) at extraction
Bunch length at PS extraction [ns]	50	25	~ 4

2.2 The PS as LHC Injector

This section provides a short description of the production of LHC multi-bunch beams in the PS, meant for LHC physics experiments. According to the production scheme, the LHC-type beams transverse emittances should be defined in the PS-Booster, whereas the longitudinal structure should be the result of a complicated series of RF gymnastics done in the PS. The beam should be cleaned by eventual tails in the SPS and eventually, the longitudinal and/or the transverse emittances might be increased by controlled blow-ups [28].

Four different LHC multi-bunch beams with the parameters of Table III are prepared in the PS. The differences come from the bunch spacing and the intensity per bunch at the extraction of the PS meant for different purposes.

Table III. Parameters of the LHC beams produced in the PS at extraction

	N° of bunches	Long. emittance [eVs]	Intensity per bunch
LHC25	12 to 72	0.35	up to 1.3e11 ppb
LHC50	12 to 36	0.35	up to 1.9e11 ppb
LHC75	8 to 24	0.35	up to 1.3e11 ppb
LHC150	4 to 12	0.35	up to 1.3e11 ppb

All LHC beams are produced using harmonic one in the PSB. Nevertheless, up to 4 bunches can be sent per batch to the Proton Synchrotron (PS) as the PSB consists of 4 superimposed rings. Until now, the 25, 50 and 75 ns LHC physics beams were produced in a double-batch transfer from PSB to PS using 4 + 2 rings. To prepare the LHC filling, it is also possible to request only 1 PSB ring for these beams resulting in 12, 6 or 4 bunches, respectively. All the other beams use single-batch transfer to the PS with one PSB ring only (except for the individual physics beam with 1 or 4 PSB rings) [35].

The 25 ns LHC physics beam is referred to as ‘nominal’ LHC beam. It is made of 6 PSB bunches injected in two consecutive cycles into the PS, where it undergoes a triple and then, after acceleration to 26 GeV/c, two double splittings for the resulting 72 bunches injected into the SPS. Combinations of up to four PS batches can fill the SPS and later the LHC for the baseline 25 ns bunch filling scheme. To achieve the nominal LHC intensity while respecting the LHC normalised transverse rms emittance limit of 3.5 μm , bunches of 16.2×10^{11} protons with normalised transverse rms emittances of 2.5 μm have to be produced in the PSB.

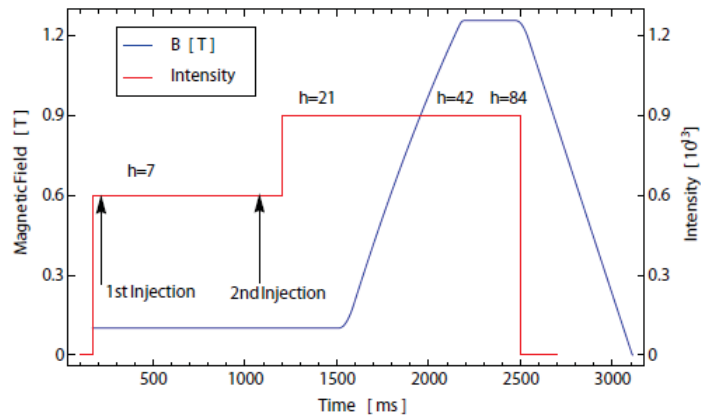


Figure 2.5. Production of the LHC 25 ns beam in the PS with the double batch injection on the 1.2 s long flat bottom plateau. The blue curve is the magnetic field as a function of time, the red is the beam intensity in number of protons and as a function of the harmonic number changed by the successive RF gymnastics.

The 50 ns LHC physics beam emerged as the first LHC beams to be required. The increased bunch spacing allows tailoring the luminosities to the needs of the four main experiments. The 75 ns beam variant was proposed for early LHC operation to leave out 2 bunches by tripling the bunch separation at PS extraction from 25 to 75 ns. Two double splittings in the PS led to 24 bunches at PS extraction.

In the next section we will see in details how the RF gymnastics are performed to produce the required bunch spacing.

2.3 Alternative schemes for 25/50 ns beam production

Beside the classical production scheme of the LHC-type beam, based on triple splitting at injection energy plus two double splitting on the extraction flat top and described in [28], another one was proposed to increase the brightness. It is the BCMS (Batch Compression Merging and Splittings), and consists in the injection of eight bunches on the 9th harmonic, batch compression from $h=9,10,\dots,14$, bunch merging between $h=7$ and $h=14$ (from 8 to 4 bunches) followed by a triple splitting (see figure 2.6) all done at low energy. These evolved RF gymnastics are performed at an intermediate kinetic energy ($E_k = 2.5 \text{ GeV}$) to avoid transverse emittance blow up due to space charge and to relax the requirements on the longitudinal emittance at injection. The resulting 12 bunches are accelerated to the extraction flat top where two bunch splittings occur to obtain the final 25 ns bunch spacing. The advantage with respect to the traditional scheme results from the smaller splitting factor of the PSB bunches (6 instead of 12). This scheme will be used for the production of the LHC physics beam during the 2015 run.

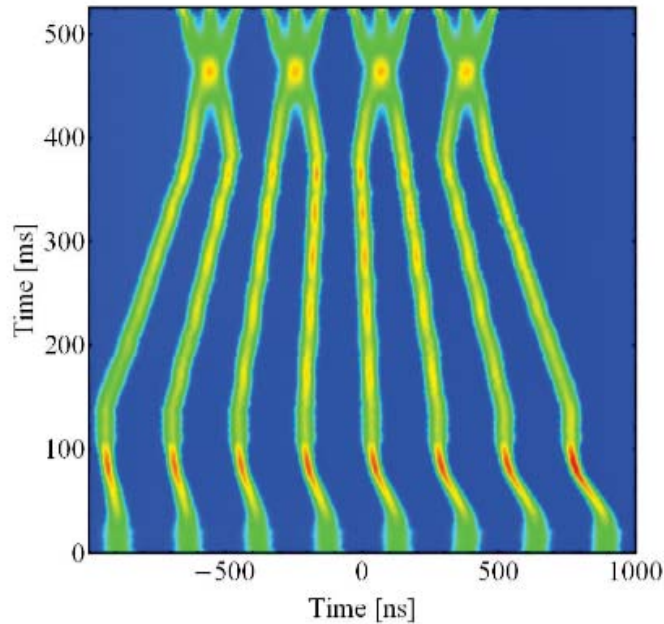


Figure 2.6. RF gymnastic for the production of the BCMS scheme at intermediate energy. The batch compression is followed by a bunch merging and a triple splitting [27]

2.4 The LHC Injectors Upgrade project

Luminosity (L) is one of the most important parameters of a collider like the LHC. It's a measurement of the number of collisions that can be produced in a detector per cm^2 and per second. The bigger is the value of L , the bigger is the number of collisions. To calculate the number of collision we need also to consider the cross section ; for a given physics process, like unelastic or elastic proton-proton collision. The instantaneous luminosity in the LHC (L_{LHC}) can be expressed as:

$$L_{LHC} = \left(\frac{\gamma}{4\pi} \frac{1}{\beta^*} f_{rev} F \right) \cdot \left(n_b \frac{N_b^2}{\varepsilon_n} \right) \quad (2.1)$$

where γ is the usual relativistic factor, β^* the betatron function at the interaction point, f_{rev} the beam revolution frequency, F a form factor depending upon the geometry of the bunch crossing, n_b the number of bunches per ring, N_b the number of protons per bunch and ε_n the normalised transverse emittance of the beam.

Eq. (2.1) shows that, independently of the modifications in the LHC, the instantaneous luminosity directly depends upon the characteristics of the injected beam. Maximizing the integrated luminosity requires the highest possible circulating current in the collider (proportional to $N_b n_b$) and hence from the injectors, with beam brightness.

2.4.1 Main principles of the upgrade

The parameters demanded by the HL-LHC will not be reached without a major upgrade of the LHC injector chain. The injectors can account for an increase of luminosity by producing more intense beams within constant or even smaller transverse emittances and hence increasing the beam brightness proportional to N_b/ε_n .

One topic the LIU project investigates is an increase of the PS injection energy from 1.4 GeV to 2 GeV, decreasing the tune spread induced by space charge. This fact, together with a well chosen working point, enables to conserve transverse beam parameters along the injection flat bottom of 1.2 s long for the production of the 25 ns beam.

In all synchrotrons, the RF systems represent another obvious limitation because of their power capability (in the case of PSB and SPS), because of their impedance for the beam (PS and SPS) and for reliability reasons (PSB, PS and SPS). All RF systems will therefore be subject to major changes or extensions, some being even planned for replacement (PSB). Longitudinal beam stability is planned to be obtained with the combined effect of reduced impedances and a new feedback [36].

The maximum intensity N_b for bright bunches in the PS is limited by coupled-bunch (CB) instabilities after transition crossing. The CB stability limit versus N_b and ε_n is illustrated in fig. 2.7. The mode spectrum shows that the CB instabilities are most likely excited by the main 10 MHz accelerating cavities. Three different upgrade paths are thus under investigation: improved direct and 1-turn FBs around the cavities, a new global CB-FB, potentially with a dedicated kicker, and the possibility of delivering naturally more stable bunches to the SPS.

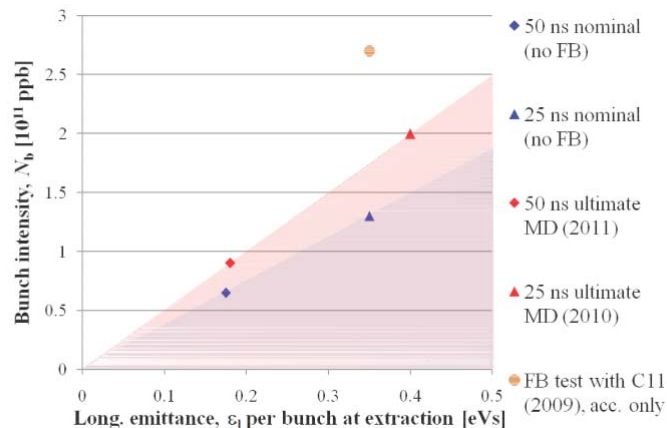


Figure 2.7. Longitudinal stability limits according to observations from 2009 to 2011 [37]

This thesis work will focus its attention on this kind of instability, trying to study and control the longitudinal coupled-bunch oscillations which constitute an important limitation for the CERN PS high intensity beams.

Chapter 3

Wakefield and Longitudinal Beam Instabilities

Modern accelerators have to provide charged particle beams with a high current to achieve high brightness [38], fact that presents a variety of challenges in the development of these accelerators. In storage ring or in low rep. rate pulsed machines, one of the most important factors limiting the maximum attainable beam current are beam instabilities, as presented in Chapter 2.

Charged particles in a synchrotrons are accelerated, guided and confined by external e.m. fields and the motion of a single charge is governed by the Lorentz force (eq. (1.1)). Acceleration is usually provided by the electric field of RF cavities and magnetic fields are produced in:

- the bending magnets for guiding the charges on the reference trajectory (orbit)
- the quadrupoles for transverse confinement
- the sextupoles for chromaticity correction.

However there is another source of e.m. fields, the beam itself, circulating inside the pipe. These fields depend on the total current, the geometry of the beam pipe and the surrounding materials and they are responsible of the so called 'beam instabilities'.

3.1 Basic mechanism driving an instability

Assume a bunched beam circulating in a synchrotron. The bunch, corresponding to a beam current I_B , will induce electromagnetic fields in the beam pipe and give rise to image or wall currents $-I_W$ of the same magnitude but opposite sign to the beam current [39], since the beam pipe itself is very often a conductor [40]. In turn, these currents generate an electromagnetic field that acts back on the beam.

The vacuum chamber has a finite conductivity and, moreover, changes its shape, cross-section, etc. along the beam path, and therefore presents an impedance to this wall current. The impedance $Z = Z_R + iZ_i$ can be resistive (real), capacitive or

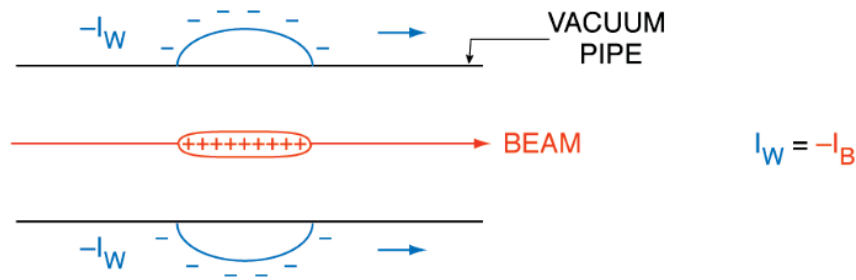


Figure 3.1. Image or wall current induced by a circulating bunch

inductive (imaginary). Thus the wall current induces a voltage $V \sim I_W Z$ which gives rise to a longitudinal electric field, which may act back (accelerating or decelerating) on the bunch. While Z depends on the geometry and material of the vacuum enclosure and on the exciting frequency, V is proportional to the wall current and thus the beam current: instabilities are intensity dependent, and in general stronger at higher beam currents.

Instabilities are investigated with the following scheme:

- start with a nominal, unperturbed particle distribution (i.e. longitudinal position, energy, density, etc.);
- apply a small perturbation which has a simple form – called ‘mode’ – and determine forces acting back on the beam;
- calculate how the pattern would change under the forces. If it disappears, the beam is stable; if it is self-sustaining or even increases, the beam is unstable.

3.2 Wakefield and potentials

As shown in Chapter 1, by collective effects we mean all those modifications to the beam behaviour which are due to beam-induced forces. We illustrated before the case of the beam interacting with itself (space charge and beam-beam effect) and the case of the beam interacting with a localized electron cloud (e-p instability). Now we are going in detail of the third kind of interaction, the one between the beam and the machine: the wake fields.

Wake fields depend on the particular charge distribution of the beam. It is therefore desirable to know what is the effect of a single charge (i.e. find the Green function) in order to reconstruct the fields produced by any charge distribution.

The electromagnetic fields created by a point charge act back on the charge itself and on any other charge of the beam. We therefore focus our attention on the source charge q_0 , and on a test-charge, assuming that both are moving with the same constant velocity $\nu = \beta c$ on trajectories parallel to the axis.

Let \vec{E} and \vec{B} be the fields generated by q_0 inside a structure, $s_0 = \nu t, r_0$ be the position of the source charge, and $s = s_0 + z, r$ be the position of the test charge q

[41].

Since the velocity of both charges is along z , the Lorentz force has the following components:

$$F = q [E_z \hat{z} + (E_x - \nu B_y) \hat{x} + (E_y + \nu B_x) \hat{y}] \equiv F_{\parallel} + F_{\perp} \quad (3.1)$$

Thus, there can be two effects on the test charge: a longitudinal force which changes its energy, and a transverse force which deflects its trajectory. If we consider a device of length L , the energy gain is:

$$U = \int_0^L F_z ds \quad (3.2)$$

and the transverse deflecting kick is :

$$M = \int_0^L F_{\perp} ds \quad (3.3)$$

Note that the integration is performed over a given path of the trajectory. These quantities, normalized to the charges, are called wake potentials (Volt/Coulomb) and are both functions of the distance z :

$$\text{Longitudinal wake potential } [V/C] : w_{\parallel} = -\frac{U}{q_0 q} \quad (3.4)$$

$$\text{Transverse wake potential } [V/Cm] : w_{\perp} = \frac{1}{r_0} \frac{M}{q_0 q} \quad (3.5)$$

The minus sign in the longitudinal wake-potential means that the test charge loses energy when the wake is positive. Positive transverse wake means that the transverse force is defocusing.

3.3 Coupling Impedance

The wake fields are generally useful to study the beam dynamics in the time domain (generally instabilities in a LINAC). If we consider the equation of motion in the frequency domain (generally done to study instabilities in circular accelerators), we need the Fourier transforms of the wake fields. Since these quantities have Ohms units they are called coupling impedances. The longitudinal coupling impedances is defined as:

$$Z_{\parallel}(\omega; r, r_q) = \frac{1}{v} \int_{-\infty}^{+\infty} W_{\parallel}(s; r, r_q) e^{-i\omega \frac{s}{v}} ds \quad (3.6)$$

Similarly, the transverse coupling impedance can be defined as:

$$Z_{\perp}(\omega; r, r_q) = \frac{-i}{v} \int_{-\infty}^{+\infty} W_{\perp}(s; r, r_q) e^{-i\omega \frac{s}{v}} ds \quad (3.7)$$

The coupling impedances and wake functions are the description of the same physical phenomenon, the wake effect of a single charge (or a beam with zero duration) and they are used to convey the complementary information in the frequency

domain and time domain, respectively. Sources of coupling impedance can be any discontinuity of vacuum chamber walls and finite conductivity of the vacuum chamber (the resistive wall impedance) in the accelerators. Vacuum chamber discontinuities are necessary for example to accommodate a variety of accelerator components. Different vacuum chamber sections can contribute to wakefields of different ranges in space and time.

According to the effective range of a wakefield, there are two types of coupling impedance: broadband impedance and narrow-band impedance. For example, a typical coupling impedance of an RF cavity with adjacent beam pipes is shown in fig. 3.2. The impedance spectra of this system contain a number of peaks. The sharp peaks of the impedance spectra below the cut-off frequency of the beam pipe represent the fundamental mode and HOMs of the RF cavity [42].

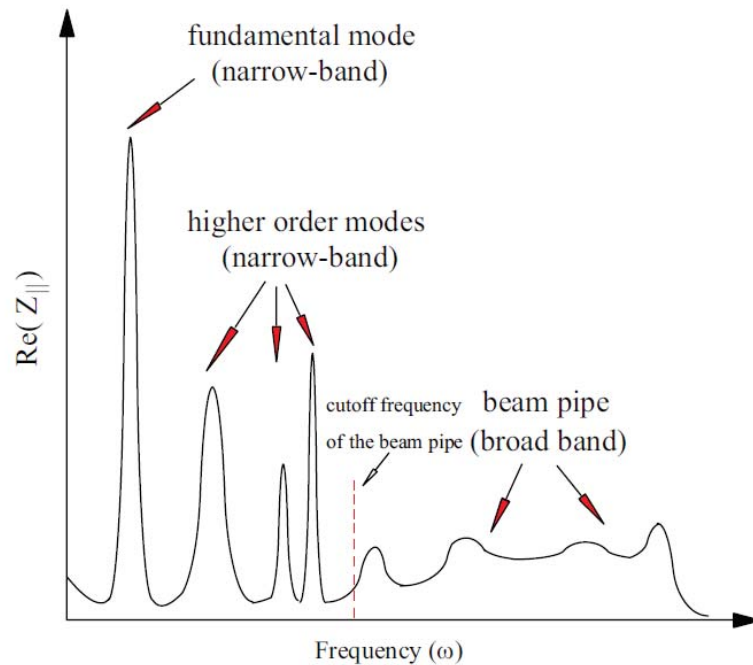


Figure 3.2. The real part of a longitudinal coupling impedance for an RF cavity with adjacent beam pipes [6]

A broadband impedance corresponds to a wakefield with a short decay time, therefore a short effective range (shorter than a few RF bucket lengths). Typically this type of wakefield can only be seen by particles in the same bunch and does not effect particles in the trailing bunches. Therefore, the broadband wakefield can excite instabilities in a single bunch.

In contrast to the broadband impedance, a narrow-band impedance corresponds to a long range wake effect, which impacts bunches behind the source bunch. The narrow-band wakefield induces coupled-bunch motions between electron bunches

circulating. This type of wakefield is usually excited inside an RF cavity and is dominated by high-Q resonant modes of the cavity itself, which appears as narrow peaks in fig. 3.2.

3.4 Longitudinal wake field of a resonant mode

The machine impedance is a function of the angular frequency ω , and typically it is maximal at the resonance frequencies of cavity-like objects, which thus represent the most critical machine components, prone to drive instabilities. Therefore a closer look at these objects is justified. The characteristic features of such objects are quite similar to a parallel RLC circuit (fig. 3.3) where we call I the beam current, R the shunt impedance, ω_r the resonance angular frequency, Q the quality factor (eq. (3.8) and (3.9)).

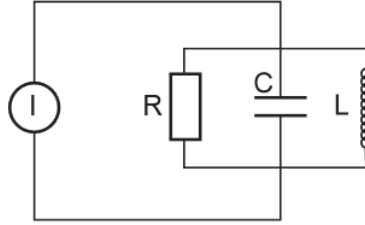


Figure 3.3. Parallel RLC circuit

$$\omega_r = \frac{1}{\sqrt{LC}} \quad (3.8)$$

$$Q = R\sqrt{\frac{C}{L}} = \frac{R}{\omega_r L} \quad (3.9)$$

where ω_r is the revolution frequency. The differential equation of the circuit is:

$$\ddot{V} + \frac{\omega_r}{Q}\dot{V} + \omega_r^2 V = \omega_r \frac{R}{Q} \dot{I} \quad (3.10)$$

with solution:

$$V(t) = V_0 e^{-\alpha t} \cos \left[\omega_r \sqrt{1 - 1/4Q^2} t + \phi \right] \quad (3.11)$$

This represents a damped oscillation with the damping rate $\alpha = 1/\tau = \omega_r/2Q$.

One interesting case is the longitudinal wake-potential of a resonant higher order mode (HOM) in an RF cavity [19]. When a charge crosses a resonant structure, it excites the fundamental and higher order modes. Each mode can be treated as an electric RLC circuit loaded by an impulsive current, as shown in Fig. 3.4

Just after the charge passage, the capacitor is charged with a voltage $V_0 = Cq_0$. The passage of the impulsive current charges only the capacitor, which changes its

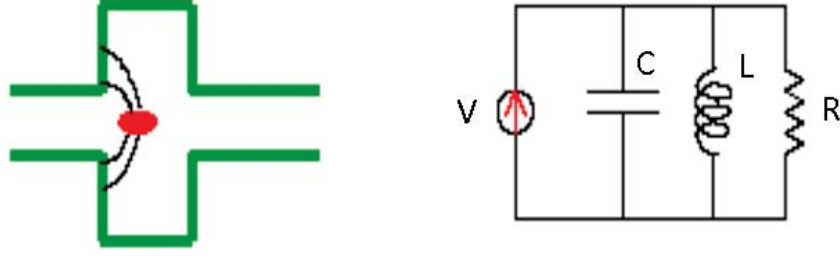


Figure 3.4. RF cavity and the equivalent RLC parallel circuit model driven by a current generator

potential by an amount $V_c(0)$. This potential will oscillate and decay producing a current flow in the resistor and inductance. For $t > 0$ the potential satisfies the following equation:

$$\ddot{V} + \frac{1}{RC}\dot{V} + \frac{1}{LC}V = \frac{1}{C}\dot{I} \quad (3.12)$$

Applying the boundary conditions ($V(t = 0^+) \equiv V_0$ and $\dot{V}(t = 0^+) = \frac{V_0}{RC}$) we are able to obtain the solution $V(t)$, and, more important, the expression of the wake potential:

$$w_{\parallel}(z) = \frac{-V(z)}{q_0} = w_0 e^{-\Gamma z/c} \left[\cos(\bar{\omega}z/c) - \frac{\Gamma}{\bar{\omega}} \sin(\bar{\omega}z/c) \right] \quad (3.13)$$

where $\bar{\omega}^2 = \omega_r^2 - \Gamma^2$ and $\Gamma = 1/2RC$.

Eq. (3.13) is the expression of the wakefield of a resonant HOM in a RF cavity.

In order to evaluate the impedance $Z(\omega)$ of the resonator, we excite the circuit with the current, ($I = I_0 e^{j\omega t}$ ($-\infty < \omega < \infty$)) and look for solutions of the form $V = V_0 e^{j\omega t}$. Note that the range of ω includes negative frequencies simply because it allows doing all calculations with the $e^{j\omega t}$ rather than the complicated trigonometric functions. By eq. (3.11), and considering that $Z(\omega) = V_0/I_0$ one then gets:

$$Z(\omega) = Z_r(\omega) + iZ_i(\omega) = R \frac{1 - iQ \frac{\omega^2 - \omega_r^2}{\omega\omega_r}}{1 + \left(Q \frac{\omega^2 - \omega_r^2}{\omega\omega_r} \right)^2} \quad (3.14)$$

$Z(\omega)$ is complex because in general V_0 is not in phase with excitation I_0 . The real and imaginary parts of the impedance of a resonator are shown in fig. 3.5.

The expression for the impedance of a narrow-band resonator (high Q cavity) can be simplified near the resonance frequency to:

$$Z(\omega) \approx R \frac{1 - i2Q \frac{\Delta\omega}{\omega_r}}{1 + \left(2Q \frac{\Delta\omega}{\omega_r} \right)^2} \quad (3.15)$$

A narrow-band impedance like this one features a high quality factor Q and thus a low damping rate: once the beam has induced a signal into this object, it will

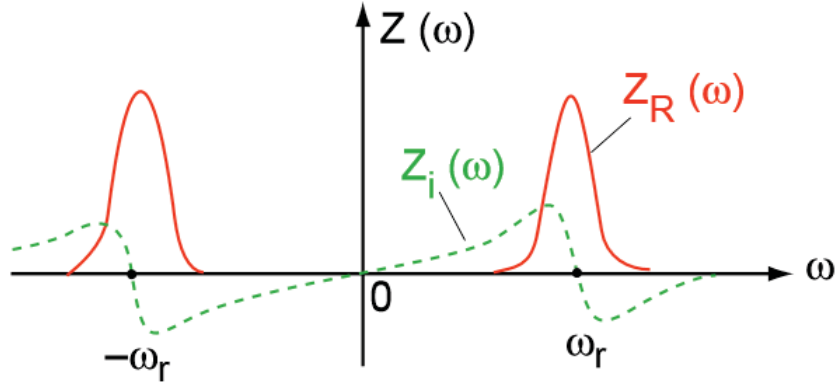


Figure 3.5. Real and imaginary parts of impedance Z of a resonator

oscillate during many machine turns, memorizing the fields induced during many passages of all bunches (multi-bunch effects). The converse is true for a broad-band cavity: Q is low, the damping rate is large, the induced fields collapse rapidly and are not memorized long enough to have repercussions on subsequent bunches, but only on the bunch itself (single-bunch effects).

3.5 Coupling impedances of a resonant mode

In this section we just want to give some remarks on the longitudinal impedance of a resonant mode that will be useful in future. The expression of the longitudinal impedance is:

$$Z_{\parallel}(\omega) = \frac{R_s}{1 + iQ\left(\frac{\omega}{\omega_r} - \frac{\omega_r}{\omega}\right)} \quad (3.16)$$

The parameters R_s, ω_r and Q , that can be evaluated by computer codes, can be related to the parameters RLC of the parallel circuit as explained before. The transverse impedance is:

$$Z_{\perp}(\omega) = \frac{c}{\omega} \frac{R_{s\perp}}{1 + iQ_r\left(\frac{\omega}{\omega_r} - \frac{\omega_r}{\omega}\right)} \quad (3.17)$$

This impedance can be also used as a simplified impedance model of a whole machine for the short range wake fields assuming $Q_r \sim 1$ (it is called Broad Band Impedance Model).

3.6 Instabilities in circular accelerators

To study of collective effects, it is convenient to distinguish between short range and long range wakefield, the former influencing essentially the single bunch (potential well distortion and deformation of the longitudinal distribution, longitudinal emittance growth, microwave instability) and the latter the multibunch dynamics (Robinson and coupled bunch instability) [43]. We just introduced the concepts of

longitudinal and trasverse wake field and the related coupling impedances necessary to deal with collective phenomena and now we are going to investigate the effect of wake field focusing on the longitudianl plane.

A bunch in a storage ring going through a cavity induces electromagnetic fields which oscillate and slowly decay away. In the next turn the same bunch might find some remnant field and will get influenced by it. The phase of the field seen in the next turn can be such that a small initial synchrotron oscillation of the bunch is increased. In each turn the oscillation gets amplified resulting to an exponentially growing instability. In many cases the fields created by the beam are small compared to the guide fields and their effects can be treated as a perturbation. In particular we are interested in the case of a charged particle passing into a cavity (fig. 3.6) that loses some of its energy in the form of electromagnetic field, which remain trapped reflecting back and forth at given frequencies, thus producing resonant modes. This fields are called long range wake fields and they influence the multi-bunch dynamics.

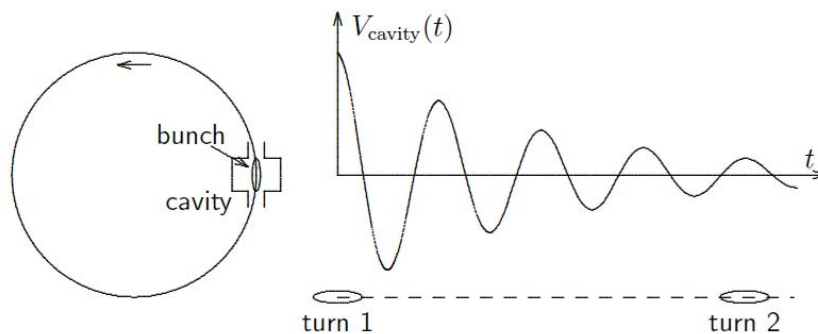


Figure 3.6. Charged particle passing into a cavity

3.7 Longitudinal coupled-bunch instabilities:qualitative analysis

A combination of many bunches and narrow-band resonant impedance enables the latter to memorize the fields for many bunch passages: the induced field due to the first bunch drives the motion of the second bunch, which in turns excites the third bunch, and so on until the first bunch appears back at the cavity for a second time, eventually leading to coupled-bunch instabilities.

Taking as an example a machine with $n_b = 4$ bunches performing synchrotron oscillations, all four bunches may oscillate in phase. However in addition to this in-phase oscillation mode (mode $\mu = 0$), three other 'modes' of coupling are possible with synchrotron oscillation phase shift between consecutive bunches of $\frac{\pi}{2}, \pi, \frac{3}{2}\pi$ ($\mu = 1, 2, 3$). These four modes are depicted in fig. 3.7 which shows the motion of the four bunches in the longitudinal phase plane. For a machine with n_b bunches, there are n_b modes, with bunch-to-bunch phase shift of $\frac{2\pi\mu}{n_b}$. All this modes are possible, but

may grow unstable only in the presence of a high impedance at the mode's frequency [52].

Now we are going to see under what conditions do the bunches become unstable.

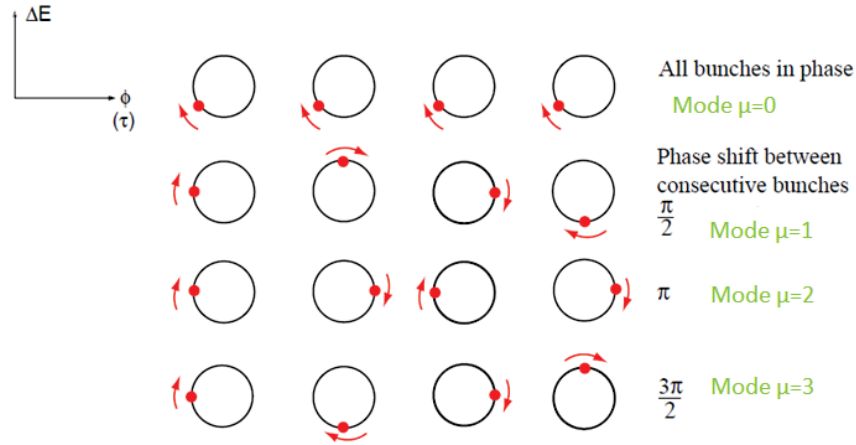


Figure 3.7. Motion of the four bunches in the longitudinal phase plane

Figure 3.8 shows the voltage induced into the resonator by each of the four bunches during one machine revolution time, and the motion of each bunch in the longitudinal phase plane: there is no motion in this case as there are no coherent synchrotron oscillations. The voltage induced by bunch 2 cancels with the one induced by bunch 4, and likewise the voltages generated by bunches 1 and 3 cancel. Hence there is no net induced voltage: the beam is stable.

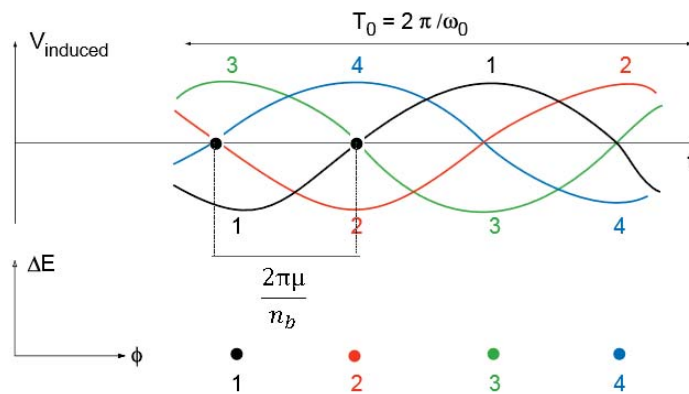


Figure 3.8. Voltages induced by each of four bunches in a cavity tuned at the revolution frequency. Bunches do not perform synchrotron oscillations in this case

In fig. 3.9 instead the four bunches do perform synchrotron oscillation with a bunch-to-bunch phase shift of $\pi/2$ (mode $\mu=1$). While the voltage of bunches 2 and 4 cancel as in Fig. 3.8, bunches 1 and 3 induce a voltage. This voltage in turn affects bunch 2 which gets accelerated while bunch 4 is decelerated, thus increasing

their synchrotron oscillation amplitude, and the bunches are unstable. It is easy to figure out that one-quarter of a synchrotron oscillation later (usually many machine turns), bunches 2 and 4 will drive 1 and 3 unstable.

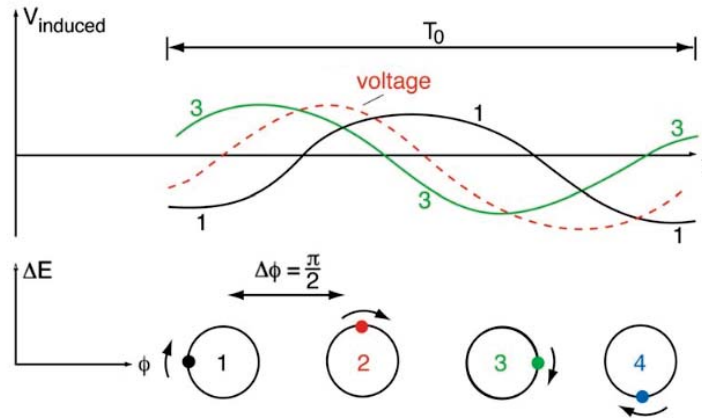


Figure 3.9. Voltages induced by two out of four bunches performing coupled synchrotron oscillations with a bunch-to-bunch phase shift of $\pi/2$

3.8 Basic principle of Longitudinal Multi-bunch Instabilities

To study the PS case, we analyze the effect of one bunch on the others ignoring the internal structure of the bunch, which is then considered as a rigid macroparticle with charge en_b and it can only oscillate of dipole motion. We start from the equation of motion of the bunch centre of mass, and by indicating with z_n and ε_n the variables referring to the n^{th} bunch ($n = 0, 1, \dots, n_b - 1$) and introducing the notation $\dot{z} = dz/dt$, we can write:

$$\dot{z}_n = -c\alpha_c\varepsilon_n \quad (3.18)$$

$$\dot{\varepsilon}_n = \frac{eV_{RF}(z_n - U_0)}{T_0E_0} - \frac{eV_w^n}{T_0E_0} - \frac{D}{T_0}\varepsilon_n \quad (3.19)$$

where z is the longitudinal displacement of a particle with respect to the synchronous one, ε is the variation energy with respect to the nominal particle's energy, c is the speed of light, T_0 the revolution period of a synchronous particle, E_0 the nominal energy, α_c the momentum compaction, $D = \frac{2U_0}{T_0}$ is the damping coefficient and V_w^n is the voltage seen by the n^{th} bunch and induced by the long range wake field. It is important to observe that, due to the macroparticle model, the wake function is that of a point charge, and we do not consider any distribution function.

If we suppose to have n_b bunches, having an equilibrium distance L_0/n_b one from another, combining eq. (3.18) and eq. (3.19) they give a second order differential equation [44]:

$$\ddot{z}_n + \frac{D}{T_0} \dot{z}_n + \omega_{sn}^2 z_n = \frac{c\alpha_c e}{T_0 E_0} \sum_{h=0}^{n_b-1} \sum_{q=-\infty}^{\infty} Q_h(dw/dz) \Big|_{(q-\frac{h}{n_b}+\frac{n}{n_b})L_0} z_h(t - qT_0 + \frac{h}{n_b}T_0 - \frac{n}{n_b}T_0) \quad (3.20)$$

Since usually $2\pi hz \ll L_0$, then we can linearly expand $V_{RF}(z)$ around z obtaining:

$$V_{RF}(z) = \hat{V} \cos(\phi_s) + \frac{2\pi h \hat{V} \sin(\phi_s)}{L_0} z + \dots \quad (3.21)$$

The synchrotron frequency ω_s , depending on the bunch n under consideration is:

$$\omega_{sn}^2 = \frac{c^2 \alpha_c e}{L_0 E_0} \left[\frac{2\pi h \hat{V} \sin(\phi_{sn})}{L_0} + \sum_{h=0}^{n_b-1} \sum_{q=-\infty}^{\infty} Q_h \frac{dw}{dz} \Big|_{(q-\frac{h}{n_b}+\frac{n}{n_b})L_0} \right] \quad (3.22)$$

and the synchronous phase Φ_{sn} has been chosen in order to have:

$$e \hat{V} \cos(\Phi_{sn}) = U_0 + e \sum_{h=0}^{n_b-1} \sum_{q=-\infty}^{\infty} Q_h w_{\parallel} \Big|_{(q-\frac{h}{n_b}+\frac{n}{n_b})L_0} \quad (3.23)$$

The equation (3.20) represents the dipole oscillation of the n^{th} bunch under the forcing effect of the long range wake field induced in previous turns by the particle.

We want to obtain under which conditions the motion is stable or unstable. Similarly to the perturbation theory of the Fokker-Planck equation, starting from the linearized Vlasov equation [45] and working in the frequency domain, we end up with the following eigenvalue system (for theoretical description see [45]) from eq (5.1):

$$(\Omega - m\omega_s) \sigma_m(q\omega_0 - \Omega) = -i \frac{2\pi m c e^2 N_b n_b}{T_0^2} \sum_{l=-\infty}^{\infty} i^{(m-l)} \sum_{p=-\infty}^{\infty} \frac{Z_{\parallel}[(n_b p - \mu)\omega_0 - \Omega]}{(n_b p - \mu)\omega_0 - \Omega} \sigma_l[(n_b p - \mu)\omega_0 - \Omega] F_m[(n_b p - \mu)\omega_0 - \Omega, q\omega_0 - \Omega] \quad (3.24)$$

where Ω is the coherent frequency of the azimuthal oscillation mode, m is the azimuthal mode of the perturbation of the stationary distribution Ψ_1 function, and μ the oscillation mode:

$$\Psi_1(\hat{z}, \phi; t) = e^{i\Omega t} \sum_{m=-\infty}^{\infty} R_m(\hat{z}) e^{-im\phi} \quad (3.25)$$

where R_m is the radial function of the azimuthal mode, and

$$\sigma_m(\omega) = \int_0^{\infty} R_m(\hat{z}) J_m\left(\frac{\omega}{c} \hat{z}\right) \hat{z} d\hat{z} \quad (3.26)$$

$$F_m(\omega, \omega') = \int_0^\infty J_m\left(\frac{\omega}{c}\hat{z}\right)J_m\left(\frac{\omega'}{c}\hat{z}\right)\frac{\delta\Psi_0(\hat{z})}{\delta\hat{z}}d\hat{z} \quad (3.27)$$

whit J_m the Bessel function of first kind and m^{th} order and R_m the corresponding radial function. The eigenvalue system is valid for equally spaced bunches (but theory can be developed also for uneven fills [46]). The corresponding eigenvectors can be demonstrated to be of the kind:

$$a_n^{(\mu)} = a_0^{(\mu)} \exp\left[i\frac{2\pi}{n_b}n\mu\right] \quad (3.28)$$

the physical meaning of which is that every oscillation mode has a phase shift from one bunch to another equal to:

$$\Delta\Phi = \frac{2\pi\mu}{n_b} \quad (3.29)$$

As an example, for the mode $\mu = 0$, all the bunches oscillate in phase (zero mode), while for $\mu = \frac{n_b}{2}$ there is a phase shift of π (pi mode).

To solve the problem we suppose there is no coupling between different azimuthal modes, only $l=m$ remains and each azimuthal mode can be studies independently from the others. Of particular interest is the case in which there is a single high quality resonator as source of impedance close to the frequency $(n_b p_1 - \mu_1)\omega_0$ (where p is an integer number, $-\infty < p < +\infty$ and ω_0 is the revolution frequency) eq. (3.24) becomes :

$$\Omega^{(\mu_1)} = m\omega_s - i\frac{2\pi m c e^2 N_b n_b}{T_0^2} \frac{Z_{||}[(n_b p_1 - \mu_1)\omega_0 - m\omega_s]}{(n_b p_1 - \mu_1)\omega_0 - m\omega_s} F_m[(n_b p_1 - \mu_1)\omega_0 - m\omega_s, (n_b p_1 - \mu_1)\omega_0 - m\omega_s] \quad (3.30)$$

The imaginary part of Ω gives the growth or damping rate depending on the sign:

$$-Im[\Omega] = \alpha = \frac{1}{\tau} = -\frac{m c \eta e^2 N_b n_b}{2L_0 E_0 T_0 \omega_s} [(n_b p_1 - \mu_1)\omega_0 - m\omega_s] Re[Z_{||}(n_b p_1 \omega_0 - \mu_1 \omega_0 - m\omega_s)] G_m(x) \quad (3.31)$$

with:

$$G_m(x) = \frac{2}{x^2} e^{-x^2} I_m(x^2) \quad (3.32)$$

the form factor which accounts the bunch lenght σ_z and:

$$x = \frac{[(n_b p_1 - \mu_1)\omega_0 - m\omega_s]\sigma_z}{c} \quad (3.33)$$

Above transition ($p_1 < 0$) for $\omega_r > h\omega_0$ we have instability (see Table IV). This effect is generally known as Robinson instability.

Table IV. Robinson Instability

	$\omega_r > h\omega_0$	$\omega_r < h\omega_0$
Above transition ($\eta > 0$ and $p_1 < 0$)	unstable	stable
Below transition ($\eta < 0$ and $p_1 < 0$)	stable	unstable

These results will be used in next chapters to study the particula case of CERN PS with the pourpose to benchmark the new simulation code introduced to study and analyze coupled-bunch instabilities with theory and even to check the consistence of measurements from past years on this machine.

Chapter 4

Simulation Code and Benchmarking

In the previous chapter, it was pointed out that the CERN PS is a very versatile machine. During the last years it became a key-accelerator with a central position in the LHC accelerator chain and with the largest number of beam destinations in the CERN complex, even if a significant part of its working time is dedicated to providing beams to LHC and particular attention is given to high intensity beams. As the intensity per bunch has increased over the years, limitations directly related to high intensity beams were discovered and constrained the number of particles that can be accelerated. Therefore, an effort has to be done to understand these limitations and several studies are under way to improve the beams required for the different experiments. Currently the main limitation in the PS are due to beam losses caused by aperture restrictions and large transverse emittances, space charge, and beam instabilities driven by wakefields [33].

The analytical study of the longitudinal dynamics of a beam interacting with resonant modes of an RF cavity is generally performed only in the case of small oscillations of equally spaced bunches around their synchronous phase. A complete analytical treatment of the dynamics in the presence of a bunch-by-bunch feedback system to control longitudinal coupled bunch instabilities has also been developed. The purpose of this chapter is to describe the main features of the LCBC (Longitudinal Coupled Bunch Simulation Code) a simulation code that executes a track of the longitudinal oscillations of the bunches. My study consists of an extensive campaign of simulations not only to fully benchmark the code with theory but even to find out if the 10 MHz cavity system used to accelerate the bunches in the PS, is really the most probable impedance source for this kind of instability [47].

4.1 Longitudinal Coupled Bunch simulation Code (LCBC)

The first version of the program was developed to track longitudinal oscillations of bunches for *DAΦNE* [48] (the e^+e^- Storage Ring at the Laboratori Nazionali di Frascati of Istituto Nazionale di Fisica Nucleare (LNF-INFN)) with the aim of including the main phenomena affecting the longitudinal beam dynamics: the

feedback, the effect of the HOMs and the synchrotron oscillations. The code has been modified to study the longitudinal dynamic in the CERN PS introducing a feedback system in frequency domain instead of the bunch-by-bunch one used for *DAΦNE*.

The code models each bunch as a single particle of given charge. Under this condition it is possible to simulate only the "rigid" oscillations that are the most dangerous for the beam stability.

In fig. 4.1 is shown a simplified flow chart of the code [9]. The input data have been divided into three files: one for machine and cavity parameters, another for all the bunches, and the last one for the feedback system. The synchrotron motion of all bunches is tracked first along the ring and the feedback system, and then through the cavity. This choice reduces the computation time. As output data, the code produces the phase oscillations of each bunch and the mode amplitude in radians of each oscillation mode (used in the evaluation of the instability growth rates).

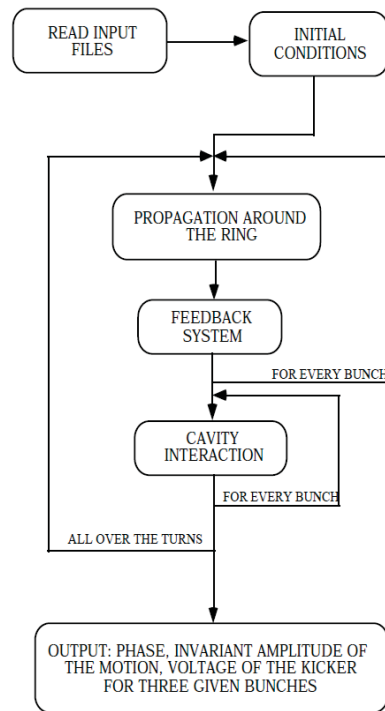


Figure 4.1. Flow chart of the code developed for *DAΦNE* with the previous FB system in time domain [9]

The core of the algorithm used for the PS case can be divided into three main parts:

- propagation around the ring: for each macroparticle n we use in place of the variable position z_n the phase $\Delta\varphi_n$ so the equations of motion are like:

$$(\Delta\varphi_n)_0 = (\Delta\varphi_n)_i + \frac{2\pi h\eta}{E_0}(\epsilon_n)_i \quad (4.1)$$

$$(\varepsilon_n)_0 = (\varepsilon_n)_i - U_0 \quad (4.2)$$

where:

$$\Delta\varphi_n = \varphi_{sn} - 2\pi h \frac{z_n}{L_0} \quad (4.3)$$

where L_0 is the circumference length covered by the synchronous particle; E_0 is the nominal energy of the synchronous particle at the output of RF cavity; ε is the energy deviation; α_c is the momentum compaction, U_0 is average value of the energy radiated during a revolution of the synchronous particle and with the index i an o indicating input and output from the vacuum chamber;

- feedback effect: the FB system will be described in detail later: its interaction with particles consist in an exchange of energy ΔE_{fb} while the phase stay constant;
- beam-cavity interaction: between the effects of the RF cavity, the ones which produce the multibunch instabilities are included, that is the one produced by long range wakefields. As explained in Chapter 2 each HOM is simulated as a parallel RLC circuits. When a charge q crosses the cavity, it perturbs the total voltage. The induced voltage of each mode depends on the shunt resistance R_s and the quality factor Q of that mode. We assume that the cavity-beam energy exchange occurs at a single point in the ring. In the RLC parallel circuit it is possible to follow the evolution of tension $v(t)$ with time. When a charge q goes through the cavity, it produces on each resonant mode an additional voltage ΔV :

$$\Delta V = -\frac{\omega_r R_s}{Q} q \quad (4.4)$$

where ω_r is the resonance angular frequency. In order to take into account the bunch length, assuming a Gaussian distribution, the shunt resistance is corrected by a factor [49]:

$$\exp(-\omega_r \sigma_m / c)^2 \quad (4.5)$$

where σ_m the RMS bunch duration.

For a detailed description of the code see [9].

4.2 Benchmarks

For comparing the growth rates given by the simulation code with the analytical ones, I have simulated the instability exciting only one mode of oscillation.

To do that, I have considered a single HOM with a resonant angular frequency equal to:

$$\omega_r = q\omega_0 + \omega_s \quad (4.6)$$

with $q = n_b p \pm \mu$ (see par. 3.8), $\omega_0 = \frac{2\pi c}{L_0}$ (c is the speed of light and L is the length of the machine) and ω_s given by (3.22). With all the bunches at the equilibrium phase, a small perturbation excites the selected mode of oscillation. I have then evaluated the growth rate with an exponential fit over the invariant amplitude of the motion. For simplicity, in this benchmark's simulation, the length of the beam (eq. (4.5)) is not taken into account.

I consider n_b equally spaced bunches performing coupled oscillations. They oscillate longitudinally within the RF-buckets and only the dipole-mode $m = 1$ is taken into account in eq. (3.8). In table V we can see the parameters used in this simulations.

Table V. Parameters used for benchmark simulations of the LCBC code.

Parameters	Value
Q	10^5
$R_s(\Omega)$	10^2
Beam energy (GeV)	13
Harmonic number	21
Number of bunches	21
RF voltage (kV)	165
Total beam intensity (ppp)	$38 \cdot 10^{11}$
Synchrotron frequency [kHz]	2.49218875

This is the same case explained in Chapter 3 in which there is a single high quality resonator as source of impedance. Due to Robinson instability, above transition energy, positive sidebands of the beam spectrum, evaluated at multiples of $\omega_0 + \omega_s$ are unstable, while the negative sidebands, evaluated at multiple of $\omega_0 - \omega_s$ are stable. So a mode in correspondence of the line $q = n_b p + \mu$ is unstable mode (fig. 4.2).

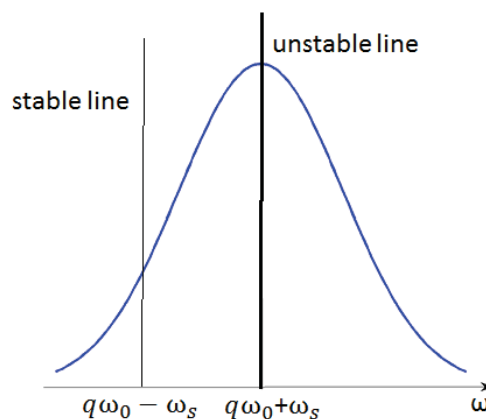


Figure 4.2. Real part of the shunt impedance with indication of the lines of stable and unstable modes

After selecting the unstable mode the rise time of instability has been evaluated by using eq. (3.31) and compared with the growth rate of the code's output.

Fig. 4.3 shows the result obtained with $n_b = 21$: starting from a situation of perfect equilibrium, $\mu = 19$ coherent mode of oscillation is excited.

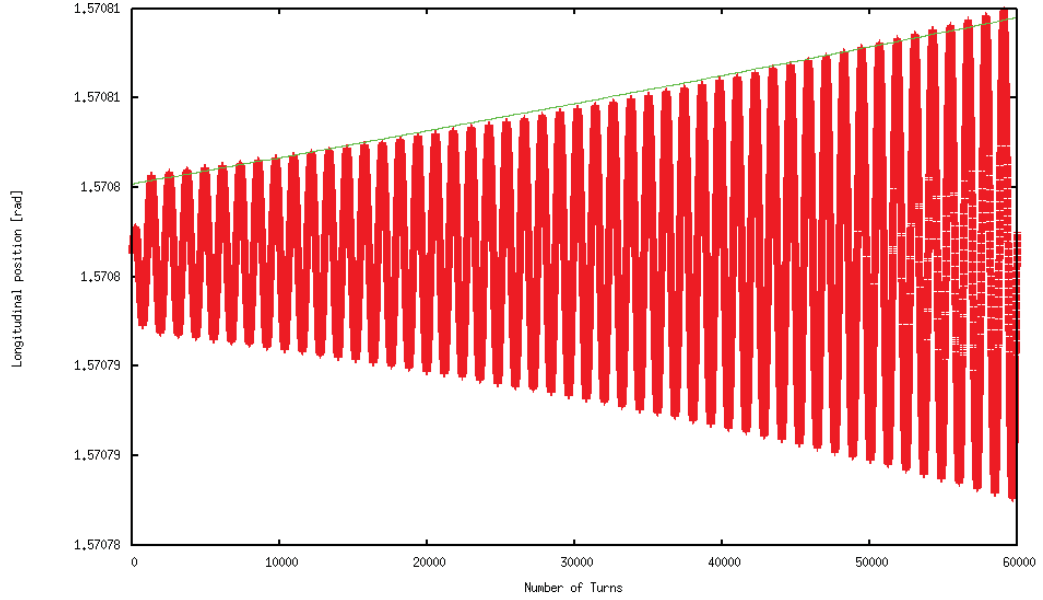


Figure 4.3. Growth rate mode $\mu = 19$ in function of the number of turns in the machine

The green line in fig. 4.3 is the exponential fit used to evaluate the growth rate and it is of the kind:

$$f(x) = A \cdot \exp(x \cdot \alpha) \quad (4.7)$$

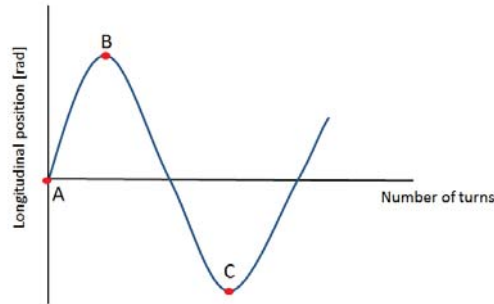


Figure 4.4. Fit

where the growth rate is obtained as:

$$\alpha = [\log\left(\frac{\Delta_1}{2}\right) - \log\left(\frac{\Delta_2}{2}\right)] / n^{\circ} \text{turns} = 7.67917 \quad (4.8)$$

wit $\Delta_{1,2} = B - C$ at turn 0 and 60000.

With the parameters of table V the growth rate is:

$$\alpha = \frac{1}{\tau} = -\frac{mc\eta e^2 N_b n_b}{2L_0 E_0 T_0 \omega_s} \omega_r \text{Re}[Z(\omega_r)] = 7.86674 \quad (4.9)$$

The sum of the squared differences or 'residuals' (SSR) between the input data points and the function values, evaluated at the same places, is $1.01542 \cdot 10^{-5}$

In table VI the rise time of instability obtained with eq. (3.31) is compared with the exponential fit of eq. (4.8): the comparison results satisfactory.

Table VI. Theoretical and simulated rise time of instability for mode $\mu = 19$ in harmonic number 21 with 21 bunches

Theoretical τ [ms]	126
Simulated τ [ms]	130

As a crosscheck we can verify that the selected mode is the right one by detecting from the output of the simulation code the phase displacement between two consecutive bunches, and using eq. (3.29):

$$\Delta\Phi = \omega_s \Delta n T_0 = 2\pi \frac{\mu}{n_b} \quad (4.10)$$

where Δn is the distance (in number of turns) between the bunches. From this formula we can easily extrapolate the mode number:

$$\mu = \frac{\omega_s \Delta n T_0 n_b}{2\pi} = 19 \quad (4.11)$$

which corresponds to the one excited in the simulations by the HOM.

In the next section I will focus the work on the new feedback system implemented in the code. Some simulations will be presented to have a complete understanding of it.

4.3 Review of Feedback System Theory

Coupled-bunch instabilities excited by the interaction of the particle beam with its surroundings can seriously limit the performance of circular particle accelerators. These instabilities can be cured by the use of active feedback systems based on sensors capable of detecting the unwanted beam motion and actuators that apply the feedback correction to the beam. They can even be controlled by reducing the magnitude and number of high-order modes, carefully controlling the resonant frequencies of the resonators to avoid coupling to the beam or by adding damping to the motion of each bunch. External feedback system does the latter.

A feedback system consists mainly of three parts (fig. 4.5): a detection system to measure beam oscillations and to provide the system with an error signal; a signal processing unit to derive a correction signal and a beam deflector to act with a kick on the beam. The signal processing unit can be accomplished in either the frequency (mode-by-mode feedback) or in the time domain (bunch-by-bunch feedback). The bandwidth required by the feedback system is determined by the minimum bunch

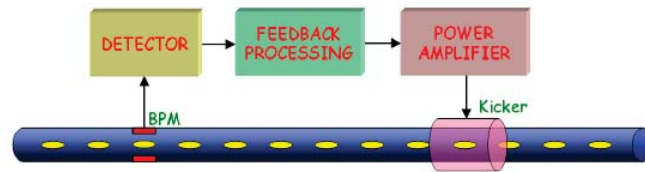


Figure 4.5. Diagram of a feedback system

spacing.

In a mode-by-mode feedback (frequency domain) each mode is identified with the help of a special narrow band filter centred around one of the revolution harmonics. Each mode is then processed individually leading to a feedback that consists of many narrow band systems running in parallel. A mode by mode feedback is the appropriate choice if only a few coupled bunch modes have to be damped. For example such a system has been in operation in the PS Booster for more than 20 years.

In a bunch-by-bunch feedback (time domain) each bunch is treated individually. Moreover, the feedback implementation can be analog or digital, depending on whether the signal is handled in the analogic domain or sampled and processed digitally. Despite the fact that most of the more recent feedbacks are digital bunch-by-bunch systems, analogic or mode-by-mode implementations are still in use in a number of accelerators [50].

A bunch-by-bunch feedback individually steers each bunch by applying small electromagnetics kick every time the bunch passes through the kicker. The result is a damped oscillation lasting several turns. There are as many processing channels as the number of bunches. Since the bunch oscillation is sinusoidal, the turn-by-turn position of the one bunch measured at a given location is a sampled sinusoid. In order to introduce damping, the force applied by the feedback must be proportional to the derivate of the bunch oscillation. Consequently, the kick signal applied by the actuator to each bunch can be generated by shifting by $\pi/2$ the signal of the position of the same bunch when it passes through the kicker.

4.3.1 Frequency domain FB: the PS choice

With a mode-by-mode feedback each coupled-bunch oscillation mode is detected separately with a pass-band tracking filter centred around the revolution harmonic corresponding to the mode number. Additionally, the spectral component at the revolution frequency is removed by a narrow-band notch, keeping only the synchrotron frequency side-bands. The filtered synchrotron frequency side-band signals are then de-phased, amplified and fed back to the beam via a longitudinal kicker. Coupled-bunch feedbacks in lepton machines normally detect all modes simultaneously by measuring the phase oscillations of each bunch in the time domain. In the PS the revolution frequency of the protons changes during acceleration, which makes the generation of correctly phased bunch-synchronous trigger difficult. Damping

mode-by-mode rather than bunch-by-bunch has the additional advantage that the modes are decoupled for equidistant identical bunches, which remains mostly valid even for unequal filling patterns. This type of feedback makes it easy to measure the interaction of each individual mode with the longitudinal coupling impedance and with the feedback system itself. The basic components of the FB system are a bank of parallel filters producing the correction kick signals, phase shifted by $\frac{\pi}{2}$, a broad-band power amplifier and a longitudinal broad-band kicker which operate at different synchrotron frequency side-bands than the detection. The maximum kick strength is determined by the energy gain needed to achieve the required damping rate and the maximum tolerable synchrotron phase error. The design of the kicker structure must be optimized in terms of shunt impedance and bandwidth in order to reduce the power requirement on the final stage, because broadband power is very expensive.

4.4 Overview of the feedback system in the LCBC code

The existing bunch-by-bunch FB system used for *DAΦNE* has been replaced in the code with a frequency domain one similar to the final implementation of the machine.

The feedback system in the LCBC code consists of three parts: a phase error detection subsystem, a signal processing subsystem and an energy correction part. We suppose to know the synchrotron frequency for each bunch b which oscillate as:

$$\phi_b = A_b \sin(\omega_s t + \sigma_b) + \phi_{s,b} \quad (4.12)$$

and the phase σ_b at each oscillation. By doing a sinusoidal fit with three parameters, we obtain $A_b, \sigma_b, \phi_{s,b}$, and so we get:

$$\phi_b - \phi_{s,b} = A_b \sin(\omega_s t + \sigma_b) \quad (4.13)$$

which must be equal to the sum of all the oscillation modes:

$$A_b \sin(\omega_s t + \sigma_b) = \sum_{\mu=0}^{n_b-1} A_\mu \sin\left(\omega_s t + \frac{2\pi}{n_b} \mu_b + \sigma_\mu\right) \quad (4.14)$$

If we now write the equation of all the bunches it is possible, from eq. (4.14) to obtain unknown quantities A_μ and σ_μ . If we suppose to damp only one mode of the kind:

$$A_\mu \sin\left(\omega_s t + \frac{2\pi}{n_b} \mu_b + \sigma_\mu\right) \quad (4.15)$$

the phase of the kick ΔV_{fb} must be:

$$\Delta V_{fb} = \frac{g}{\omega_s} \frac{d\phi_b}{dt} = \frac{g}{\omega_s} A_\mu \cos\left(\omega_s t + \frac{2\pi}{n_b} \mu_b + \sigma_\mu\right) \quad (4.16)$$

where g is the feedback's gain in $[\frac{V}{rad}]$.

Then the same kick, in amplitude, but with a difference phase, is applied to all the bunches.

To evaluate the damping time we start from the longitudinal equation of motion:

$$\dot{\phi}_b = \omega_{rf}\eta\varepsilon \quad (4.17)$$

$$\dot{\varepsilon} = \frac{eV_{rf}(\phi_b)}{T_0E_0} - \frac{e\Delta V_{fb}}{T_0E_0} \quad (4.18)$$

Considering that:

$$V_{rf}(\phi_b) = \hat{V}\cos\left(\frac{\pi}{2} + \phi_b\right) = -\hat{V}\sin\phi_b = -\hat{V}\phi_b \quad (4.19)$$

we can write the longitudinal dipole equation of motion of a bunch in presence of the feedback as:

$$\ddot{\phi}_b + \frac{\omega_s}{\hat{V}}g\dot{\phi}_b + \omega_s^2\phi_b = 0 \quad (4.20)$$

from which we get a feedback damping rate of:

$$\alpha_{fb} = \frac{1}{\tau} = \frac{1}{2} \frac{\omega_s}{\hat{V}}g = \frac{1}{2} \frac{\omega_{rf}\eta}{\omega_s T_0 (E_0/e)}g \quad (4.21)$$

Note that even if the bunches are not equally spaced, for a given mode, the phase difference between two consecutive bunches remains $2\pi\mu/n_b$.

4.4.1 Application of the feedback system to damp an unstable mode

When several HOMs are present in the cavity, it is difficult to calculate analytically the rise time of all the possible modes of oscillation. There could be compensation between different HOMs, or, at the opposite, their effects could sum up.

In this section I will show some simulation results based upon the PS system using the LCBC code to validate the implementation of the feedback in the code in presence of several HOMs.

I first excite mode $\mu = 19$ in harmonic number $h = 21$ with a full machine (21 bunches) and evaluate the rise time. In tableVII one can see the parameters used for the simulation.

Table VII. Parameters used to benchmark the FB system in the code (for beam parameters see table V)

Parameters	Value
Initial phase amplitude	0.005
Oscillation phase shift between bunches	5.68478
Shunt impedance	100
Quality factor	5×10^5

This simulations has been performed with a full machine, with equally-spaced bunches and it is possible to use the theory of Chapter 1. Let's look at the instability

of the first bunch.

In fig. 4.6 are reported both the mode amplitude and the longitudinal position of the bunch as a function of the number of turns.

I then proceed by evaluating the rise time of instability which will be used in eq. (4.21) to obtain the correct value of the gain of the FB. In this case I obtain from the exponential fit on the phase a value of 151 ms for the rise time.

The second step consists in checking if the evaluated gain is correct, so I switch on the feedback but do not excite the mode. If the gain g is correct, one should see that the same value of the rise time, with the opposite sign, will correspond to the damping rate.

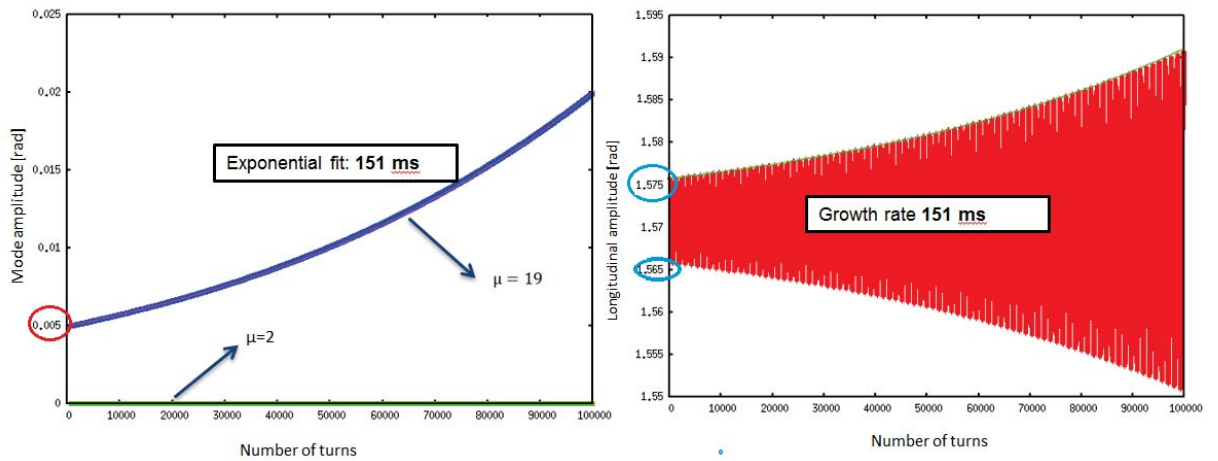


Figure 4.6. Longitudinal position (on the right) and amplitude (on the left) of one bunch with FB off and with excitation

In fig. 4.7 one can see that if I do not excite any instability, the feedback with the gain evaluated before works correctly and I get a damping rate equal to the growth rate in module.

Finally I switch on the FB and observe that there is quite an equilibrium between the instability and the damping effect (fig. 4.8). In fact we can see, in fig. 4.8 that the regime amplitude values 1.56 and 1.576 correspond to the starting ones in fig. 4.7 as eyelight in pictures.

The LCBC code has then been proved to be able to correctly simulate the frequency domain FB system.

In the next chapter we will go through the validation of the code by comparing simulations results with measurements and the analysis of the 10 MHz cavities impedance system which is considered to be the main cause of instability in CERN PS.

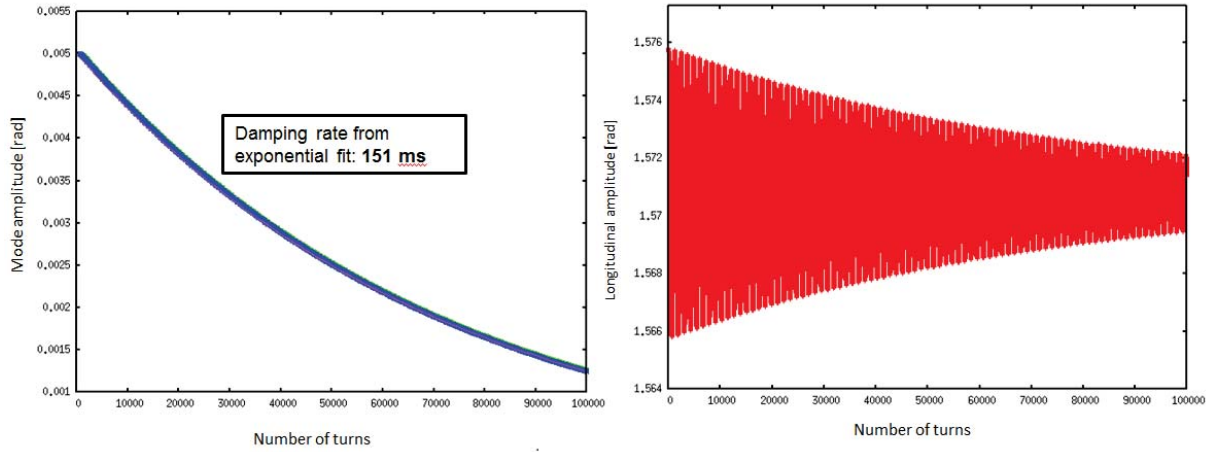


Figure 4.7. Longitudinal position (on the right) and amplitude (on the left) of one bunch with FB on and without excitation of an HOM

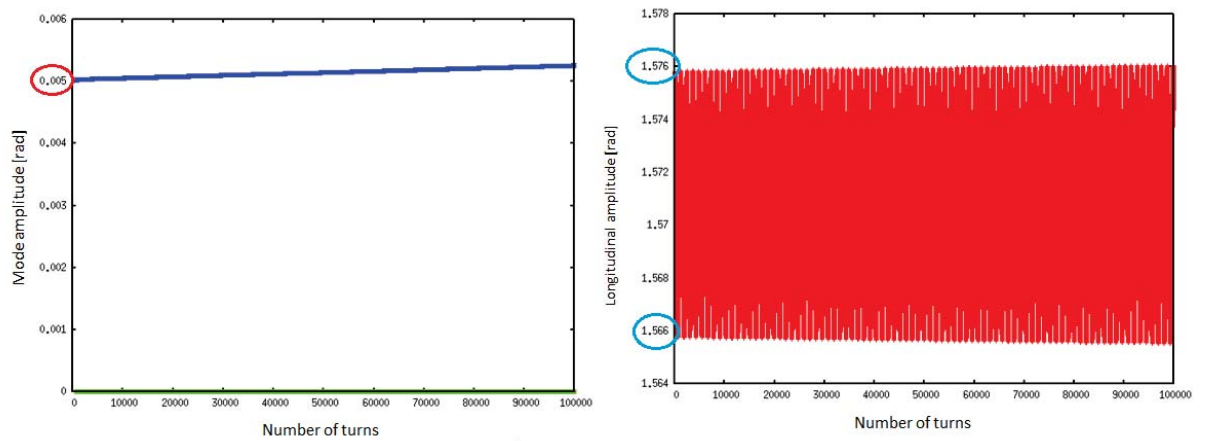


Figure 4.8. Longitudinal position (on the right) and amplitude (on the left) of one bunch with FB on and the mode excited

Chapter 5

Coupled bunch studies for the CERN Proton Synchrotron

Longitudinal coupled-bunch instabilities are observed in the CERN PS during acceleration and on the flat-top. Up to present intensities oscillation modes are damped using a feedback system limited to the first two dominant oscillation modes, but it will become insufficient for the beam parameters planned within the upgrade. During the first long shutdown (LS1) in 2013-2014, a new feedback will be installed, covering all modes [51].

In the beam spectrum measured with a wall-current monitor, coupled-bunch oscillations manifest themselves as synchrotron frequency sidebands f_s , of the revolution frequency harmonics f_{rev} . For LHC-type beams in the PS with bunch spacings below 100 ns, only dipole modes are important. Each mode occurs twice in the spectrum, as upper and lower sidebands. As exemplar an energy of about 14 GeV (during acceleration) and an RF voltage of $V_{RF} \cong 165$ kV, the sidebands are separated by only 400 Hz from the revolution frequency harmonics [52].

To study experimentally CB oscillations, the low-level part of the existing FB has been connected to a spare 10 MHz accelerating cavity. As powerful longitudinal kicker (up to 20 kV), it is tunable from 2.8 MHz to 10 MHz, covering $h = [6..21]$ [52]. To excite CB oscillations using the FB, a perturbation was injected to generate a sideband at $nf_0 \pm f_s$ (with f_0 the revolution frequency). Following the excitation of well-defined oscillation mode, damping time and corresponding longitudinal kick strengths is analysed. The simulation program LCBC has been used to study the beam behaviour of the CB (coupled bunch) FB (feedback). Using this program I have started an extensive simulation program to benchmark the code with measurements and to predict the FB requirements for the increased intensities of LIU using the parameters of the upgrade.

5.1 External Excitation

If we look at the coupled-bunch oscillations in time domain, as showed in Chapter 3, bunches have with different phase and amplitude. If we look in frequency domain,

as illustrated in fig. 5.1, for equally spaced bunches, each oscillation mode can be identified by the lines that occur in the bunch spectrum, namely:

$$\omega_p = (pn_b \pm \mu)\omega_0 \pm \omega_s \tag{5.1}$$

where ω_s is the synchrotron frequency, μ the mode number, ω_0 the revolution frequency, n_b the number of bunches and p is an integer number, $-\infty < p < +\infty$. So each mode μ is observable as an upper side-band or as a lower sideband depending on the sign of equation (5.1).

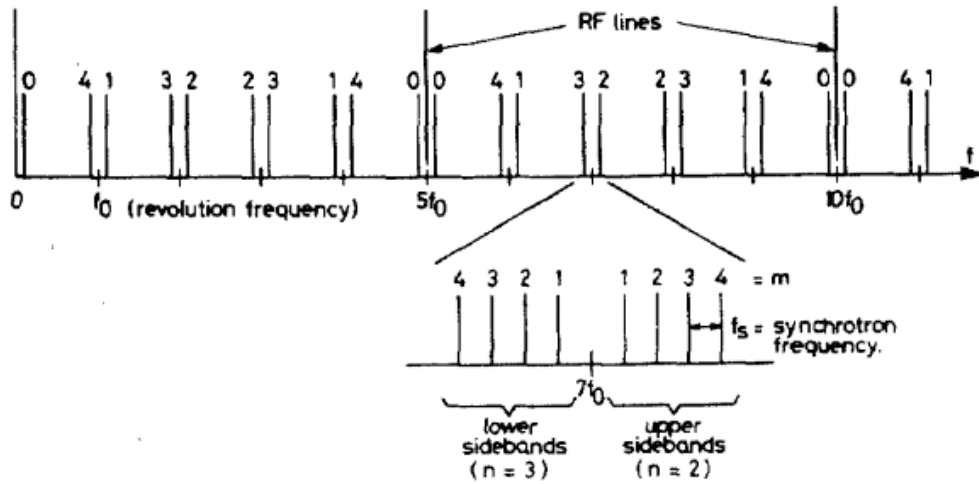


Figure 5.1. Synchrotron frequency sidebands of the f_{rev} harmonics [55]

In the case of the LHC-type beams in the PS ($h = 21$) we have the situation shown in fig. 5.2.

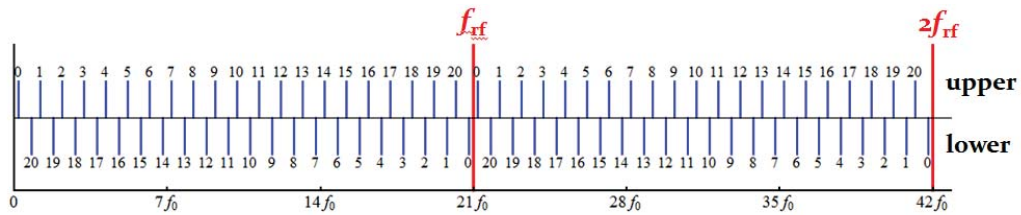


Figure 5.2. Synchrotron frequency sidebands for LHC-type beams

Figure 5.3 shows as an example the mode spectrum following the excitation of the upper SB (sidebands) at $19f_0$ for 21 bunches in $h = 21$ (full machine). As expected, the $\mu = 19$ mode is excited most strongly. Also visible are the CB mode excited by imperfect suppression of the unwanted SB at $h - \mu$ and a third mode at $2\mu - h$.

So if we excite each mode individually and measure the mode spectrum for an equally spaced pattern, we have a clean observation of all possible modes.

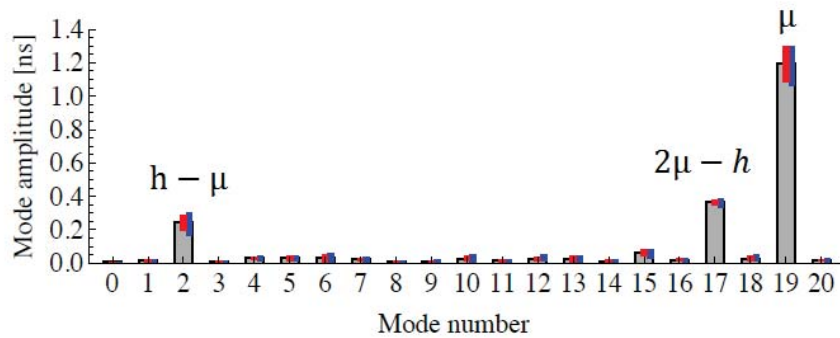


Figure 5.3. Example mode spectrum of 21 bunches in $h = 21$, excited at the upper SB of $19f_0$

From this analysis becomes clear that the CB modes are only weakly coupled to each other and that a feedback in the frequency domain can treat them successfully one by one.

The measured mode pattern becomes more complicated with the operational filling pattern for LHC-type beams in the PS, where only a maximum of 18 bunches on $h = 21$ are accelerated before final splitting to obtain a final bunch spacing of 25 ns or 50 ns, leaving a gap for extraction purposes. With only 18 bunches the CB mode number becomes n_{batch} and no longer corresponds directly to an harmonic of f_0 : each mode n_{batch} generates a spectrum of f_s SBs due to the convolution with the filling pattern.

The validation of the simulations was done by implementing an external excitation to be used as alternative to an HOM to excite the beam. It is a simple sinusoidal forcing that is given in energy to each bunch at every turn, by setting the amplitude, the frequency ($19f_0$) and the initial phase.

By using LHC-type beams, 18 bunches are accelerated in $h = 21$ with input parameters indicated in table VIII. The energy of 13 GeV was chosen as a test case being sufficiently far away from transition and with the instabilities already well established.

The damping rates have been measured, but since there are no equally spaced bunches a mode spectrum is excited due to this filling pattern:

$$n_{batch} = \frac{18}{21}\mu \cong 16 \quad (5.2)$$

In fig. 5.4 we can see the measurements and the results of simulations performed in the same conditions (see table VIII), the good agreement between the two is apparent..

The code has been validated with the PS data obtained with external excitation in the specific case of LHC-type beams, with 18 bunches are accelerated in $h = 21$. From fig. 5.4 one can see that in both cases mode $\mu = 16$ is excited due to the unequal pattern in the ring. As explained before, the CB mode excited by imperfect

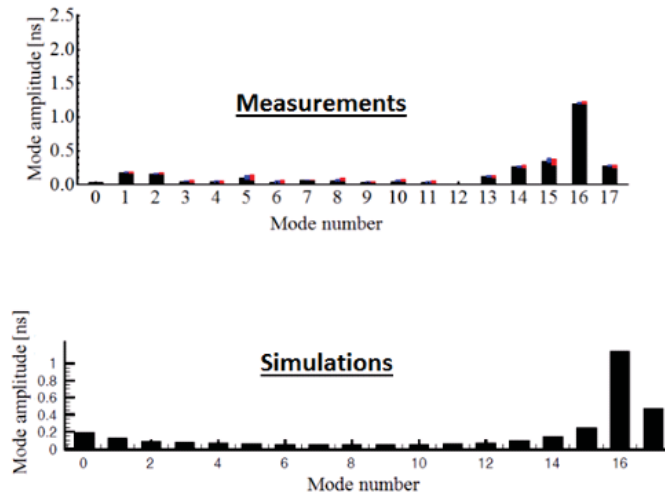


Figure 5.4. Example mode spectrum of 18 bunches in $h = 21$, excited at the upper SB of $19f_0$ [53]

Table VIII. Parameters used for benchmark simulations of the LCBC code.

Parameters	Value
Beam energy (GeV)	13
Harmonic number	21
Number of bunch	18
RF voltage (kV)	165
Total beam intensity (ppp)	$38 \cdot 10^{11}$
Amplitude of excitation (V)	200
Synchrotron frequency [MHz]	2.49218875

suppression of the unwanted SB are visible at $h - \mu = 21 - 19 = 2$ and at $2\mu - h = 2 \cdot 19 - 21 = 17$.

5.2 10 MHz RF cavity system

The CERN PS is equipped with ten 2.8-10 MHz tunable ferrite-loaded cavities for acceleration, as well as 20, 40, 80 and 200 MHz cavities for RF manipulations and longitudinal emittance blow-up. To simplify the mode identification, seven bunches (full ring) have been injected and accelerated at $h = 7$ (3.33 MHz). Then we have the triple splitting for acceleration at $h = 21$ as described in Chapter 2. The 20, 40 and 80 MHz RF systems were switched off with their gaps short circuited. The CB instabilities start shortly after transition crossing and develop during acceleration. Firstly, growth rates were measured by analyzing the beam signal around a specific harmonic of the revolution frequency and secondly, the spectrum of the CB modes has been extracted from mountain range measurements.

In this section I will describe the 10 MHz system and showing results of simula-

tions compared to measurements of past years.

The main sources of longitudinal coupled bunch instabilities in the PS are thought to be the 10 MHz RF cavities (fig. 5.5). The coupling impedance of the cavities is not a simple resonator due to the presence of a feedback loop and the power amplifier. A simplified model of the system is presented in fig. 5.6: it includes a ferrite loaded cavity and power amplifier with a tuned grid resonator and the fast feedback around the amplifier [56].



Figure 5.5. On of the CERN PS 10 MHz cavity

The input voltage V_{ref} controls the current generator composed of the driver amplifier and the grid resonator and produces I_p that is g_p time bigger then the input voltage. The voltage V_G controls the final amplifier ($I_p \cdot Z_G = V_G$), which sends current to the parallel of R_G and Z .

I define $Z(\omega)$ as the cavity impedance:

$$Z(\omega) = \frac{R_S}{1 + iQ \left(\frac{\omega}{\omega_S} - \frac{\omega_S}{\omega} \right)} \quad (5.3)$$

and $Z_G(\omega)$ is the impedance of the grid resonator:

$$Z_G(\omega) = \frac{R_{GS}}{1 + iQ_G \left(\frac{\omega}{\omega_{GS}} - \frac{\omega_{GS}}{\omega} \right)} \quad (5.4)$$

and g_P and g_G are the effective transconductances of the driver and final amplifier defined as:

$$g_P = \frac{1}{R_{GS}} \quad (5.5)$$

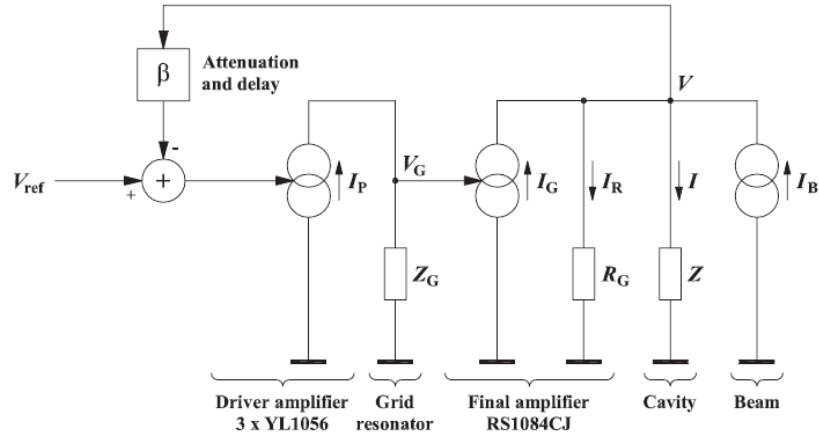


Figure 5.6. Simplified model of the 10 MHz RF system, including ferrite loaded cavities and power amplifier with a tuned grid resonator and the fast feedback around the amplifier [47]

$$g_g = \frac{1}{R_G} \quad (5.6)$$

The open loop gain is:

$$G_a = Z_F^N Z_G g_p g_g \quad (5.7)$$

where:

$$Z_F^N(\omega) = \frac{R_G \cdot Z}{R_G + Z} \quad (5.8)$$

while the closed loop one is :

$$G_{CL} = \frac{G_a}{F} \quad (5.9)$$

where F is the desensibilization factor due to the attenuation and delay of the feedback loop. According to this model, the impedance seen by the beam can be written as:

$$Z_c(\omega) = \frac{dV}{dI_b} = \frac{1}{Z_G(\omega) g_p g_g \beta + (R_G + Z)/(R_G Z)} \quad (5.10)$$

The parameters of the previous circuitual model have been chosen in order to reconstruct the measurements of open and closed loop transfer functions of 6 of the 10 cavities. The result for $Z_c(\omega)$ is shown in fig. 5.7 [47]. As we can see the impedance is centered around the line $k = \omega/\omega_0 = 7$. So we have:

$$7 \cdot \frac{2\pi}{T_0} = 2\pi f_{RF} \quad (5.11)$$

with $T_0 \simeq 2 \cdot 10^{-6}$ s the frequency is: $f_{RF} = 3.3$ MHz.

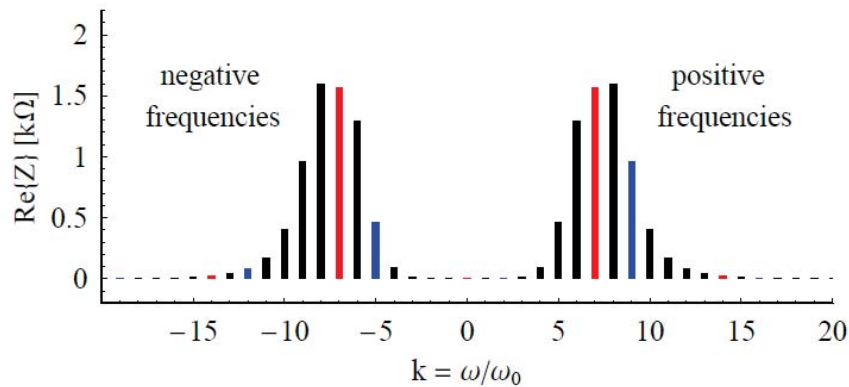


Figure 5.7. Real part of the total impedance of the 10 MHz cavities [47]

As the impedance Z_c covers several revolution harmonics around $h\omega_0$, the narrow-band approximation is not applicable for the estimation of the growth rates of the CB oscillations. For dipole modes, the growth rates $1/\tau$ are given by the eigenvalues system (eq. (3.24)). Solving the system results in the growth rate shown in table IX (for further details see ref.[47]).

Table IX. CB growth rates from eigenvalues system

Mode number	$\mu = 1$	$\mu = 2$	$\mu = 3$
Growth rate $1/\tau$	2.5 s^{-1}	3.0 s^{-1}	1.0 s^{-1}

These results predict a $\mu = 2$ mode being stronger than $\mu = 1$.

In order to use the obtained impedance in simulations I performed a fit of the impedance of fig. 5.7 to find a set of parameters (Q, R_s, ω) which allows to reconstruct $Re[Z(\omega)]$ in the most precise way. In fig. 5.8 we can see that the best fit has been found by using a sum of 4 resonant modes:

$$Re[Z(\omega)] = \sum_{i=1}^4 \frac{R_{S_i}}{Q_i^2 \left(\frac{\omega}{\omega_{r_i}} - \frac{\omega_{r_i}}{\omega} \right)^2 + 1} \quad (5.12)$$

In the fig. 5.8 the red curve is the same as fig. 5.7 (I just took the positive frequency part) and the green one is the result of the fit.

In table X are shown the values obtained from the fit and that will be used in the next section for simulations.

5.3 Simulations at 3.3 MHz for $h = 7$

Using the previously obtained parameters, I evaluated the growth rates of instability for the same modes of table IX to crosscheck the code with the results of the eigenvalue system.

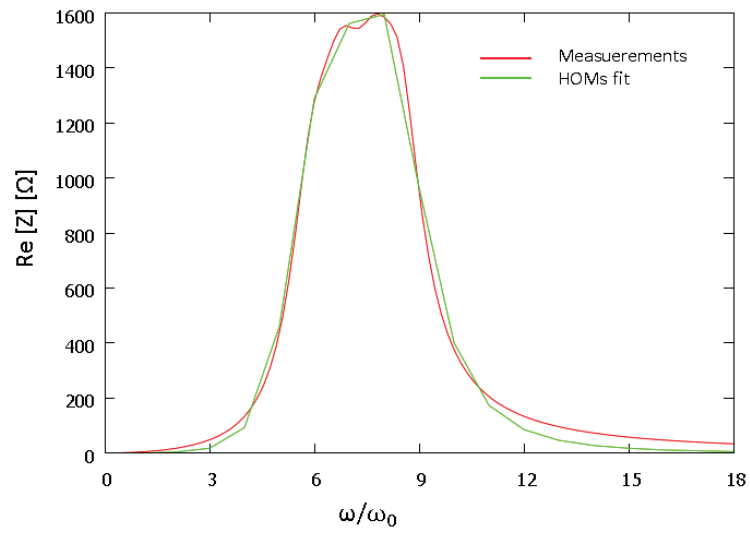


Figure 5.8. Real part of the total impedance of the 10 MHz cavities and best fit obtained and used in simulations for $h = 7$

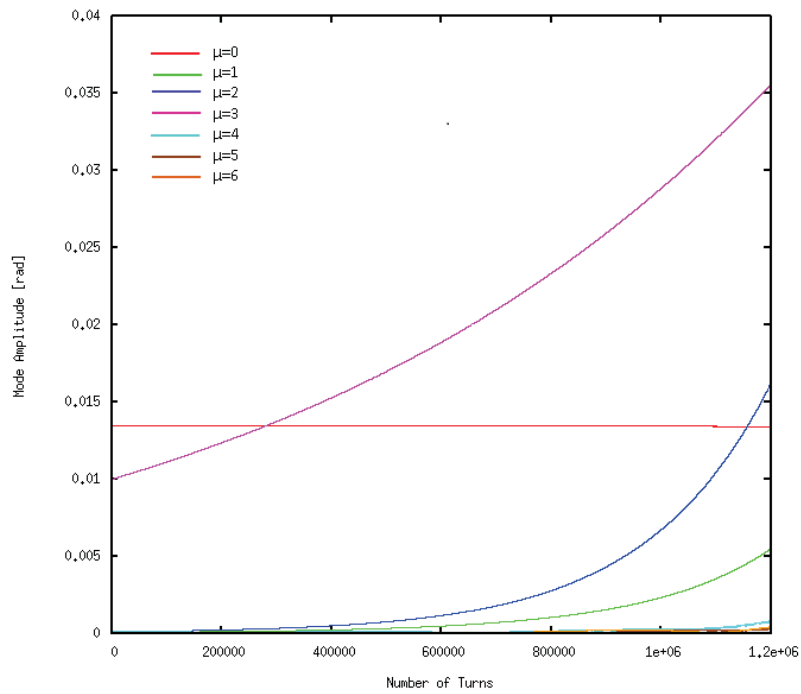


Figure 5.9. Mode pattern for $h = 7$ using 7 bunches

Table X. Parameters resulting from the fit on the real part of the 10 MHz system impedance indicating the HOMs used in simulations to excite the coherent oscillation modes for $h = 7$

Frequency ω/ω_0	Quality factor	Shunt Impdance [Ω]
8.5009	5.9696	747.343
6.79973	4.0167	821.522
7.76648	4.76129	728.578
5.94224	3.77121	733.168

I studied separately each mode ($\mu = 1, 2, 3$) by choosing the corresponding oscillation phase shift between bunches and I evaluate the rise times of instability and compared them with the ones in table IX. For example, for mode $\mu = 3$ and using eq. (3.29), I have:

$$\Delta\Phi = \frac{2\pi \cdot 3}{7} \simeq 2.7 \quad (5.13)$$

For this value, the simulation shows that the coherent oscillation mode $\mu = 3$ is the one which shows itself before the others. Using an average energy of 13 GeV and a total beam intensity of $9 \cdot 10^{12}$ as indicated in table XI, I obtain the mode pattern shown in fig. 5.9. As we can see, mode 3 grows before the others due to the fact that we forced an oscillation phase shift between bunches relative to this mode. The clear presence of mode $\mu = 0$ is due only to initial conditions on the synchronous phase.

Table XI. Parameters used for simulations for $h = 7$.

Parameters	Value
Beam energy (GeV)	13
Harmonic number	7
Number of bunch	7
RF voltage (kV)	165
Total beam intensity (ppp)	$9 \cdot 10^{12}$

Now, using an exponential fit of the kind of eq. (4.7), I evaluate the growth rates for the 3 modes of interest. In table XII, I compared the results with values from the eigenvalues system: the agreement is very good.

Table XII. Comparison between CB growth rates for $h = 7$ and for 7 bunches as simulations by LCBC code and values from the theoretical eigenvalues system.

Mode Number	1	2	3
CB Growth Rate from tab. IX	400 ms	333 ms	1 s
CB Growth Rate from simulations	544 ms	467 ms	1.91 s

5.4 Simulations at 10 MHz for $h = 21$

Until now, the LCBC code was validated for the case $h = 7$. Now I will show $h = 21$, during acceleration the working at frequency becomes the case for:

$$21 \cdot \omega_0 = 2\pi f \rightarrow f \simeq 10\text{MHz} \tag{5.14}$$

As previously done with $h = 7$, I have developed a model for the impedance at 10 MHz by using the results of measurements done in 2009 of the open and closed loop transfer functions of the RF system (see the simplified model of fig. 5.6 and fig. 5.10).

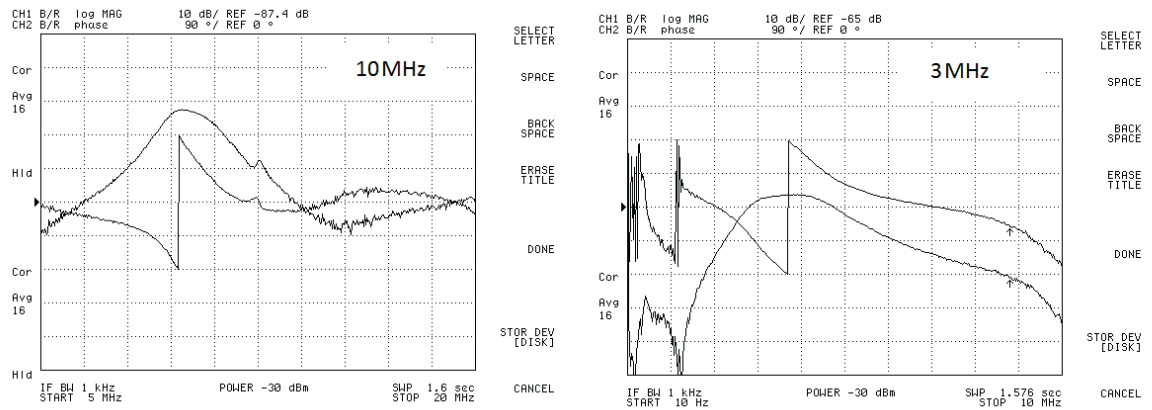


Figure 5.10. Open and closed loop transfer function of one of the cavities at 3.3 MHz (right) and 10 MHz (left)

If I shift the closed loop transfer function at 3.3 MHz to 10 MHz, as in fig. 5.11, it overlaps quite well the measured one at 10 MHz. I therefore conclude that it is simply possible to the study by shifting the impedance given by eq. (5.12) (see fig. 5.12).

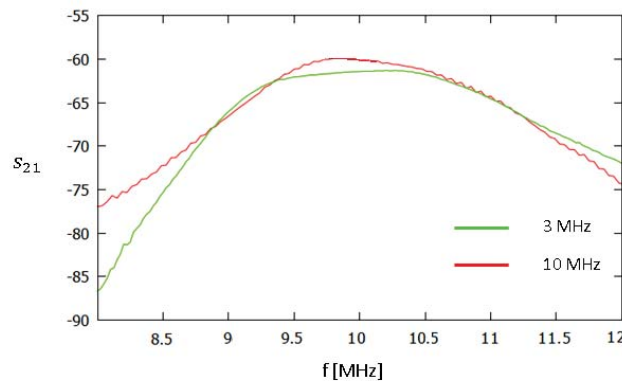


Figure 5.11. Closed loop transfer function at 3.3 Mhz (shifted) and at 10 MHz

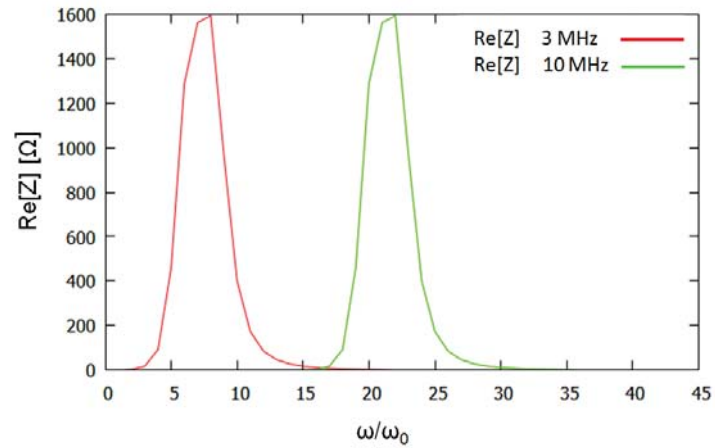


Figure 5.12. Machine model impedance at 3.3 and 10 MHz

By performing a fit on the new impedance using the same eq. (5.12), the resulting parameters are indicated in table XIII and the resulting impedance is in fig. 5.13.

Table XIII. Parameters resulting from the fit on the real part of the 10 MHz system impedance indicating the HOMs used in simulations to excite the coherent oscillation modes for $h = 21$

Frequency ω/ω_0	Quality factor	Shunt Impdance [Ω]
21.8008	12.4459	750.35
20.8558	13.5905	824.954
19.9068	16.3653	732.464
22.5028	13.0183	735.866

Again, using the impedance model just shown, I checked which is the pattern of the oscillation modes at this frequency. Measurements done in 2013 show the evolution of the mode spectra for LHC50ns beam during acceleration in the two cases of a full machine (21 bunches) and with 18 bunches (see fig. 5.14 and fig. 5.15).

To reproduce this results, I used a bunch length of 6.5 ns and an average energy of 13 GeV as indicated in table XIV.

Table XIV. Input parameters for LHC50ns beams during acceleration

Parameters	Value
Beam energy (GeV)	13
RF voltage (kV)	165
Total beam Intensity	$9.8 \cdot 10^{12}$
Bunch length σ [ns]	6.5

LCBC shows that with the HOMs of table XIII, all the coherent oscillation modes are excited. In both measurements and simulation there isn't an exponential trend so it is no possible to perform a fit on each oscillation mode curve to evaluate the rise time, but the amplitude ratio of each mode is compatible in simulations and

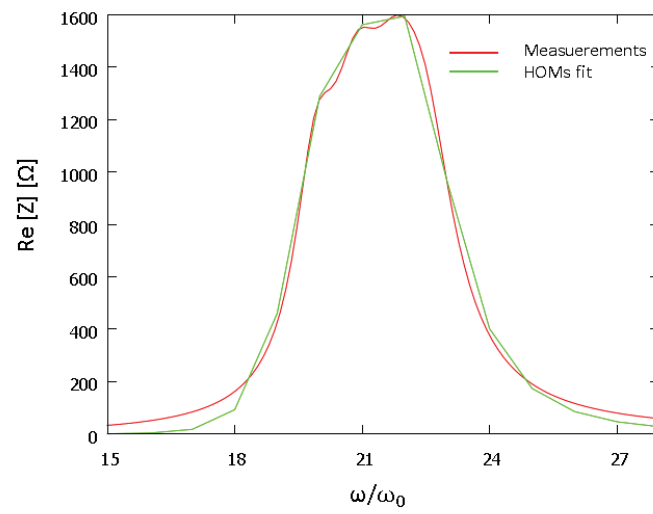


Figure 5.13. Real part of the total impedance of the 10 MHz cavities and best fit obtained and used in simulations for $h = 21$

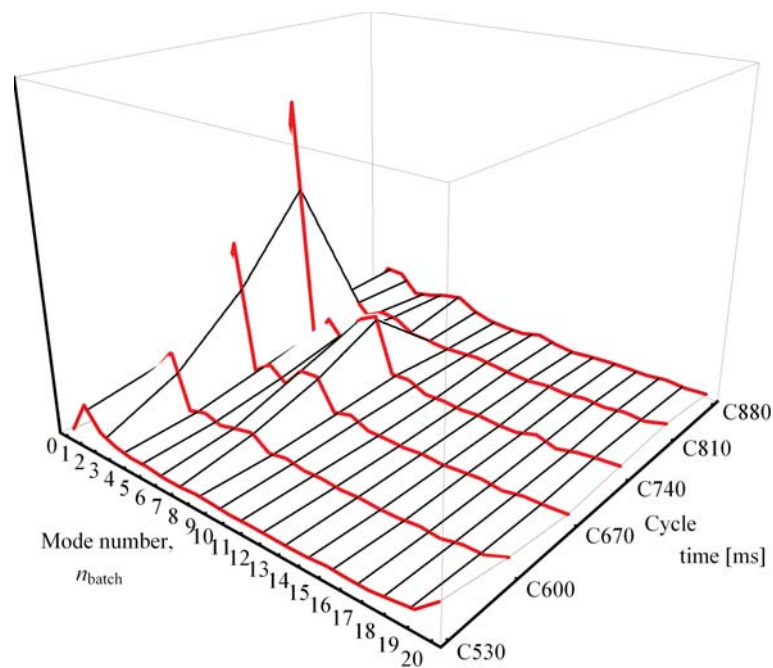


Figure 5.14. LHC50ns: Development of the CB mode spectrum during acceleration for $h = 21$ with 21 bunches[54]

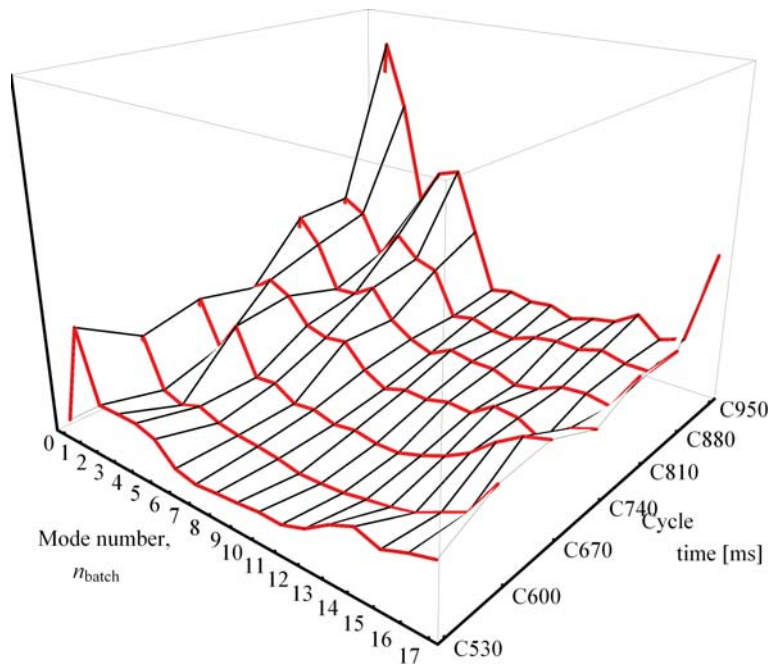


Figure 5.15. LHC50ns: CB mode spectrum during acceleration for $h = 21$ with 18 bunches[54]

measurements and the mode trend is the same. Comparing fig. 5.14 and fig. 5.17 and fig. 5.15 and fig. 5.16 we can see that in both cases simulations show that mode 1, in case of 18 bunches, and mode 2, in case of a full machine, are the ones which appear before the others.

The code proved to be a valid instrument to study longitudinal CB instability, simulation results have been compared both with the theory of the CB through the benchmark with the results of the eigenvalues system either with the outcome of previous measurements in different conditions (not only in the simple case of a full machine with equally spaced bunches but even with 18 not equally spaced bunches). The results obtained are fully consistent. Now let's see if, with these machine parameters, the FB in frequency domain introduced in the code works correctly.

5.5 Suppression of one mode at 10 MHz for $h = 21$

As previously shown in chapter 4.4.1, I preceded to demonstrate that the LCBC code is able to dump one of the CB modes of the 10 MHz cavity system.

I used parameters of table XIV in case of 21 bunches in $h = 21$, and using the impedance model at 10 MHz I chose to study the oscillation mode $\mu = 2$ by using an oscillation phase shift of:

$$\Delta\Phi = \frac{2\pi\mu}{n_b} \sim 0.6 \quad (5.15)$$

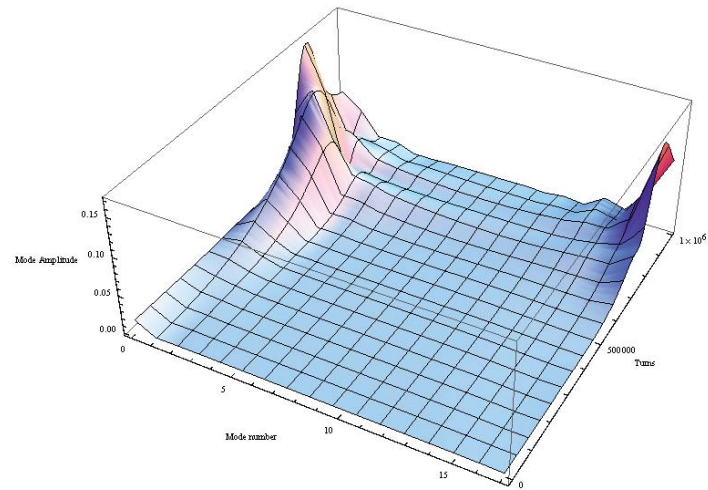


Figure 5.16. Simulation of the LHC50ns CB mode spectrum during acceleration for $h = 21$ with 18 bunches

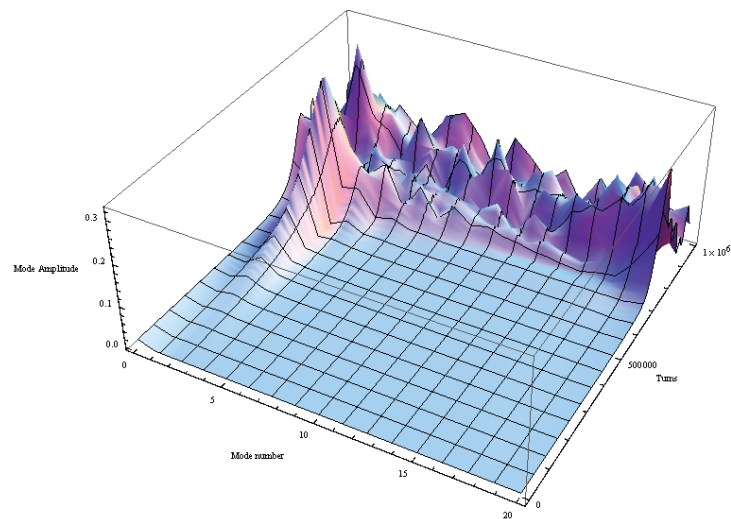


Figure 5.17. Simulation of the LHC50ns CB mode spectrum during acceleration for $h = 21$ with 21 bunches

First, I evaluated the rise time of instability using eq. (4.7). In fig. 5.18 is shown on the left the pattern of all the modes excited by the HOM while on the fig. 5.19 is presented only the trend of the oscillation mode 2 with the fit. I obtained a rise time of instability $\alpha = 1/\tau = 3.5433$. Now, using eq. (4.21) and considering $\omega_s = 2.49218875$ MHz and $V_{RF} = 165$ kV, I got that the feedback gain is equal to 472.44.

The second step consists in checking if the evaluated gain is correct. I switched on the feedback but without the excitation of the HOMs. Looking at fig. 5.20 one can conclude that the gain g is correct: without the effect of the HOMs the FB is able, with the choosen gain, to produce the same value of the rise time, with the opposite sign (the damping rate).

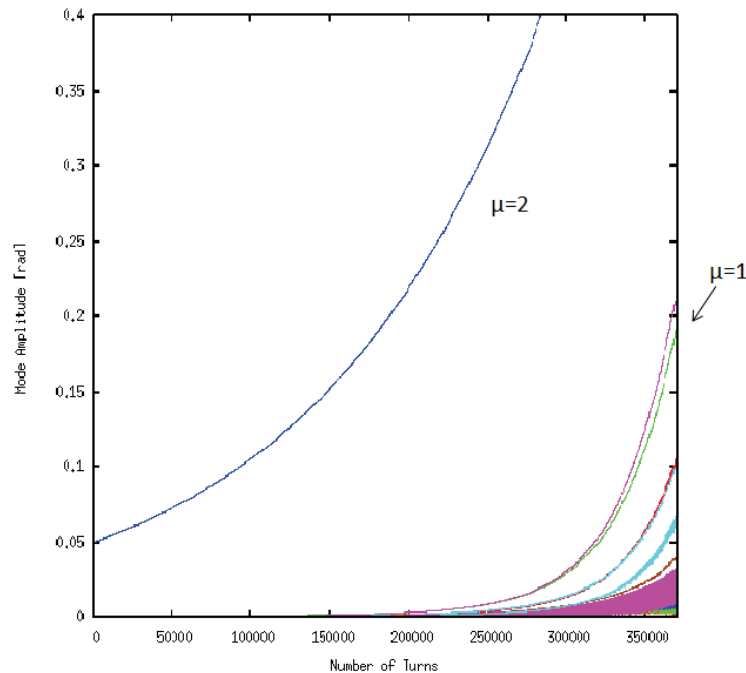


Figure 5.18. Mode amplitude of all oscillation modes excited, the blu line is referred to $\mu = 2$

Finally I switched on the FB (feedback): as expected there is equilibrium between the instability and the damping effect (fig. 5.21): the regime amplitude value 0.05 corresponds to the starting one in fig. 5.18.

As eyelighted before, and as demonstrated by measurements, the oscillation mode $\mu = 2$ is the one which grows faster than the others in $h = 21$. Dumping this mode implicates, as one can see comparing the scale amplitude in fig. 5.18 and fig. 5.21, that all the others are dumped too and their amplitude is reduced. If we try now to dump another mode, for example mode 1 (the one rapresented by a green line in fig. 5.18) all others modes continue to behave as before, and only the amplitude of mode 1 is reduced.

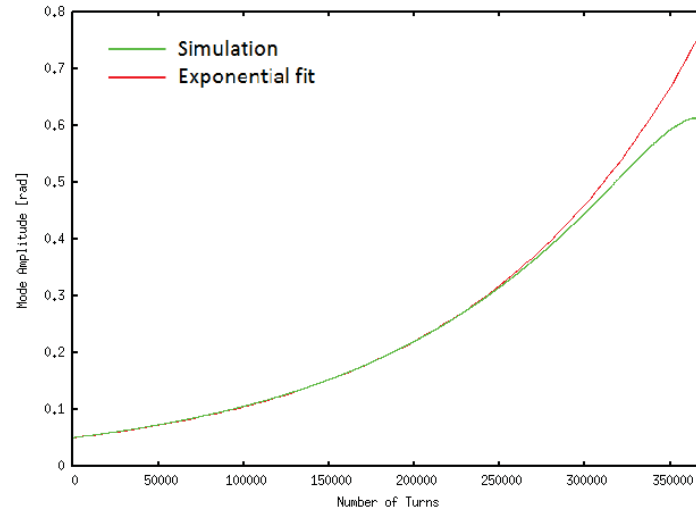


Figure 5.19. Mode amplitude of oscillation mode $\mu = 2$, the green line is referred to the mode and the red one is the fit

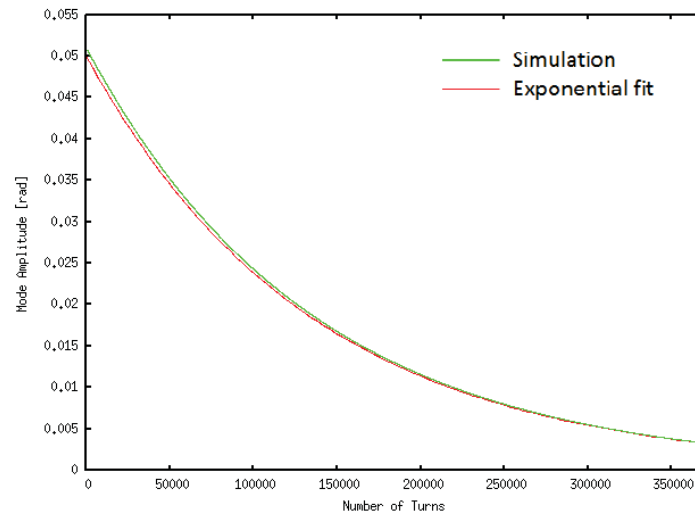


Figure 5.20. Exponential fit on the oscillation mode $\mu = 2$ when the FB is switched on

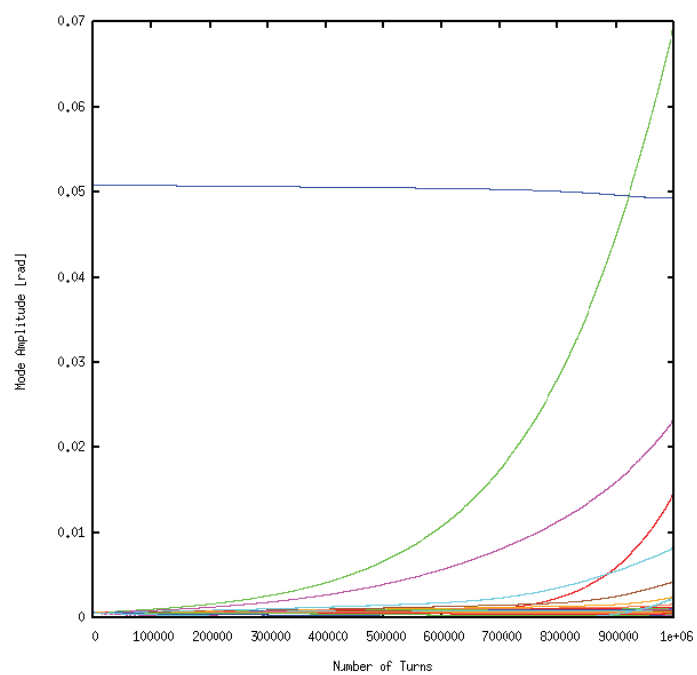


Figure 5.21. Mode pattern of all the oscillation modes once that the FB and the HOMs are on. The blue line is referred to the damped mode $\mu = 2$

Chapter 6

Preliminary results

6.1 40 and 80 MHz cavities

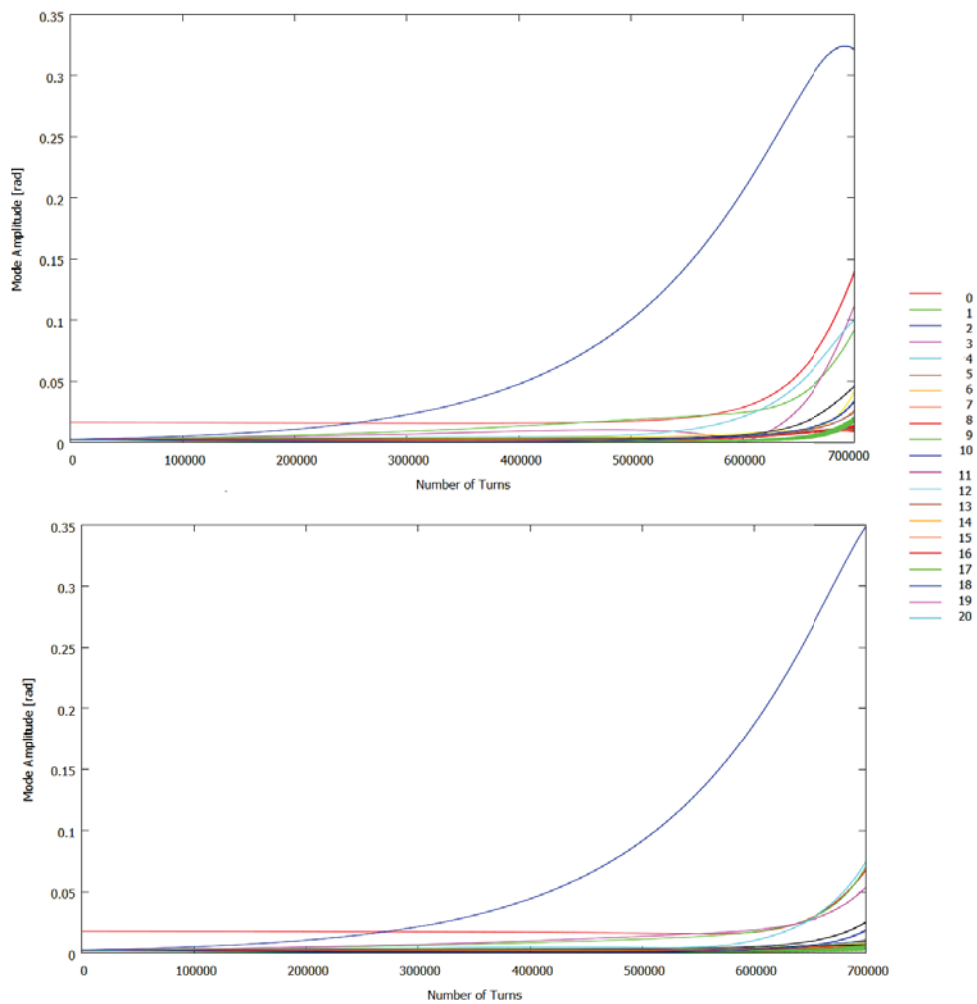


Figure 6.1. Mode amplitude of 10 and 40 MHz cavities (up) and 10 and 80 MHz cavities (down)

The 10 MHz cavity system is considered the principle cause of coupled bunch instability in the PS. During this thesis work I demonstrated the effect of the 10 MHz system, but as explained in the second chapter, the PS has a total of 24 RF cavities: 11 for 2.8-10 MHz; two 20 MHz; two 40 MHz; three at 80 MHz and six at 200 MHz. So I proceeded with further simulations to be sure that the 40 and 80 MHz system cannot be considered as an additional source of instability. For the 20 MHz cavity haven't been done simulations.

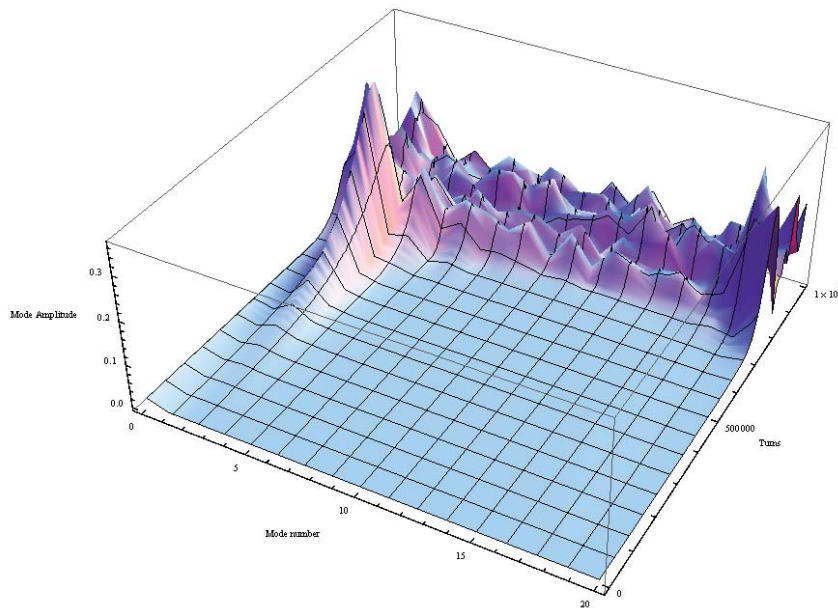


Figure 6.2. Mode amplitude of all cavities

Simulations have been performed in $h = 21$ with 21 bunches and using parameters of table XIV. In table XV are shown the characteristic parameters of the HOM used to simulate the effects of one 40 and two 80 MHz cavities as used in normal operation for the production of the 25 and 50 ns beams.

Table XV. Characteristic parameters of 40 and 80 MHz cavities

Frequency MHz	HOM's quality factor	HOM's R/Q
$f = 40$	70	33
$f = 80$	100	56

In fig. 6.1 is shown the mode pattern excited by the HOMs: the up picture shows the effects of the 10 and one 40 MHz cavity, while the other takes into account the 10 and 80 MHz ones. In both cases the oscillation mode $\mu = 2$ remain the one which grows faster than the others, which is in agreement with measurements (fig. 5.14). In fig. 6.2 the mode pattern excited is due to all cavities together: the pattern and the mode amplitude doesn't change much with respect to fig. 5.17. From these preliminary simulations I can conclude that it is correct to consider the 10 MHz cavity system as the major cause of CB instability in the PS.

6.2 Finemet© cavity

The longitudinal damper cavity for the new coupled-bunch feedback of the PS machine has to provide a correcting RF voltage to the circulating bunches to suppress the excitation of bunch oscillations. To improve longitudinal beam stability, a first dedicated coupled-bunch feedback has been installed in 2005: two 10 MHz accelerating cavities driven by the signal from the feedback low level electronics are used as longitudinal kickers.

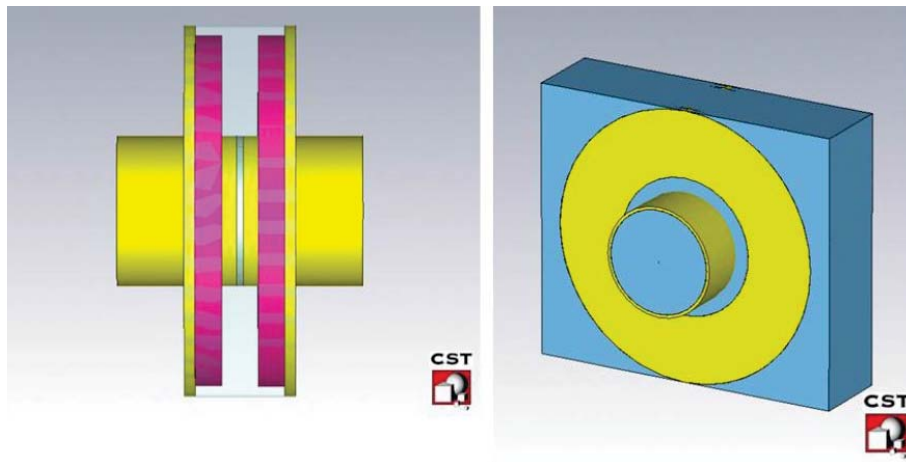


Figure 6.3. One cell CST model of the Finemet cavity [58]

In the framework of the LIU project it has been decided to install a dedicated, wideband kicker based on the wideband frequency characteristics of Finemet magnetic alloy and driven by solid-state amplifiers. However, installing a wideband cavity in the PS ring also introduces longitudinal impedance covering many revolution frequency harmonics.

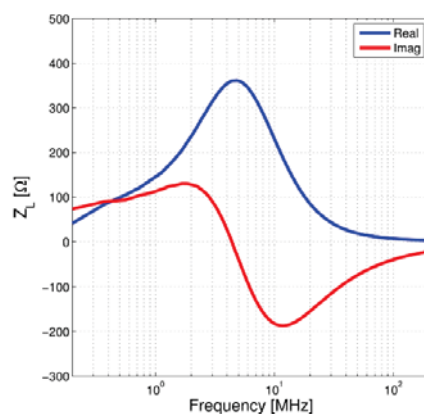


Figure 6.4. Longitudinal impedance of the one cell Finemet cavity [58]

Ferrite has been used extensively in RF cavities for particle accelerators that

require tuning. Some ferrites used can operate up to more than 100 MHz but the saturation magnetic flux intensity is often limited to 100-200 G. Recently a met-glass-like material called Finemet© was developed in Japan that can hold up to 2 kG of magnetic flux intensity. Ferrite is ceramic in nature and is manufactured by baking in an oven. Therefore, large ferrite cores are difficult to produce. On the other hand, Finemet© is in the form of a tape which can be wound into a core over 1 m in diameter, making very high magnetic flux possible. For this reason, Finemet© may open up a new way to the construction of high gradient acceleration cavities [57].

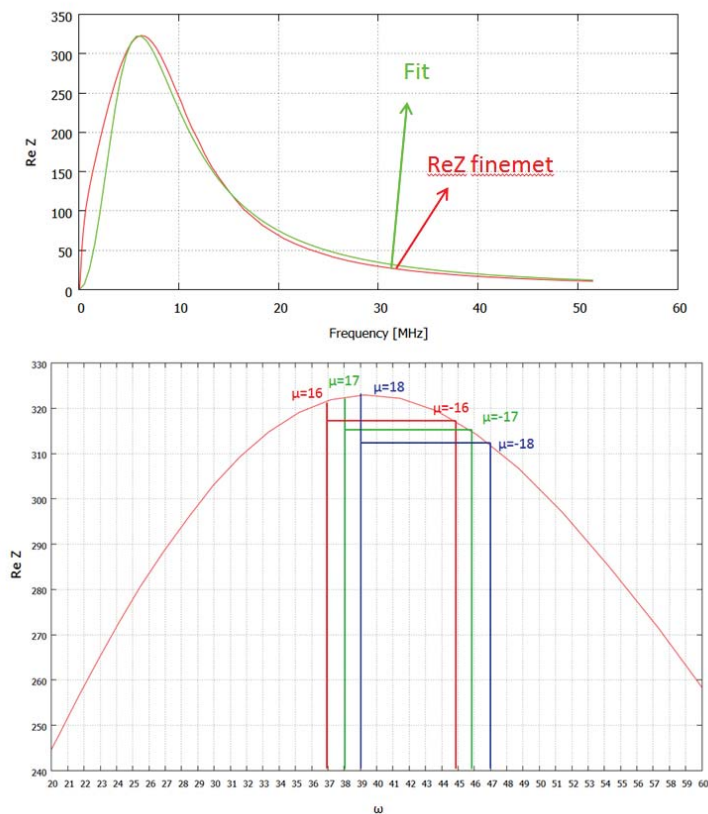


Figure 6.5. Fit of the impedance of Finemet© cavity and study of the excited modes. The real part of impedance is expressed in Ω .

To detect longitudinal CB oscillations in the frequency domain, the feedback system picks up synchrotron frequency sidebands of the beam signal at harmonics of the revolution frequency. Demodulation and filtering are applied to remove the strong component of the beam signal at exactly the revolution frequency harmonic. The filtered synchrotron sidebands alone are then amplified and remodulated with the correct phase to a multiple of the revolution frequency. The resulting signal, containing multiple carriers, is sent to the longitudinal kicker. According to the theory of CB oscillations, each mode, identified by its phase advance, appears as an upper synchrotron frequency sideband as well as lower synchrotron frequency sideband as described in Chapter 3 ; due to the symmetry of sidebands, the kicker cavity

should cover the frequency range from 0.4 to 5.5 MHz or from the 4.5 to 10 MHz [58].

The Finemet© cavity model used in these simulations is based on the one cell model shown in fig. 6.3.

I performed a fit on the real part of impedance of fig. 6.4 to obtain parameters useful for simulations as shown in fig. 6.5. I obtained:

- $Q = 0.6$;
- $f = 6 \text{ MHz}$;
- $R_s = 323 \ \Omega$

Fig. 6.5 presents the results of the study of the oscillation modes excited by the cavity. The real part of longitudinal impedance shows that the oscillation mode $\mu = 17$ should be the one which grows unstable faster than the others and it has been confirmed by simulations, as shown in fig. 6.6.

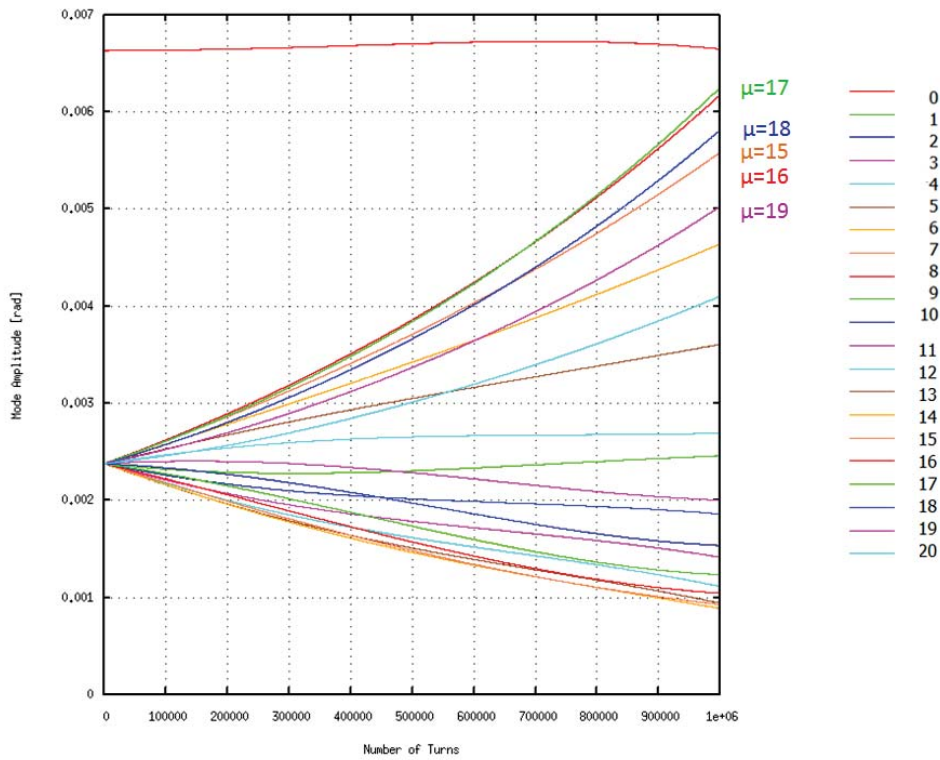


Figure 6.6. Mode amplitude of Finemet cavity

As last step was useful to check that the Finemet©, which will be used as a kicker cavity to suppress excitation of bunch oscillation, is not itself source of instability. Even in this case, preliminary simulations (fig. 6.7) show that the Finemet© cavity doesn't produce any significant effect on the modes of the 10 MHz system. This happens because its longitudinal impedance is quite broadband so that stable and

unstable frequencies generally compensate each other, and they don't excite coupled bunch oscillation modes. However a more detailed analysis and its impact on the beam dynamics will be done in the future.

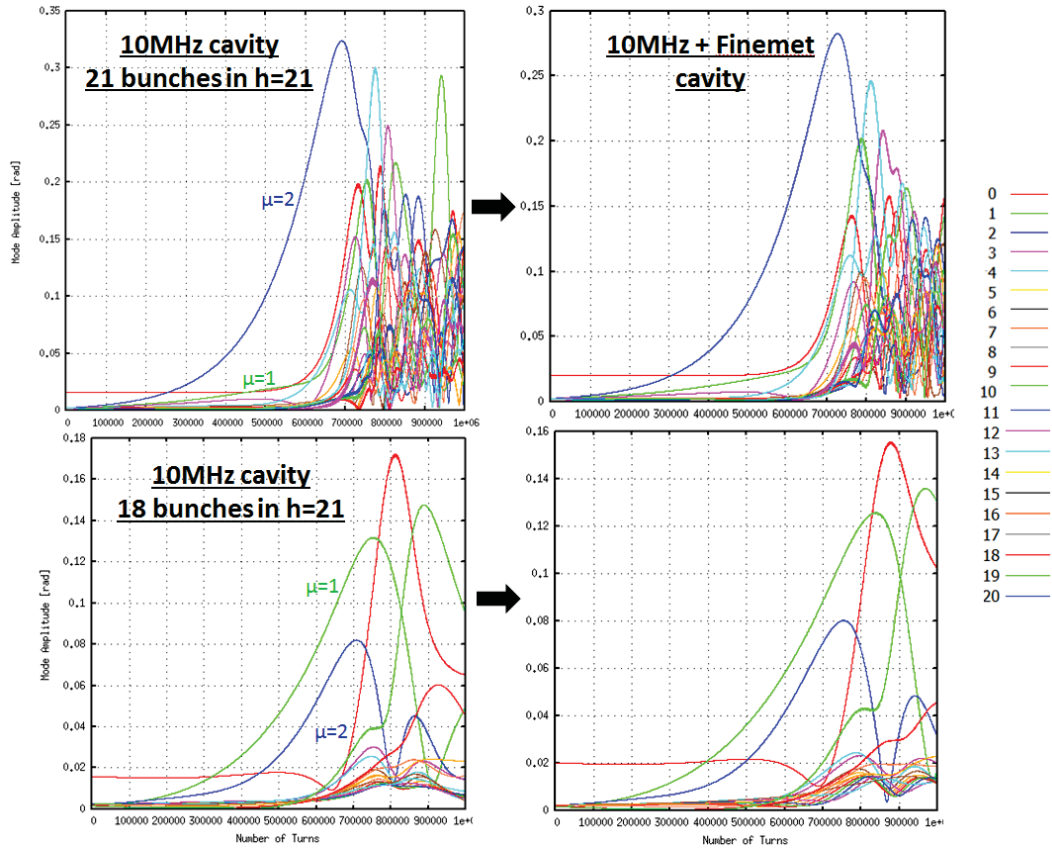


Figure 6.7. Mode amplitude of Finemet© cavity and 10 MHz cavity

Chapter 7

Conclusion

The role of the PS in the production of the beams for the LHC is to preserve at maximum the transverse emittances defined by its injector, the PS Booster (PSB), and to manipulate the longitudinal phase-space to define the bunch spacing required by the collider. In the framework of the the High-Luminosity LHC project, all the injectors should be able increase the intensity per bunch of the LHC-type beams while keeping or reducing the transverse emittances. The goal is to achieve a peak luminosity of $10^{34} \text{ cm}^{-2} \text{ s}^{-1}$ during 2015 and 40 fb^{-1} for the integrated luminosity [59]. The luminosity formula (eq. (2.1)) shows that, independently of the modifications of LHC, the luminosity depends from the characteristics of the injected beam. It is proportional to the product of beam current in the collider ($\sim n_b N_b$) and in injectors with the beam brightness ($\sim N_b/\varepsilon_n$). The beam intensity is limited by single-particle effects as well as collective effects. Collective effects are caused by the interactions between charged particles and their surroundings and become more dangerous at a high beam intensity. In the PS, the wakefield, which is the electromagnetic field produced by the interaction between protons and their surroundings, is the main source of beam instabilities. Wakefield effects can lead to longitudinal and transverse instabilities, which limit the ultimate achievable beam current because typically produces beam losses.

In the PS the maximum intensity N_b for bright bunches is limited by coupled-bunch (CB) instabilities after transition crossing, which are most likely excited by the main 10 MHz accelerating cavities. In the frame of LIU project a new wide-band FB kicker cavity will be installed to suppress these instabilities to replace the old one which is limited to the two dominant oscillation modes.

To carry on these studies it has been used a new simulation code, the LCBC, which has been proved to be an useful instrument to reproduce the behaviour of the CB FB in the PS. In Chapter 4 I preceded by doing a benchmark of this code using PS parameters, in order to verify that simulation's result are in agreement with the theory of coupled-bunch which has been illustrated in Chapter 3. Moreover a new FB system in frequency domain (mode-by-mode) has been implemented in the code to emulate the real one that will be installed in the PS during LS1. The code is able to excite a single CB oscillation and from it I evaluated the damping time. The coupling between different modes is visible and I proved that the code FB can

attack each mode individually.

In chapter 5 I used the code to reproduce results of measurements done back in 2013 in the PS. I developed a model for the 10 MHz system impedance and used it for simulations at 3.3 MHz ($h = 7$) at injection with a full machine and compared the growth rates of oscillation modes with the ones from the eigenvalues system. Then I moved at 10 MHz ($h = 21$) to see what happens during acceleration. If I shift the closed loop transfer function at 3.3 MHz to 10 MHz they overlaps quite well. I therefore concluded that it was simply possible to shift the impedance model developed at $h = 7$ to 10 MHz and use it for simulations. I checked which is the pattern of the oscillation modes at this frequency to compare it with results from measurements done in 2013 which show the evolution of the mode spectra for LHC50ns beam, and they both appear to be very similar. As last step in Chapter 6 I started doing some preliminary simulations on the 40 and 80 MHz cavities to prove that they don't add some instability to the one produced by the 10 MHz and on the Finemet cavity which will be used as a damper in the new FB system, in order to verify that the cavity which should damp unstable modes doesn't introduce itself any kind of instability. From these preliminary simulations these cavities doesn't seem to cause any problem.

Acknowledgments

Non è facile citare e ringraziare, in poche righe, tutte le persone che hanno contribuito alla nascita e allo sviluppo di questa tesi di laurea: chi con una collaborazione costante, chi con un supporto morale o materiale, chi con consigli e suggerimenti o solo con parole di incoraggiamento, sono stati in tanti a dare il proprio apporto alla mia carriera universitaria e a questo lavoro.

Desidero veramente ringraziare il Prof. Luigi Palumbo per avermi offerto la possibilità di lavorare ad un tema così interessante e ambizioso e per avermi introdotto in vasti e interessanti ambiti scientifici. Un grazie speciale al mio supervisore al CERN Simone Gilardoni per la sua disponibilità, gentilezza ed infinita pazienza nei miei confronti. And thanks to Heiko Damerau for helping and guiding me during my master thesis work with his incredible knowledge of...everything. Ma non avrei potuto fare niente di tutto ciò senza il preziosissimo aiuto del Prof. Mauro Migliorati, senza i suoi pazienti insegnamenti, le risposte a tutti i miei dubbi e gli aiuti, la tesi non avrebbe prodotto alcun risultato, a lui in particolar modo sono profondamente riconoscente.

Tutto questo non sarebbe stato possibile se non avessi ricevuto il sostegno delle persone che mi circondano, persone che con la loro presenza mi hanno incoraggiato a stringere i denti nei momenti difficili e hanno festeggiato con me le vittorie nelle tappe che mi hanno portata a tagliare questo traguardo. La mia gratitudine va ai miei amici Federica e Stelvio, per le serate insieme, le risate, e per essere semplicemente due persone straordinarie con cui ho l'onore di essere amica; Laura e Letizia, sono 10 anni che questa amicizia, nata tra i banchi di scuola, continua, ogni volta che ci vediamo è una gioia immensa. Un pensiero va alla mia grande amica Giorgia, per questi mesi vissuti insieme, per tutto quello che abbiamo condiviso, mi ritengo molto fortunata di averti conosciuto e di affrontare questo straordinario percorso insieme a te.

E poi ci sei tu Michele. Michele non ha bisogno di ringraziamenti perché'.....Michele e' Michele.

Grazie a nonno Americo e a nonna Attilia per l'affetto e i consigli che mi davano ogni qual volta ritornavo a Ginevra. Ovviamente grazie alla mia famiglia: alla mia cara e adorata Debora, sempre presente nella mia vita con i suoi suggerimenti e osservazioni dei quali non potrei fare a meno, alla mia cucciola Silvia che con il suo sorriso e la sua testardaggine ha dato sempre gioia e allegria al mio cuore.

Ma soprattutto a mamma e papà che in tutti questi anni, mi hanno spronato e

aiutata nei momenti difficili in cui credevo di non farcela e soprattutto in quest'anno pieno di novità e cambiamenti non solo per me ma anche per loro. Senza il loro sostegno continuo non potrei. . . .vivere. Vi voglio bene e grazie.

Bibliography

- [1] H. Wiedemann, *Particle accelerator physics*, ISBN-13 978-3-540-49043-2, Springer, Berlin Heidelberg New York, 2007
- [2] D. J. Simon, *The CERN PS Complex: a versatile particle factory*, Proceedings of the fifth European Particle Accelerator Conference, Sitges, Barcelona, Spain, 1996, edited by S. Myers, A. Pacheco, R. Pascual, C. Petit-Jean-Genaz, and J. Poole (IOP, Bristol, 1996) p. 295
- [3] <http://cds.cern.ch/record/615850?ln=en>
- [4] R. Cappi, R. Garoby, S. Hancock, M. Martini, N. Rasmussen, T. Risselada, J. P. Riunaud, K. Schindl, H. Schönauer, and E. J. Wilson, *The PS complex as part of the LHC injector chain*, Technical Report CERN-PS-91-07-PA. LHC-NOTE-144. CERN-LHC-Note-144, CERN, Geneva, Apr 1991
- [5] E. Wilson, *The lattice of the SPS*, 7th IEEE Particle Accelerator Conference, Chicago, IL, USA, 16 - 18 Mar 1977, pp.1458-1460
- [6] W. Wu, *Feedback System for Control of Coupled-bunch Instabilities in the Duke Storage Ring*, 2012
- [7] R. Garoby, *Plans for the upgrade of the LHC injector complex*, CERN 19/06/2012
- [8] M. Migliorati, *Simulations of the longitudinal coupled-bunch instability in the PS*, Presentation at the 84th ICE meeting, available at URL <http://emetral.web.cern.ch/emetral/ICEsection/2013/2013-06-12/ICE>
- [9] M. Bassetti, A. Ghigo, M. Migliorati, L. Palumbo, M. Serio, *A time simulation code of the longitudinal multibunch instabilities*, DAΦNE Technical Note, Frascati, June 23, 1993
- [10] E. Wilson, *An introduction to particle accelerators*, ISBN 0-19-850829-8, Oxford University Press, United Kingdom, 2001
- [11] R. Steerenberg, *Introduction to accelerator physics*, AXEL 2012, CERN-BE/OP Shutdown Lectures, Geneva, Switzerland, 2012

- [12] B. J. Holzer, *Lattice design in high-energy particle accelerators*, DESY, Hamburg, Germany
- [13] J. Rossbach, P. Schmüser *Basic course on accelerator optics*, Deutsches Elektronen-Synchrotron DESY, Institut für Experimentalphysik, Universität Hamburg, F.R. Germany
- [14] *CAS CERN accelerator school, Fifth general accelerator physics course*, University of Jyväskylä, Finland 7-18 september 1992
- [15] K. Takayama, *Note on the Courant and Snyder Invariant*, Fermi National Accelerator Laboratory, Batavia, 60510, USA, IEEE Transaction on Nuclear Science, Vol. NS-30, No. 4, August 1983
- [16] B. Holzer, *Introduction to transverse beam optics*, CERN, available at URL <http://cas.web.cern.ch/CAS/UK-2007/Lectures/PDF/Holzer/Transverse>
- [17] E. Wilson, *Transverse beam dynamics*, CERN, Geneva, Switzerland, available at URL <https://cds.cern.ch/record/941311/files/p1.pdf>
- [18] Jonathan L.F. King *Liouville's Theorem: calculus*, University of Florida, Gainesville FL 32611-2082, USA, 2 February, 2011
- [19] E. Jensen, *RF cavity design*, CERN Accelerator School Accelerator Physics (Intermediate level), Chios 2011, available at URL <http://cas.web.cern.ch/cas/Greece-2011/Lectures/Jensen.pdf>
- [20] S. Baird, *Accelerators for pedestrians*, CERN-AB-Note-2007-014 OP, 2007
- [21] E. A. Perevedentsev, *Simplified theory of the head-tail instability of colliding bunches*, Budker Institute of Nuclear Physics, Novosibirsk, 630090, Russia, Proceedings of the 1999 Particle Accelerator Conference, New York, 1999
- [22] K. Hock, *Sextupoles magnets*, Cockcroft Institute, Liverpool University
- [23] K. Schindl, *Space charge*, CERN, CH-1211, Geneva
- [24] W. Herr, *Beam-beam effects*, CERN, Cockcroft Institute Lectures
- [25] M. Chanel, *LEIR: the low energy ion ring at CERN*, CERN, PS Division, Geneva CH 1211, Switzerland
- [26] library.web.cern.ch/Library/Archives/isad/isaps.html
- [27] S.S. Gilardoni et al., *The PS upgrade programme: recent advances*, Proceeding of IPAC 2013
- [28] S. Gilardoni and D. Manglunki, *Fifty years of the CERN Proton Synchrotron*, volume I, 2011. CERN-2011-004

- [29] E. Regenstreif, *The CERN Proton Synchrotron(Part III)*, CERN Yellow Report 59-29 (1959)
- [30] *nTOF*, Collaboration (CERN) *The neutron Time-Of-Flight facility, n_TOF, at CERN (I): Technical Description*, CERN 13 feb 2013
- [31] <http://www.exploratorium.edu/origins/cern/tools/ad.html>
- [32] B. Giulia *Neutrino velocity measurement with the OPERA experiment in the CNGS beam*, Institut de Physique Nucléaire de Lyon, PhD thesis, Lyon, 20 Mai 2011
- [33] S. Aumon, *High intensity beam issues in the CERN Proton Synchrotron*, Lausanne, EPFL, 2012
- [34] A. Huschauer, *Working point and resonance studies at the CERN Proton Synchrotron*, Vienna University of Technology and CERN, September 2012
- [35] B. Mikulec, A. Blas, C. Carli, A. Findlay, K. Hanke, G. Rumolo, J. Tan, *LHC beams from the CERN PS Booster*, CERN, 1211 Geneva 23, Switzerland, Proceedings of PAC09, Vancouver, BC, Canada
- [36] R. Garoby et al., *Upgrade Plans for the LHC Injector Complex*, IPAC'12, New Orleans, May 2012, TUXA02
- [37] S.S. Gilardoni et al., *The proposed CERN Proton-Synchrotron upgrade program*, Proceedings of IPAC2011, San Sebastián, Spain
- [38] R.A. Jameson, *High-Brightness H⁻ accelerators*, MS-H811, Los Alamos National Laboratory, Los Alamos, NM 87545
- [39] M. Sands, *The physics of electron storage rings an introduction*, November 1970
- [40] K. Schindl, *Instabilities*, CAS DESY, Zeuthen, Germany, 15-26 September 2003
- [41] M. Ferrario, M. Migliorati and L. Palumbo, *Wake fields and instabilities in linear accelerators*, INFN-LNF and Università di Roma 'La Sapienza', CAS DESY, Zeuthen, Germany, 15-26 September 2003
- [42] T. W. et al, *Wake Fields and Impedances*, DESY M-91-06, 1991
- [43] B. C. Craft *Robinson instability and beam loading*, National Synchrotron Light Source, Brookhaven National Laboratory, Upton, N.Y. 11973, IEEE Transaction on Nuclear Science, Vol. NS-32, No. 5, October 1985
- [44] A. W. Chao, J. Wiley and Sons, *Physics of Collective Beam Instabilities in High Energy Accelerators* 1993

- [45] C.N. Lashmore-Davies, *Kinetic theory and the Vlasov equation*, Culham Laboratory, Abingdon, Oxon. OX14 3DB, UK (Euratom/UKAEA Fusion Association)
- [46] S. Prabhakar, et al., *Curing coupled-bunch instabilities with uneven fills*, Phys. Rev. Lett. 2001 Mar 5;86(10):2022-5
- [47] H.Damerau, S.Hancock, C.Rossi, E.Shaposhnikova, J. Tuckmantel, J.-L. Vallet, *Longitudinal coupled-bunch instabilities in the CERN PS*, CERN, Geneva Switzerland, Proceedings of PAC07, Albuquerque, New Mexico, USA
- [48] M. Bassetti, A. Ghigo, M. Migliorati, L. Palumbo, M. Serio, *A time domain simulation code of the longitudinal multibunch instabilities*, Frascati, June 23, 1993
- [49] M. Bassetti, *Finite Difference Equations Calculations of Beam-Cavity Coupling Instability*, LNF Note 67/45, Frascati 1967
- [50] M.Lonza, *Multi-bunch feedback system*, Elettra Synchrotron Light Laboratory, Trieste S.C.p.A., Trieste, Italy
- [51] S. Persichelli, M. Paoluzzi, M. Migliorati, B. Salvant *Finemet cavity impedance studies*, CERN-ATS-Note-2012-064 M
- [52] H. Damerau, S. Hancock, M. Paoluzzi, M. Migliorati, L. Ventura, *Longitudinal coupled-bunch oscillation studies in the CERN PS*, CERN, Proceedings of IPAC2013, Shanghai, China
- [53] H. Damerau, *Coupled-bunch oscillation feedback studies*, LIU-PS Working Group Meeting, 20 February 2013
- [54] H. Damerau, S. Hancock, M. Schokker, *Longitudinal performance with high-density beams for the LHC in the CERN PS*, Proceedings of HB2010, Morschach, Switzerland
- [55] F. Pedersen, F. Sacherer, *PAC77*, pp. 1397-1399
- [56] G. Favia, *The CERN PS main RF system: a study for possible upgrades in the perspective of the ultimate LHC performance*, Master thesis, Sapienza University, Rome, Italy
- [57] K.Y. Ng and Z.B. Qian, *FINEMET VERSUS FERRITE -PROS AND CONS*, FNAL, Batavia, IL 60510, Proceedings of the 1999 Particle Accelerator Conference, New York, 1999, p.872
- [58] M. Paoluzzi, H. Damerau *Design of the PS longitudinal damper*, CERN-ACC-NOTE-2013-0019
- [59] R. Garoby *Plans for the upgrade of the LHC injector complex*, LIU Project at CERN, 19/06/2012